Development and partial validation of a bioanalytical assay for the detection of a novel bone-targeting parathyroid hormone conjugate using metal-free LC-MS/MS

by

Benjamin George Wajda

A thesis submitted in partial fulfillment of the requirements for the degree of

Master of Science

in

Pharmaceutical Sciences

Faculty of Pharmacy and Pharmaceutical Sciences

University of Alberta

Abstract

In an effort to address shortcomings with current drug treatments for osteoporosis (OP) and improve the efficacy of human parathyroid hormone (hPTH(1-34)), we have employed a bisphosphonate-conjugation strategy by tethering hPTH(1-34) to a non-nitrogenated bisphosphonate (BP) moiety (BP-PTH) in order to enhance targeted drug delivery to bone. Conjugation of hPTH (1-34) to a BP imparts mineral affinity to the peptide hormone, allowing it to localize to positively-charged calcified tissues in bone. Improved drug targeting will lead to administration of lower therapeutic doses, resulting in low systemic exposure and lower concentrations being observed in plasma. Therefore, it is essential to develop a sensitive bioanalytical assay for future pharmacokinetic studies of this conjugate.

This thesis describes the development and partial validation of an LC-MS/MS assay for the sensitive measurement of BP-PTH in rat plasma. A combination of protein precipitation and solid phase extraction was used for sample preparation, allowing for concentrated samples without the need of evaporation. Chromatographic separation was performed on a reverse-phase Phenomenex bioZen PS-C18 column with a total run time of 10.50 min. The calibration curve was linear (r^2=0.996) in the range of 5 ng/mL to 25 ng/mL, the lower limit of quantification was 2.5 ng/mL. The intra- and inter-assay precision over two days (percent coefficient of variation) calculated from quality control samples was less than 10%, and the mean accuracy (percent deviation from nominal) for all samples was between 102.22%. Despite achieving satisfactory validation parameters, the chosen analytical column proved to have a short column lifetime before becoming irreversibly damaged. The method will be re-optimized with a more appropriate analytical column in the future. To our knowledge, this is the first reported method for the detection and quantification of BP-conjugated peptides in a biological matrix.

In an effort to achieve lower limits of detection of BP-PTH, TMSD derivatization was used to methylate the phosphonic acid groups present in the BP moiety of BP-PTH. Lack of specificity with the derivatization agent resulted in the creation of numerous BP-PTH derivatives, with the most abundant corresponding to derivatives containing 11-15 methylations. The generation of numerous derivatives caused by the various number of possible methylation sites on the conjugate resulted in poorer sensitivity in comparison to non-derivatized BP-PTH.

The use of a highly specific commercial hPTH (1-34) ELISA was explored as an alternative to LC-MS/MS for the detection of BP-PTH. The ELISA was unable to establish a concentration-response relationship for unmodified BP-PTH. Modifications to BP-PTH were undertaken with the aim to generate variants that were more chemically and structurally similar to hPTH (1-34) to allow for ELISA detection. Neutralization of the phosphate groups present in the BP portion of the conjugate were unsuccessful and suitable ELISA detection was not achieved.

Preface

This thesis is an original work by Benjamin G. Wajda. No part of this thesis has been previously published.

I dedicate this thesis to my loving family; mom, dad and brother;

Kathy, Paul and Davis:

Thank you for all of the unconditional support and faith in me.

Acknowledgements

I would like to express my sincerest gratitude and thanks to my supervisor Dr. Michael Doschak for giving me the opportunity to conduct research in his laboratory and providing me with a traditional graduate student experience. I thank him for his endless support in my research and in my future career aspirations. I appreciated the faith, trust and independence he gave me as his student; it helped to foster my intellectual curiosity, improve my critical thinking skills and better understand the scientific method. I will cherish the memories from our trips to Japan and Banff. Thank you for also showing me that there is more to graduate school than simply conducting experiments, and fun still needs to be had!

I would like to extend a special thank you to my supervisory committee members Dr. Carlos Velázquez, Dr. Dion Brocks and Dr. Randy Whittal for their understanding of the circumstances that required this thesis to be defended on short notice. I will be forever grateful for their understanding of the situation, as their willingness in letting me defend on a tight deadline allowed me to realize a childhood dream and start my next chapter as I begin medical school. I also appreciate their guidance, critique and discussion during the last two years.

I would also like to thank my lab colleagues and members of the Pharmaceutical Orthopaedic Research Laboratory (PORL): Dr. Shadab Alam and Dr. Waheed Asghar for their discussions and input on my project. Special thanks to Dr. Takeshi Susukida who became a lifelong friend during his stay in Canada. Thank you for being a fantastic support, friend and for the fun times, arigato!

Final thanks go to my friends, Alex for his non-stop support and encouragement during this degree, Jonas for listening to me discuss my research many times as we would drive together to coach skiing, and Megan for all of her kind support and encouragement towards the end of my degree.

List of Figures

List of Tables

List of Symbols, Abbreviations and Units

°C	Degree Celsius
ACN	Acetonitrile
amu	Atomic mass unit
BMD	Bone mineral density
BMU	Basic multicellular unit
BP-PTH	Bisphosphonate-PEG-PTH(1-34)
BPs	Bisphosphonates
cc	Cubic centimeter
CE	Collision energy
CRM	Charge-residue model
CV%	Coefficient of variation expressed as percent
D-BP-PTH	Derivatized BP-PTH
Da	Dalton
DC	Direct current
DO	Degree of oxidation
FWHM	Full width of the peak at its maximum height
ELISA	Enzyme-linked immunosorbent assay
EMA	European Medicines Agency
ESI	Electrospray ionization
eV	Electron volt
FA	Formic acid
FDA	US Food and Drug Administration
GC	Gas chromatography
HPLC	High performance liquid chromatography
hPTH (1-34)	Synthetic recombinant human PTH analog
hPTH (1-84)	Endogenous human PTH
hr	Hour
IEC	Ion-exchange chromatography
IEM	Ion-evaporation model

IS	Internal standards
kPa	Kilopascal
LC	Liquid chromatography
LC-MS/MS	Tandem mass spectrometry
LLOQ/LOQ	Lower limit of detection/ limit of quantification
LOD	Limit of detection
m/z	mass-to-charge ratio
ME	Matrix effect
mg	Milligram
min	Minute
mL	Millilitre
MRM	Multiple-reaction monitoring
MS	Mass spectrometry
MW	Molecular weight
N-BPs	Minute
ng	Nanogram
non-N-BPs	Non-nitrogen containing BPs
OP	Osteoporosis
PBM	Peak bone mass
PEG	Polyethylene glycol
ppm	Parts-per-million
PPT	Protein precipitation
psi	Pounds per square inch
PTH	Parathyroid hormone
Q1	First quadrupole
Q3	Third quadrupole
QC	Quality control
r^2	Correlation coefficient of regression
RF	Radio frequency
RP	Reversed-phase
rpm	Revolutions per minute

RT	Room temperature
SD	Standard deviation
SIM	Single ion monitoring
SPE	Solid-phase extraction
TFA	Trifluoroacetic acid
TIC	Total ion chromatogram
TMSD	Trimethylsilyldiazomethane
tR	Retention time
μg	Microgram
μL	Microlitre
UHPLC	Ultra-high-performance liquid chromatography
v/v	Volume/volume percentage
WAX	Weak-anion exchange
z	Charge

Chapter One

Introduction

1.1 Rationale

With the increasing prevalence of osteoporosis in our societies, osteoporosis is considered a serious public health problem around the world (1). While OP affects both sexes, the incidence of OP increases with age and is twice to three times more prevalent in females than males. In Canada, one in 4 women and one in 8 men are at risk of developing OP with a 40% lifetime risk of bone fracture (2). In 2008, the cost to the Canadian health care system of treating osteoporotic fractures was estimated to be in the range of $2.3 to $4.1 billion annually (3). With the aging world population, the social and economic burden of OP is growing in Canada and around the world. Improved management of OP will be necessary to reduce the economic burden on the healthcare system and improve quality of life for those living with OP.

Though there are several classes of compounds being used to treat and prevent OP, poor patient compliance, lack of selectivity, potency, and toxicity concerns causing significant adverse side-effects has created a need for safer and more efficacious next-generation therapies with reduced unwanted side-effects. Synthetic parathyroid hormone (hPTH (1-34)) is an effective bone-forming approved treatment for OP. However, due to rapid degradation in the body, treatment efficacy and potency of hPTH (1-34) is severely restricted. To address these concerns, our lab has tethered a bone-seeking bisphosphonate group to hPTH (1-34) to impart bone mineral affinity to hPTH (1-34), allowing it to be specially guided to bone surfaces to promote bone formation. Administration of this novel drug (BP-PTH) into osteoporotic female rat models over a 12-week period has shown significant bone formation when viewed with micro-CT scans in comparison to unmodified hPTH (1-34).

A sensitive and accurate bioanalytical method for the detection of BP-PTH in rat plasma is required to perform pharmacokinetic evaluation to determine biodistribution, clearance, and retention of BP-PTH to correlate serum concentration with pharmacological response. Establishing these parameters will facilitate the translation from preclinical studies to clinical drug trials in humans. The work described in this thesis will create novel contributions to the bioanalytical field by establishing new methodology capable of determining pharmacokinetic parameters for bisphosphonate-conjugated peptide drugs, which has not been reported before in literature.

1.2 Hypotheses

First Hypothesis

Metal-free LC-MS/MS for the quantification of BP-PTH will address the problematic metal chelating abilities of BP and BP-containing compounds that lead to poor linearity, sample carry-over, poor peak shape, and poor reproducibility in traditional LC-MS/MS instrumentation.

Second Hypothesis

Performing on-cartridge derivatization of BP-PTH using derivatization agent, trimethylsilyldiazomethane (TMSD), will allow for efficient and sensitive quantification of BP-PTH in rat plasma. Methylation of the negative phosphonic acid groups by TMSD will reduce the conjugates overall negative charge, and in turn, increase the sensitivity of BP-PTH in ESI+ mode to achieve lower quantification levels.

Third Hypothesis

Neutralization of the phosphonic acid groups in BP-PTH through derivatization will allow for sensitive detection of BP-PTH using a commercial ELISA specific for hPTH (1-34). Neutralization of these groups will significantly reduce electrostatic interactions between analyte and antibody, enabling improved antibody recognition and binding.

1.3 Objectives

The objectives of this thesis were as follows:

1. Optimize the plasma extraction procedure using protein precipitation and solid-phase extraction. Explore derivatization of phosphonic acid groups using trimethylsilyldiazomethane to enhance ionization in ESI+ mode to improve sensitivity.

2. Develop and optimize a sensitive LC-MS/MS method using ESI+ mode with efficient method run time that also allows for adequate separation and retention of BP-PTH on a reverse-phase analytical column. Linear range of the bioanalytical method needs to correspond with the estimated concentration of previously collected preclinical rat plasma samples.

3. Perform method validation studies in accordance to the European Medicines Agency guideline for bioanalytical assays. The assay will be assessed for linearity, selectivity, precision and accuracy, sensitivity, matrix effect and extraction recovery, and stability.

4. Using the optimized plasma extraction procedure for BP-PTH, evaluate whether a commercial ELISA specific for hPTH (1-34) is able to detect BP-PTH. Derivatization of the BP moiety will be explored as potential avenue for improved detection using commercial ELISA.

1.4 Background

1.4.1 Basic structure and function of bone

Bone is essential for numerous vital functions within the body and is absolutely necessary for the life of vertebrates. Bone provides the rigid framework of our skeletal systems, interacts with muscles allowing for the movement of limbs, protects internal organs, generates and maintains various blood cells and stores important minerals such as calcium and phosphorus. In order for bones to facilitate the movement of limbs, they must be stiff and resist deformation, while also remaining flexible to change shape without cracking, shorten and widen in compression and lengthen and narrow during tension (4).

Loads that exceed a bones elastic ability, may deform the bone further, causing permanent changes. These permanent shape changes manifest as microcracks that allow energy release and affect the mechanical properties of bone (4). Accumulation of microcracks, larger cracks or increased bone porosity can significantly reduce bones elastic ability, leading to potential fractures. If a bone is unable to absorb the energy during impact loading, it can only be released by fracturing the bone. The seemingly contradictory mechanical properties requiring bone to be stiff, yet flexible, can be explained by its mineral composition and structural design (4).

The relationship between bone stiffness and flexibility is ultimately determined by varying mineral content within bone. Bone is a mineralized connective tissue comprised of an organic matrix of type I collagen that serves as the connective tissue and an inorganic mineralized phase consisting of calcium hydroxyapatite-like crystals (5,6). The collagen matrix provides flexibility, whereas the inorganic mineral phase provides material stiffness. Greater mineral content leads to stiffer bones with reduced flexibility (5).

Despite bones "static" appearance, bone is actually a dynamic tissue that is constantly being remodeled through the formation of new bone and the breakdown of old bone by osteoblast and osteoclast cells respectively. The process of renewing bone is called bone remodeling and is required to maintain bone strength and mineral homeostasis (6,7). Physiologic influences or mechanical forces drive the modeling process which leads to gradual changes in the shape, width, strength and flexibility of bones (7). Bone remodeling is a lifelong process that begins before birth and continues until death. The cycle of bone remodeling follows three phases: 1) initiation of bone resorption by osteoclast cells, 2) transition from resorption to new

bone formation, and 3) new bone formation by osteoblast cells (6,8). Evidence suggests that a third cell type, osteocytes, act as mechanoreceptors to coordinate the interplay between osteoblast and osteoclast cells which facilitates the cycle of bone remodeling (6). Ultimately, bone remodeling is carried out by the basic multicellular unit (BMU) which coordinates the action of four major bone cells: bone-lining cells, osteocytes, osteoclasts, and osteoblasts (Figure 1) (9). Normal bone remodeling is a systemic and local process required for locomotion, healing of fractures and microdamage's in bone matrix, skeletal adaptation and maintenance of plasma calcium homeostasis (6,9). Abnormal bone absorption or resorption is the underlying cause of many bone diseases and disorders.
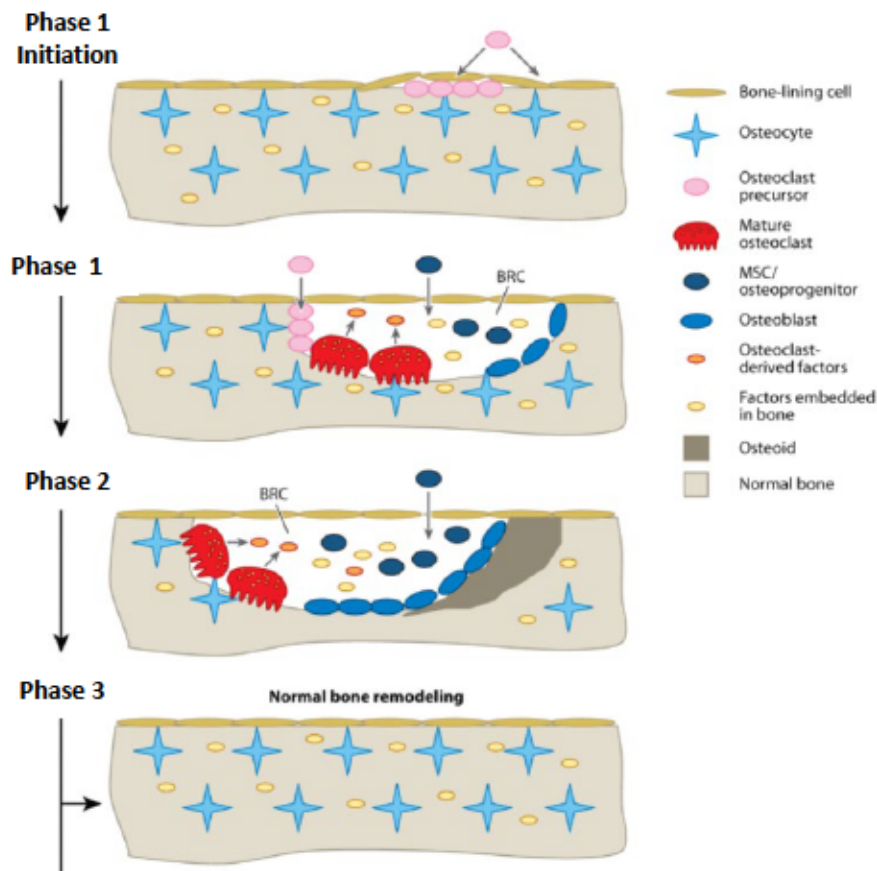
Figure 1.1: Three phases of bone remodeling.
Adapted and modified from source 9.

1.4.2 Osteoporosis: etiology and epidemiology

Osteoporosis (OP) is a skeletal disorder that is characterized by low bone mineral density, deterioration of bone microarchitecture, reduced mineralization, and an overall decrease in bone strength and stiffness (10). Osteoporosis significantly increases an individual's risk of bone fracture and is considered a serious public health problem around the world (11). Due to the asymptomatic nature of the condition, OP is often undiagnosed until patient hospitalization occurs stemming from low-trauma fractures of the hip, spine, proximal humerus, pelvis, and/or wrist (10). Vertebral fractures have been associated with increased rates of morbidity, including pain, spinal deformity (kyphosis), height reduction, disability and death (11).

Osteoporosis is the most significant cause of fractures within the older population and is also associated with people becoming bedridden, which can cause other serious complications (10). In addition to reduced mobility and pain, the quality of life changes induced by osteoporotic fractures may lead to psychological concerns such as lower self-esteem, anxiety, fear and depression (12). In the United States, the prevalence of OP is projected to reach 14 million people by 2020 (10). While OP affects both sexes and all ages, the incidence of OP increases with age is twice to three times more prevalent in females than males. In Canada, one in 3 women and one in 5 men will suffer an osteoporotic related fracture in their lifetime, which is of higher incidence than heart attack, stroke, and breast cancer combined (2). In 2010, the overall yearly cost to the Canadian health care system including direct and indirect costs of treating osteoporotic fractures was estimated to be in the range of $2.3 to $3.9 billion annually (13). With the aging world population, the social and economic burden of OP is growing in Canada and around the world. Improved management of OP will be necessary to reduce the economic burden on the healthcare system and improve quality of life for those living with OP.

Osteoporosis can be classified as either primary or secondary; with primary being associated with age and sex hormone deficiency, while secondary osteoporosis is the result of several comorbid diseases and/or medications. Primary OP often follows menopause in women due to the reduction in estrogen production leading to bone loss, while age-related OP results from gradual deterioration of the trabeculae in bone (10). In males, as aging occurs, sex hormone binding globulin may inactivate testosterone and estrogen, contributing to a gradual decrease in bone mineral density (BMD) that may result in primary osteoporosis (10,14). Secondary OP has been linked to conditions such as hypogonadism, diseases (e.g., coeliac disease), medications

(e.g., glucocorticoids) and imbalances of calcium and vitamin D. Management of inflammatory diseases such as rheumatoid arthritis commonly utilize glucocorticoid therapy, with many treatment plans requiring patients to be on long-term glucocorticoid therapy, the risk for developing secondary OP increases. Long-term usage of glucocorticoids has been associated with secondary osteoporosis and BMD has been shown to decline substantially within three to six months of therapy (15). With high rheumatoid arthritis prevalence amongst older aged populations in North America, potential for individuals to develop secondary OP is significant. Furthermore, it appears that the causes of secondary OP may differ amongst sexes. In men, alcohol abuse, glucocorticoid use and hypogonadism have been identified as contributing to osteoporosis (16). The three most common causes of secondary osteoporosis in postmenopausal women have been identified as hypercalciuria, malabsorption (vitamin D deficiency), and hyperparathyroidism (10,17). Of these three major secondary causes attributed to osteoporosis in postmenopausal women, hyperparathyroidism and calcium malabsorption contributed to 78% of incidences (18).

1.4.3 Osteoporosis pathogenesis

Osteoporosis can occur to varying degrees for two main reasons 1) failure to achieve peak bone mass and 2) abnormal bone remodeling through either excessive bone resorption or decreased bone formation (19). Failure of the basic multicellular unit to effectively coordinate the bone remodeling processes is the underlying cause of bone resorption and formation imbalances. Additionally, the incidence of fragility fractures is affected by the frequency, direction and force of falls. The lifelong process of bone remodeling which is caused by the resorption of old bone by osteoclasts and the formation of new bone by osteoblasts is vital for the maintenance of bone strength. Imbalances in this process where resorption exceeds the formation of new bone may result in the pathophysiological changes characteristic of osteoporosis (10). Though development of osteoporosis can be attributed to the two aforementioned causes, the roles of genetics, endocrine hormones, environment and mechanical factors, and nutrition all contribute to both main causes of OP.

1.4.3.1 Peak bone mass

Peak bone mass (PBM) is defined as the amount of bony tissue present at the end of skeletal maturation and is often reached in the late teens or early 20's (20). Achieving peak bone mass is crucial protective factor for the prevention of osteoporosis and reducing fractures in adulthood (19). Fractures have been reported to be reduced by up to 50% in post-menopausal with only a 10% increase in peak bone mass (19,21). Furthermore, a World Health Organization (WHO) generated mathematical model utilizing several experimental variables to determine the association between PBM and development of OP calculated that an increase of only 10% in PBM could delay the onset of OP by 13 years (21,22).

1.4.3.2 Irregular bone remodeling: imbalances between resorption and formation

The cells responsible for remodeling bones under normal physiological conditions are the same cells responsible for the abnormal remodeling process which occurs in disease states. The cellular basis of osteoporosis ultimately results from an increased number and life span of osteoclasts in comparison to a decrease in the life span and number osteoblasts, creating an imbalance between bone resorption and bone formation. Osteoblastogenesis and osteoclastogenesis must be properly balanced to ensure normal bone homeostasis, when the activity of osteoclasts exceeds the activity of osteoblasts, osteoporosis will result. In cases where imbalances lead to osteoporosis, osteoblasts are effectively unable to adequately form new bone in resorption cavities, leading to thickness decreases in bone cavities, thinner trabeculae, and reduced trabeculae connectivity (23). Increased intracortical remodeling also occurs, causing cortical bone to be more porous. Ultimately, the net outcome of these changes is the physical manifestation of osteoporosis, which leads to increased bone fragility and higher fracture risk.

The cells that comprise the coordinated action of the BMU (bone-lining cells, osteocytes, osteoclasts, and osteoblasts) are susceptible to mediators that may result in irregular bone remodeling. Of these mediators, the osteoprotegerin (OPG) and receptor activator of NF-$\kappa\beta$ (RANK) system and its ligand (RANKL) are the most influential mediators of osteoclasts, while low-density lipoprotein receptor-related protein 5 (LRP5) is a crucial mediator of osteoblast activity (19). Production of the TNF-like cytokine RANKL, stimulates the bone resorption process. Oligomerization and activation of the cell-surface receptor RANKL triggers the activation of various intracellular pathways, particularly NF-$\kappa\beta$, which induces osteoclastogenic

genes (19, 24). Furthermore, inflammatory cytokines such as tumor necrosis factor alpha (TNF-α) and interleukin-1 (IL1) may cooperate with RANKL to enhance signaling by RANK and promote osteoclastogenesis (25). OPG acts in a reciprocal manner to RANK and instead hinders the bone resorption process. OPG encodes a soluble TNF-α receptor that acts as a decoy for RANKL (26). Overexpression of OPG has been shown to block the later stages of osteoclast differentiation (24, 27).

Bone formation is stimulated by the activation of the LRP5 pathway by Wnt proteins, which also inhibits bone resorption. Activation of LRP5 is achieved through the Wnt/β-catenin cascade. The Wnt/β-catenin is activated upon binding of Wnt to frizzled receptor and LRP5 and LRP6 coreceptors (28). Wnt binding induces a multitude of intracellular events that stabilize β-catenin through hypophosphorylation, which accumulates in the cytosol and translocates to the nucleus (28,29,30). Within the nucleus, stabilized β-catenin binds with T cell factor/lymphoid enhancer binding factor (TCF/LEF) transcription factors and mediates gene expression to regulate osteoblast expansion and function (29, 30). Wnt signalling can be inhibit by several antagonists through Wnt receptor binding or Wnt ligand binding. Dickkopf (Dkk) proteins inhibit osteoblast function and block bone formation by binding to LRP5/6, preventing Wnt from interacting (29). Secreted frizzled-related proteins (sFRPs) work as antagonists by binding Wnt directly to inhibit activity (29). Additionally, mutations causing loss-of-function in human LRP5 have been associated with osteoporosis-pseudoglioma syndrome (30).

The complex intracellular pathways of both osteoclastogenesis and osteoblastogenesis leave ample opportunities for hormones, growth factors, cytokines, drugs and other mediators to influence the normal balance between bone formation and remodeling. Logically, it would seem that an imbalance favouring significantly more bone resorption than formation would have the largest impact on bone fragility, porosity, strength and fracture risk, impaired bone formation is also an important component of the pathogenesis of numerous bone disorders. Even in situations where bone formation activity is significantly greater than resorption, bone disorders will occur, such as osteopetrosis. Consistent irregularities in the bone remodeling process lead to disruptions in the delicate harmony between both osteoblast and osteoclast cells, which will result in bone disorders.

1.4.4 Determinants of Osteoporosis

1.4.4.1 Genetic factors

The interplay of several physiological factors influences bone mass accumulation during growth and are determinants of peak bone mass (21). Genetic factors, vitamin D and bonetropic nutrients (calcium, proteins), endocrine factors (sex steroids, IGF-I, 1.25(OH)$_2$D), and environmental factors such as nutrition, exercise, body weight and smoking (19,21). Twin and family studies have shown that genetic factors appear to be the most prominent determinant contributing between 50 to 85% of variance in peak bone mass (19,21,31). Furthermore, mass parent-offspring comparison studies show a significant relationship for the risk of OP in families, with both paternal and maternal inheritance (21). Through the use of genome-wide association studies, various genetic variants responsible for regulating bone mass have included sclerostin (SOST), LRP5, OPG, oestrogen receptor 1 and RANK pathway genes (8).

To date, there has been 24 genes and loci that have shown genome-wide significant evidence for association with BMD, though each gene contributes a small amount to the genetic variance in predisposition to osteoporosis (19,31). Sandhu and Hampson note that is may be explained due to the fact that genome-wide association studies often focus on identifying common variants of small effects, instead of uncommon variants that have large effects (19). Though there appears to be a clear hereditary component of osteoporosis, genetic factors have not yet influenced clinical decision making. Developing an understanding of gene-environment interactions as a determinant of BMD in response to nutrition and physical activity has not yet been explored, but could provide valuable insight into further understanding the pathogenesis of osteoporosis (21).

1.4.4.2 Hormonal factors

Hormones and growth factors play a substantial role in the regulation of proper bone formation, remodeling and as determinants for the achievement of peak bone mass. Estrogen is the major hormonal regulator of bone metabolism in both men and women. Though the protective effects that estrogen has on bone is undisputed, the precise mechanism(s) of action are very complex and has been challenging to define (32). Direct effects of estrogen on osteocytes,

osteoclasts, and osteoblast lead to inhibition of bone remodeling through maintenance of bone formation while reducing bone resorption (32).

Postmenopausal osteoporosis is mainly the result of reduced estrogen levels associated with menopause that lead to an increase in bone resorption (9). In postmenopausal osteoporosis, the extent of bone resorption exceeds that of bone formation. Estrogen exhibits its protective effects on bone remodeling by targeting the regulatory RANKL/RANK/OPG axis. Estrogen has been shown to stimulate expression of OPG in mouse osteoblasts and stromal cells (33). OPG is a RANKL antagonist that competes with RANK for binding of RANKL, leading to lower bone resorption activity. Additionally, estrogen directly inhibits the RANK activated JNK pathway in osteoclast precursors (9,34). A variety of cytokines regulate osteoclast activity and differentiation, most particularly IL-1, -6, -7 and TNF (9). One mechanism explaining estrogens protective effects is through the modulation of these cytokines. IL-1 and TNF enhance mature osteoclast cell activity and upregulate expression of IL-6, which stimulates osteoclastogenesis (9). Estrogen suppresses IL-1, -6 and TNF expression in osteoblast cells, enhancing bone formation (9). Deficiencies in estrogen increases the secretion of IL-1 and TNF, stimulating osteoclastogenesis indirectly through upregulation of IL-6. In addition, IL-1 and TNF also function to upregulate RANKL gene expression in osteoblasts (26).

More recent advances in attempts to better understand the molecular and cellular mechanisms of estrogen deficiency in the pathogenesis osteoporosis has shown that estrogen promotes mature osteoclast apoptosis through induction of the Fas/Fas ligand system (35). Fas ligand (FasL) and its receptor Fas are a part of the TNF superfamily of ligands/receptors that are involved in apoptotic pathways. The modulation of mature osteoclast apoptosis by estrogen is considered a mechanism with protective effects that reduces bone loss and the incidences of osteoporosis. For years it was understood that estrogen was the sole mediator responsible for pathogenesis of osteoporotic bone remodeling, however Sun et al. was the first group to report that follicle-stimulating hormone (FSH) is involved in the pathogenesis of postmenopausal osteoporosis (9, 36). Sun et al. states that FSH is required for hypogonadal bone loss. The group showed that neither FSHβ nor FSH receptor knockout mice showed bone loss despite severe hypogonadism (36). Furthermore, they suggested that the skeletal action of FSH is estrogen independent by stating bone mass increases through reduced osteoclastic resorption in haploinsufficiinet FSHβ[+/1]

mice (36). Ultimately, they concluded that high concentrations of FSH causes hypogonadal bone loss.

In advancing aged males, the decrease in sex hormone concentrations is significantly smaller than in menopausal females, with a relatively small reduction in serum testosterone, but a proportionally larger increase in sex hormone binding globulin (SHBG) (37). Hypogonadism in males is a significant cause of osteoporosis, therefore, the reduction in serum testosterone presumably contributes to age-related bone loss in males. Conversion of testosterone to 5α–dihydrotestosterone (DHT) results in greater affinity for androgen receptors. Colvard et al. note that human osteoblast-like cells show specific androgen receptors which may mediate the effects of testosterone on bone (38). It is believed that androgens have a role in the proliferation and differentiation of osteoblasts, regulate osteoblast-to-osteoclast signaling by inhibiting osteoclast recruitment (37,38).

A study of 48 men with a median age of 44 years old found that the ratio of serum testosterone to SHBG was significantly correlated with bone density in the forearm (39). Additional evidence regarding testosterone induced bone formation stems from the belief that the actions of testosterone on the male skeleton may be partially regulated by aromatization to oestradiol (26,37). Several studies support this hypothesis through their findings that bone density is positively correlated to serum oestradiol and not serum testosterone concentration (37,40,41). Furthermore, mutations of the aromatase gene have shown no bone density improvements when subjected to intramuscular testosterone, but bone density increases when transdermal oestradiol was administered (41,42).

Parathyroid hormone (PTH) is another hormone that plays a crucial role in regulating the rate of bone remodeling. PTH is an 84-amino acid residue peptide hormone that works antagonistically with calcitonin for the maintenance of calcium homeostasis through increasing bone resorption (43,44). PTH regulates bone remodeling and increases plasma concentration levels by increasing renal tubular calcium reabsorption and indirectly increasing intestinal calcium absorption through stimulation renal calcitriol or 1,25 dihydroxyvitamin D (45). The corresponding ligand for PTH is the PTH-1 receptor, which is a G-protein-coupled receptor that is primarily expressed in the bone and kidney (45,46). Another PTH receptor known as PTH 2 receptors, are present in the central nervous system, pancreas, testis, and placenta (47). Despite

being a hormone responsible for the catabolism of bone and increasing calcium plasma concentrations, intermittent release of PTH lead to increased bone formation (43, 44).

Though the exact cellular events explaining the anabolic effect of PTH are not fully understood, studies have shown that insulin-like growth factors I and II (IGF-I, II) and transforming growth factor-β (TGF-β) play a role in mediating bone formation (44,47,48). PTH can induce skeletal expression and stimulate the synthesis of IGF-1 which has pro-differentiation and pro-survival effects on osteoblasts (47). TGF-β is a secretory product of both osteoblasts and osteoclasts which is capable of stimulating osteoblast proliferation and collagen synthesis (44). Furthermore, osteoclasts are able to activate and release latent TGF-β that has been deposited in bone matrix at sites of resorption, leading to differentiation of nearby osteoblasts (48). Effects of TGF-β on both osteoclasts and osteoblasts has led to suggestions that TGF-β serves as an osteoblast regulator and an important mediator of coupling bone formation to bone resorption for the maintenance of skeletal homeostasis (48).

Ultimately, PTH enhances bone formation by promoting osteoblast growth and replication while also reducing osteoblast apoptosis. Interestingly, mice that lack osteoclasts show no response to PTH, which suggests that PTH also stimulates osteoclastogenesis and is required for full anabolic action (45,46). Individuals suffering from primary hyperparathyroidism (one or more overactive parathyroid glands secreting excess PTH) has been shown to be an important secondary cause of bone loss in postmenopausal women (44). Secondary hyperparathyroidism in postmenopausal women causes accelerated bone turnover and can lead to increased rates of bone loss.

1.4.4.3 Nutritional factors

Proper nutrition plays a crucial role in achieving peak bone mass and is a protective factor against the development or severity of osteoporosis. It is well accepted that proper levels of calcium and vitamin D are the primary nutrients considered for osteoporosis prevention in adults, though recent studies have shown that additional nutrients such as potassium, magnesium, phosphorus, vitamins A, B, C, E, K and proteins and fats are important factors for bone health (49). Adequate dietary amounts of protein, calcium, vitamin D, fruits and vegetables have a positive effect on acquisition and maintenance of bone mass while high caloric diets have been associated with lower bone mass and higher fracture rates (50). Though osteoporosis is primarily

a condition experienced in older aged adults, proper nutrition intake during childhood can help an individual improve their bone mass. This can allow these individuals to reach peak bone mass, reducing the potential impacts of osteoporosis later in life. Due to diet being a modifiable and controllable risk factor, it is an effective starting point for osteoporosis treatment and prevention programs (50).

Approximately 99% of the body's calcium is located in bone and calcium balance determines the degree to which bone formation is expressed over bone resorption. Positive balances occur when formation exceeds resorption and when resorption exceeds formation a negative balance occurs (51). Proper calcium intake is required to ensure a positive calcium balance for bone building. Inadequate calcium intake may lead to secondary hyperparathyroidism, leading to increased bone turnover and accelerated bone loss (50). An individual's calcium balance is determined by various factors such as the amount of calcium intake, efficiency of calcium absorption in the intestine, and amount of calcium that is lost from the body in the form of feces, urine, tears and sweat (51). Due to these factors, adequate dietary calcium amounts will vary between individuals.

Globally, there is no consensus on adequate daily calcium intake, with some nations recommending more or less than others as a recommended dietary allowance. The Institute of Medicine in the United States recommends a daily dietary allowance of 1000mg/day for individuals under the age of 50 to a tolerable limit of 2500mg/day (51,52). Females aged 51-70 have recommended dietary allowances of 1200mg/day and the same tolerable limits of men aged 51-70, 2000mg/day (51,52). Individuals aged 71 and older are recommended to have calcium intakes of 1200mg/day with a tolerable upper limit of 2000mg/day (51,52). The recommendations are based off ideal skeletal health endpoints, which consists of optimal calcium absorption, bone density, osteoporotic fractures and osteomalacia (51). Though increased calcium intake is inferior in slowing cortical bone loss in comparison to hormones such as estrogen, it still plays an important protective role against bone loss (53). Numerous epidemiologic and prospective studies support the role of proper calcium intake as a preventative measurement of osteoporotic fractures (51).

The vitamin D metabolite 1,25,hydroxyvitamin D is responsible for stimulating the absorption of calcium from the gut (53). Prolonged vitamin D deficiency (25-hydroxyivitamin D < 10ng/mL) is associated with osteomalacia which results in decreased mineralization of bone

matrix (51, 53). Furthermore, biochemical, observational and randomized controlled trials have indicated that normal serum levels of 25-hydroxyvitamin D (25(OH)D) is required for normalized PTH levels for proper bone cell function (54). Insufficient levels of 25(OH)D are associated with secondary hyperparathyroidism, enhanced bone turnover and bone loss, lower bone mineral density, and increased risk of minimal fractures (53,54).

Phosphorus plays a role in maintaining the usual net calcium balance by promoting fecal calcium loss and reducing urinary excretion of calcium (53). Therefore, individuals on a high-phosphorous diet tend to maintain a healthy calcium balance. Furthermore, phosphorus, along with calcium and magnesium, are the major mineral ions in bone: they must be present in adequate amounts in extracellular fluid for normal bone mineralization.

Protein is responsible for comprising approximately one-third of its mass and around 50% of bone volume (55). The bone-protein matrix is continuously remodeled and many of the collagen fragments that are released during the proteolysis phase of remodeling cannot be recovered. Therefore, a suitable dietary intake of protein is required to ensure proper bone health. Protein has been reported to be both beneficial and detrimental to proper bone health. The effect protein has on bones is dependent on numerous factors, including the source of the protein, level of protein in the diet, weight loss, calcium intake and acid/base balance in the diet (55). The major effects of protein on bone include 1) comprising the structural matrix of bone, 2) balancing IGF-1 levels, 3) increase intestinal calcium absorption and urinary calcium (55).

1.4.4.4 Lifestyle factors

Healthy lifestyle behaviours such as consuming a healthy balanced diet and regular exercise could lessen the impact of osteoporosis. High-caloric diets, heavy alcohol consumption, lack of exercise and smoking are lifestyle factors that have all been linked to decreased bone mass and higher rates of fracture (56). Cigarette smoking has been shown to lead to changes in the level of microarchitecture of trabecular bone, resulting in decreased mechanical stress and bone resistance (57). The increased risk of cigarette smoking as a factor contributing to osteoporosis is independent of gender. For instance, women who smoke are almost twice as likely affected by osteoporosis than non-smoking women (57). Bijelic et al. reported that the prevalence of osteoporosis was much higher in groups of smokers (31.3%) compared to former smokers (28.6%) or non-smokers (7.5%) (57).

Almost all epidemiological studies of alcohol use and bone health have shown that chronic heavy alcohol consumption can increase the risk of developing osteoporosis in the future and have substantial negative effects on bone health (58). The risk is elevated if chronic alcohol consumption occurs during adolescence or young adulthood. Results of a random-effects meta-analysis indicated that persons consuming 1-2 alcoholic drinks per day had 1.34 times the osteoporosis risk in comparison to those who abstain from alcohol (59). Persons consuming more than 2 alcoholic drinks per day had 1.63 times the osteoporosis risk (59). Though alcohol has been shown to effect osteoblasts, reducing bone turnover, the specific mechanisms through which alcohol exerts effects on bone are not fully understood (58). Mechanical stress through muscle contraction and weight-bearing exercise has been shown to increase bone density, while reduced mobility, bed-rest or limited weight-bearing exercises has been shown to reduce bone mass (60). Research on the effect of exercise and bone mass in osteoporotic patients showed an improvement in bone mineral density by 1 percent over time and by 2.5 percent above patients in a non-exercising control group (60,61).
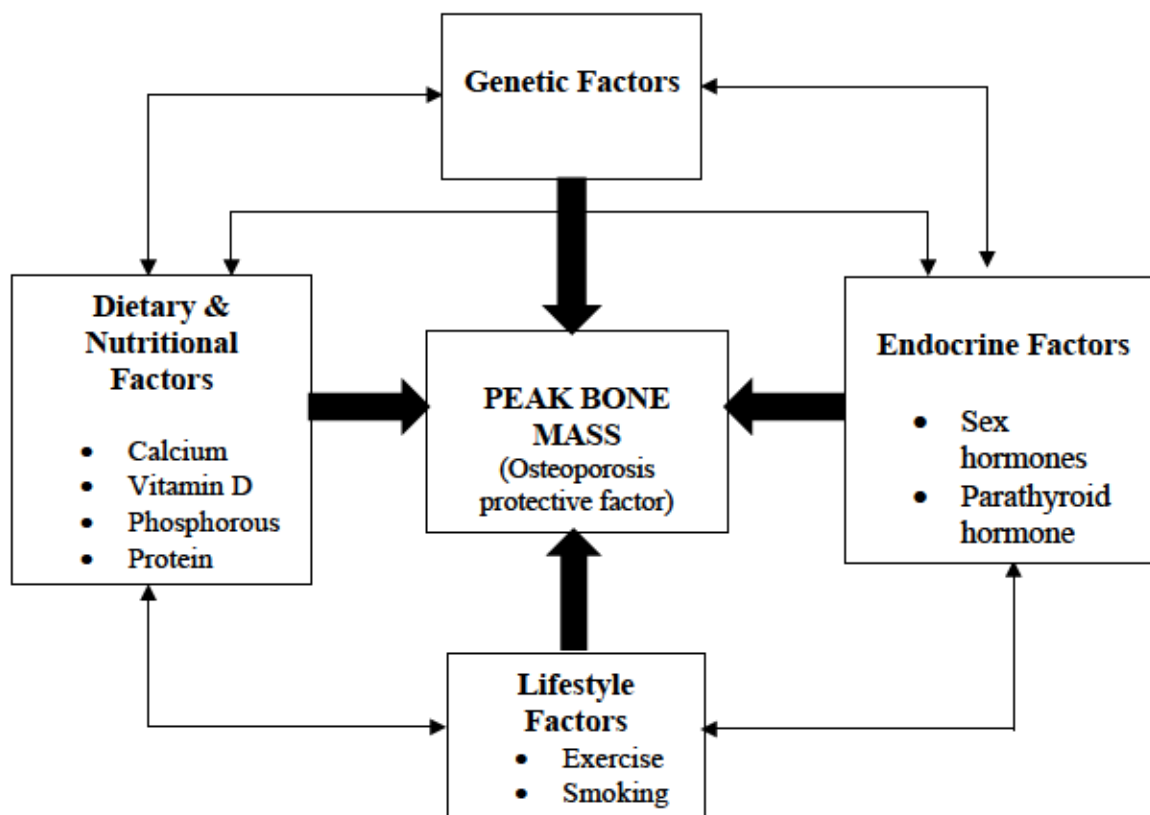
Figure 1.2: Physiological determinants of peak bone mass. Thin arrows demonstrate the interdependency of the four major factors that directly contribute to peak bone mass (thick arrows). Figure adapted and modified from Figure 1 in source 20.

1.4.5 Current Treatments for Osteoporosis

The most common therapeutic options can be classified as either anabolic agents or antiresorptive agents, or simply those that stimulate bone formation and those that inhibit bone resorption (62,63). Anabolic agents play a role in bone formation by stimulating osteoblast maturation and augmenting osteoblastic function and survival, leading to a direct increase in bone mineral density (62,63). Antiresorptive agents work to enhance osteoclastic apoptosis to promote bone strength and reduce bone resorption, effectively allowing bone formation to continue in excess of resorption. Currently, there are several classes of compounds that are being used to treat and prevent OP. These include nitrogen-containing bisphosphonates (BP), selective estrogen receptor modulators (SERMs), hormone replacement therapy, and biologic compounds such as romosozumab, (monoclonal antibody), calcium and vitamin D supplements, parathyroid hormone (PTH), and calcitonins (CT).

Reduction of bone resorption must be a paramount component of any therapeutic approach for the maintenance or improvement of bone strength. Specific stimulation of bone formation is essential, in theory, optimal pharmacological interventions should attempt to decrease bone resorption (endosteal and intracortical) while stimulating formation at all skeletal envelopes (19). This optimal approach would prevent decay of bone tissue while simultaneously increasing bone mass that may lead to improved reduction of non-vertebral fractures, which occur predominantly at cortical bone sites (19). In addition to pharmacological treatments for osteoporosis, non-pharmacological interventions have also shown to be important in reducing the prevalence of osteoporosis, managing risks and improving overall bone health.

1.4.5.1 Pharmacological interventions

Currently, pharmacological interventions are the most common way to treat and alleviate osteoporosis and osteoporotic symptoms in those medically diagnosed with the disease. Currently used treatments are examined below.

1.4.5.2 Hormone replacement therapy

The idea that hormone replacement therapy (HRT) prevents bone loss and osteoporosis in postmenopausal women is well established (64). The underlying cause of postmenopausal osteoporosis is estrogen deficiency leading to bone loss. Therefore, HRT is a logical approach

for the management of bone loss in peri- and postmenopausal women (65). HRT may consist of estrogens alone or be used in combination with progestin to decrease fracture risk (62). Studies have shown that doses of 0.625 mg conjugated equine estrogens daily, 2 mg oral estradiol-17β daily and 0.05 mg transdermal estradiol-17β daily will conserve bone mass (64,66-68). Observational studies, case-control studies, meta-analysis, and randomized clinical trials (Women's Health Initiative, Heart and Estrogen/progestin Replacement Study (HERS), Women's Interventional study of long Duration Oestrogen after Menopause (WISDOM)) have examined the anti-fracture efficacy of HRT (66-68).

Findings from these studies concluded that HRT decreases fragility fracture risk by 20-35%, with termination of HRT decreasing BMD and promoting bone turnover (66-68). Despite HRT's ability to prevent bone loss, the overall health risks generally outweigh the benefits from high dose HRT. Unwanted side effects of estrogen or combinations with progestins include thromboembolic events, stroke, coronary heart diseases, induced vaginal bleeding and breast tenderness (69). Furthermore, HRT may also increase the risk of ovarian cancer, myocardial infraction and contribute to a reduction in global cognitive function (69). Though HRT is an acceptable treatment for osteoporosis, it is only recommended after all other treatments have been considered. Patients taking HRT should use the lowest effective dose and for the shortest possible time (70).

1.4.5.3 Selective estrogen receptor modulators (SERMs)

Selective estrogen receptor modulators (SERMs) are drugs for the treatment of osteoporosis that bind with high affinity to estrogen receptors and can act as either estrogen agonists or antagonists, depending on the target tissue (71). As a partial estrogen receptor agonist, SERMs are able to maintain bone density while simultaneously exerting estrogen antagonistic effects in breast tissues women and endometrium (62,71). SERMs are chemically diverse synthetic molecules that lack the steroidal structure of estrogen but maintain a tertiary structure which allows them to bind to estrogen receptors (72). Due to their selective estrogen agonist and antagonistic properties in different tissue types, SERMs were developed as a treatment for estrogen deficiency diseases (i.e. osteoporosis) as they are efficacious without the adverse effects of estrogens (62,72).

There are currently two classes of SERMs for clinical use: triphenylethylene derivatives tamoxifen and toremifene for breast cancer usage and the benzothiophene derivatives raloxifene and bazedoxifene (71,72). Raloxifene is a second-generation estrogen receptor antagonist while bazedoxifene is a third-generation antagonist. Both are used for the treatment of osteoporosis. A large four-year osteoporosis fracture study referred to as the Multiple Outcomes of Raloxifene Evaluation (MORE) trial, demonstrated the effectiveness of raloxifene's ability to maintain BMD and reduce bone loss in both spine, neck and femur of participants (62,69,73). The study also concluded that postmenopausal women suffering from osteoporosis saw a reduction of 30% in vertebral fractures while using raloxifene (73). These findings were confirmed by the Raloxifene Use for the Heart (RUTH) trial (74), but also demonstrated that raloxifene decreases the risk of breast cancer but may also increase the risk of thromboembolism and stroke (74). Future SERMs should be developed with the focus of conserving bone density, reducing likelihood of fractures and minimizing adverse side effects to the breasts and endometrium (62).

1.4.5.4 Vitamin D and calcium supplements

Vitamin D and calcium supplementation is a baseline therapy for both the management and prevention of osteoporosis (62). Despite healthy levels of calcium and vitamin D being recognized as important and required nutrients for the maintenance of bone health and prevention of bone disease, the additional intake of calcium and vitamin D as supplements has been subjected to debate (63). Balance studies have shown that calcium has a threshold effect level, where above this level of intake, no additional bone formation occurs (75). In addition to a recommended daily intake, the effectiveness of calcium supplementation is likely to vary during different stages of skeletal development (childhood, adolescence, adulthood, and postmenopausal) (63,75). In childhood, calcium supplementation has shown an increase in bone mineral density while also having a potential beneficial effect on peak bone mineral density (76). In individuals suffering from postmenopausal osteoporosis, studies have shown that the effect of calcium supplementation is minimal and less effective compared to oestrogen replacement (75). In a large clinical trial involving healthy postmenopausal women, calcium with vitamin D supplementation showed a small but significant increase in hip bone density (77).

Despite the wide usage of calcium with or without vitamin D supplementation, there is no conclusive evidence showing an ability for supplementation to reduce fracture risk (63,77,78). Any benefits from calcium and vitamin D supplementation to reduce fracture risk are marginal at best, if any at all, and any such benefit is outweighed by the low risk of serious adverse events (78). Adverse events include increase in kidney stones, increased risk of acute gastrointestinal symptoms, myocardial infarction and hypercalcaemia (77,78). A meta-analysis study recommends daily doses of 1200 mg calcium and 800 international units of vitamin D daily for the majority of postmenopausal women suffering from osteoporosis (79).

1.4.5.5 Bisphosphonates

Bisphosphonate (BPs) drugs are the first line therapy for the treatment of osteoporosis and are extensively prescribed with more than 150 million prescriptions dispensed to outpatients between 2005 and 2009 (80). BPs are a class of anti-resorptive drugs that are stable analogs of naturally occurring inorganic pyrophosphate, an endogenous inhibitor of bone mineralization found in body fluids (81). The phosphate-carbon-phosphate (P-C-P) configuration of bisphosphonates provides resistance to chemical and enzymatic hydrolysis resulting in a long skeletal half-life and a stable and absorbable compound that can be taken orally and excreted unaltered (82,83). Though the majority of BPs are taken orally, zoledronic acid is given as a once-yearly dose intravenously. A once-yearly intravenous dose may offer increased compliance and persistence compared with oral bisphosphonates and lower adverse effects due to bypassing the gastrointestinal system (84).

BPs have tremendous affinity toward hydroxyapatite in bone and work therapeutically by inhibiting excessive bone resorption by inducing osteoclast apoptosis, resulting in a return to homeostatic bone turnover, preventing age related bone loss and deterioration of bone microarchitecture (82). The two phosphonate groups are required for cell-mediated antiresorptive activity and for binding to hydroxyapatite material in bone (83). Though several classes of BPs exist, they differ in their pharmacological properties, such as affinity for bone mineral and inhibitory effect on osteoclastic bone resorption, they share a common chemical structure with side chain variation (81). The R1 and R2 side-chains attached to the carbon atom determine the binding affinity and antiresorptive potency of the compound. R1 substituents such as primary

amino (-NH$_2$) or hydroxyl (-OH) groups improve binding to hydroxyapatite, while variations in the R2 substituent may drastically change the antiresorptive potency (83). The classes of BPs can ultimately be reduced to either nitrogen-containing (N-BPs) or non-nitrogen containing (non-N-BPs) compounds. Nitrogen containing BPs (such as alendronate, risedronate, ibandronate, and zoledronic acid) have more potent antiresorptive abilities than non-nitrogen containing BPs (clodronate, etidronate, tiludronate and midronic acid) and are the most commonly used drugs for the treatment of osteoporosis (82). Numerous large-scale phase III randomized controlled trials in postmenopausal women with osteoporosis reported significant reduction in vertebral fractures after three years of treatment with risedronate, alendronate, ibandronate, and zoledronic acid and reduction in non-vertebral fractures with alendronate, risedronate, and zoledronic acid (82,85-89). Bridging studies demonstrated an enhanced effect on BMD with intermittent dosing of weekly oral alendronate or risedronate, and monthly oral risedronate (90-92). The American Association of Clinical Endocrinologists and American College of Endocrinology (AACE/ACE) guidelines recommend alendronate, risedronate, and zoledronic acid as the first line treatment option for most patients at high risk of fracture (hip, non-vertebral and spine fractures) (93).

The numerous studies showing the promising effects of improving BMD using BPs with an acceptable safety profile has led in part, to increased prescribing of BPs and minimal monitoring for side effects (94). Unfortunately, their effectiveness in clinical practice has been limited due to poor patient persistence and low compliance with treatment regimes (94). Poor compliance may be explained by the undesirable dosing requirements (i.e. fasting overnight, taking alone with 240 ml of water with no other food or beverage and remaining upright for 30 min), never receiving proper instructions, failing to remember dosing instructions or not believing in the rationale for the dosing requirements (82,94). Low patient persistence for taking medication may be due to side effects, perceived side effects, fear of side effects, cost, or distrust in the physiological benefits of BPs (82). Common adverse side effects with nitrogen-containing bisphosphonates (such as alendonrate, risedronate, zoledronate) include atypical femoral shaft fracture (95), osteonecrosis of the jaw (96), esophageal cancer (80) and adyamic bone turnover in general leading to the accumulation of bone micro-cracks and poor-quality bone matrix. Adequate compliance and persistence with BP treatment regimens is necessary for therapeutic efficacy. Failure to adequately follow proper treatment regimens has been reported to lead to a

smaller BMD response (97), increased fracture risk (98), and greater healthcare costs when compared with proper compliance (82,99).
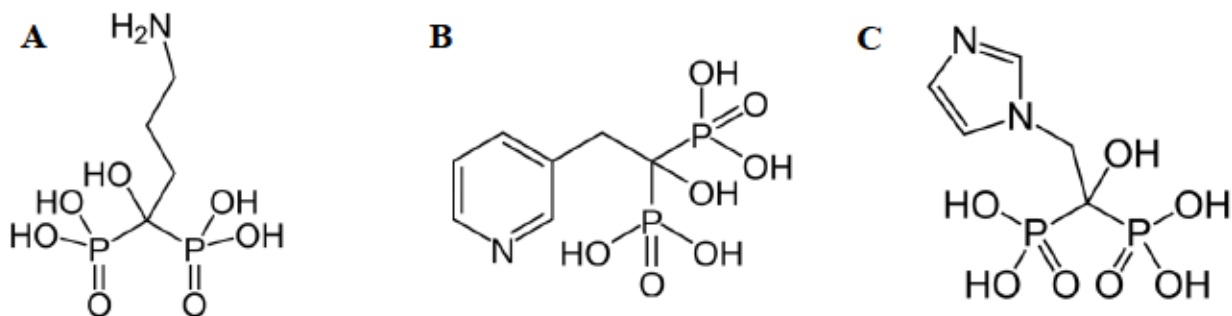
Figure 1.3: Chemical structures of common bisphosphonates. Alendronate (A), risedronate (B) and zoledronic acid (C).

1.4.5.6 Calcitonins

Calcitonin is a 32-amino acid polypeptide hormone that is secreted by the parafollicular cells of the thyroid gland in humans (100). Commercially available calcitonin uses synthetic salmon calcitonin and is an approved treatment for postmenopausal osteoporotic women who are at least 5 years beyond menopausal when other medications are not suitable. Calcitonin is currently only approved by the US FDA for the treatment of established osteoporosis and not for prevention (100). Despite human and salmon calcitonin differing structurally in 50% of their amino acid sequence, the pharmacological properties of both calcitonins are the same, but with salmon calcitonin being substantially more potent (approximately 40-50 times more than human calcitonin) (100). Calcitonin has proven anabolic ability and works to cause rapid loss of the ruffled border of osteoclasts in bone and reduces the number of osteoclasts in bone over the long term (101,102). Clinical trials have shown a small but significant increase in BMD after calcitonin administration over 3-5 years (103,104). A 5-year study using 200 IU daily doses known as the Prevent Recurrence of Osteoporotic Fractures (PROOF), demonstrated a reduction in vertebral fracture risk with benefits on hip and other non-vertebral fractures being less clear (105). There are two forms of administration for calcitonin; nasal form, which is well tolerated, and subcutaneous injection which is generally less tolerated than nasal administration and leads

to headache, nausea, diarrhea and flushing (62). Calcitonin is regarded as a second- or third-line class of drugs for the treatment of osteoporosis (62).

1.4.5.7 Parathyroid hormone

PTH analogs represent a class of anabolic agents for the treatment and management of severe osteoporosis (106). Unlike endogenous PTH, exogenous PTH has been shown to have an anabolic effect on bone which was observed in both human and animal studies (62). Endogenous PTH (hPTH (1-84)) is an 84-amino acid peptide that plays a crucial role in the maintenance of calcium and skeletal homeostasis. Early structure-function studies of PTH have demonstrated that all of the biological activity of intact hPTH (1-84) lies in the N-terminal sequence containing residues 1-34 (106). In 2002, a synthetic recombinant human PTH analog (PTH (1-34)), named teriparatide was authorized by the US FDA for the treatment of osteoporosis. PTH (1-34) is capable of stimulating bone formation and resorption, increasing or decreasing bone mass, depending on the rate of administration (107). To achieve the potent anabolic effects, PTH (1-34) must be given exogenously be intermittent injection. Continuous infusions and daily subcutaneous injections of PTH (1-34) both stimulate bone formation, but have varying effects on bone resorption and bone mass (107). Continuous infusions generate a consistent elevation of serum PTH concentration, which has been shown to lead to greater bone resorption in comparison to daily subcutaneous injections (107). Intermittent subcutaneous injection increases the rate of bone remodeling and results in a positive remodeling balance, leading to increased bone formation, causing osteon thickening (structural units of remodeled bones) (43,106). New bone forms on the inactive bone surfaces, resulting in trabecular architecture more closely resembling normal bone (43108). PTH (1-34) forms new periosteal bone apposition (the formation of layers of osteoblast-like cells and the deposition of new bones), this apposition results from reduced osteoblast apoptosis and increased differentiation of preosteoblasts to osteoblasts (43,109). A combination of new bone being formed and an increase in the remodeling rate ultimately results in a mechanism that can explain the increase of new bone tissue and increases in trabecular thickness (106). This combination and it's bone positive effects are not observed with the use of antiresorptive agents. In addition to increasing trabecular thickness, PTH (1-34) has also been reported to increase trabecular connectivity, which was assessed by microcomputed tomography of iliac crest bone biopsies (110). A large study with

1637 postmenopausal concluded that PTH (1-34) increases vertebral, femoral, and total-body BMD and decreases vertebral and nonvertebral fractures by 65-69% and 35-40%, respectively (107). A 40-μg dose increased BMD more than a 20-μg dose with similar effects on the risk of fracture, but was more likely to have side effects (107). In comparison with alendronate, PTH (1-34) significantly outperforms alendronate in terms of increasing lumbar BMD and decreasing frequency of nonvertebral fractures (111). A potential safety issue with PTH (1-34) is an elevated risk of osteosarcoma, which was first observed in a life-long carcinogenicity study using high-dose PTH (1-34) in rats from infancy to death (112). Despite these findings, there have been no reports of osteosarcoma in clinical trails (43). Isolated cases have shown occurrences of osteosarcomas in patients with long-standing hyperparathyroidism, however there is no direct evidence to suggest that elevated parathyroid hormone levels cause an increase in osteosarcomas (43,113). Hypercalcemia and hypercalciuria has been associated with a small number of patients undergoing PTH (1-34) administration which is often resolved with a decrease in calcium intake (114,115). No serious medication-related adverse effects have been attributed to the use of PTH (1-34), though nausea, dizziness, local injection site reactions, arthralgia and leg cramps are the most commonly reported adverse effects (43,108). PTH (1-34) is limited for use for high-risk or severe osteoporotic patients largely due to its high cost relative to other antiosteoporosis drugs or for patients with a lack of tolerance to bisphosphonates (62).

1.4.5.8 Non-pharmacological interventions

The effectiveness of pharmacological interventions for osteoporosis to improve bone density and reduce fracture risk are well documented. However, non-pharmacological interventions are also of significant importance as they play an important role in the prevention and management of this disease. Non-pharmacological approaches are focused on the use of exercise for prevention and treatment, implementation of multidisciplinary programs with an emphasis on balance training to minimize the likelihood of falls, nutrition recommendations and rehabilitation programs to assist with the recovery phase following a fragility fracture (116). Nutrition recommendations encourage adequate protein intake (1.2g/kg daily) for preservation of musculoskeletal function in postmenopausal women and man over 50 years of age (117). Recommended calcium intake is 1000-1200mg daily (preferably through nutritional intake) and a vitamin D blood level between 30-50 ng/ml, if supplementation is required a minimum dose of

400 IU is recommended (117). Proper nutrition is essential for the prevention and management of osteoporosis. To reduce the risk of fragility fracture through fall prevention, exercise with weight, balance and resistance load is recommended in order to improve mobility, strength and physical performance (116,117). Exercises should focus on balance and muscle strengthening later in life to reduce fall risk, which may also create more hopeful outcomes after fall incidents. Though exercise later in life may not significantly further increase bone mass, repetitive high-impact and resistive exercise in prepuberty is an important determinant of future peak bone mass and bone strength, while continued exercise in adolescence and adulthood can help maintain these gains (116). Following an osteoporotic induced fractured, early mobilization and a multi-disciplinary rehabilitation program may help in the return to prefracture activity levels.

1.4.6 Pharmacokinetics of Bisphosphonates

As a drug class, bisphosphonates that are taken orally suffer from poor absorption, usually less than 1% on average, with the concomitant intake of food or beverages further limiting absorption (118). Despite newer potent bisphosphonates, oral bioavailability is less than 1% (119). Their low absorption is likely attributed their poor lipophilicity which prevents transcellular transport across epithelial barriers in the stomach, duodenum and ileum (120). Due to their low absorption, they are readily excreted intact from the circulation. Renal excretion is the only route of elimination of bisphosphonates, with renal clearance of bisphosphonates in humans ranging from 0.9 to 1.5 mL/min• kg (120). It is suggested that the excretion of many bisphosphonates by the kidney is concentration dependent, saturable and performed by an active transport mechanism (120). The distribution of BPs within the skeletal system is not homogeneous, with BPs binding more strongly at the sites of active bone turnover than at sites with low bone turnover (121). After a single IV or oral administration, negligible amounts are deposited in non-calcified tissue, with nearly all of the BP binding to the skeleton or being excreted in the urine (121). Pharmacokinetic parameters using plasma concentration and urine excretion data of a 70mg alendronate tablet taken orally has been determined in male volunteers (122). The apparent volume of distribution with a one compartment open model was determined to be 1821.86 ± 471.38 L, urinary excretion was found to be 314 ± 395.43 µg/h and the apparent first-order absorption rate was 2.68 ± 0.95 h^{-1} (122).

1.4.7 Pharmacokinetics of Human Parathyroid Hormone (1-34)

Synthetic human parathyroid hormone (hPTH(1-34)) known as teriparatide has a concentration-time profile which is characterized by rapid absorption and elimination with a monoexponential decline in concentrations (123). Pharmacokinetic parameters of a once-daily subcutaneous administration of teriparatide (20 µg, 40 µg, 80 µg) in large samples of postmenopausal women and in men have been determined (123,124). There are no age-related differences between ages 31 to 85 years and the recommended dose for both genders is 20 µg /day. Maximum drug concentration is achieved within 30 minutes, with rapid elimination (half-life of 1 hr) and a total duration of exposure of approximately 4 hr (123,124). After approximately 4 hr, teriparatide concentrations are non-quantifiable. Absorption was assumed to follow a first-order process and elimination was assumed to occur from the central compartment using a two-compartment model (123). Apparent clearance was determined to be approximately 62 L/hr in women and 94 L/hr in men, which is consistent with both hepatic and extra-hepatic clearance (124). Volume of distribution was 0.12 L/kg with intersubject variability in systemic clearance and volume of distribution is 25 to 50% (124). Absorption rate constant was determined to be 0.63 h^{-1} in postmenopausal women (123). The extensive absorption of teriparatide corresponds to a bioavailability of approximately 95% (124). Peripheral metabolism of teriparatide is believed to be performed by non-specific enzymatic mechanisms in the liver with renal excretion.

1.4.8 Mechanism of Action: Bisphosphonates

Bisphosphonates ability to act only on bone is attributed to their strong affinity to hydroxyapatite. Upon binding to hydroxyapatite, they are deposited underneath osteoclasts. The amount of deposition on bone forming and bone resorption areas depends on the amount of bisphosphonate that is originally administered (125). Large active doses cause resorption and formation surfaces to be approximately equally covered, while small active doses result in the resorption surface being primarily covered (125,126).

At the molecular level, N-BPS and non-N-BPs interact with osteoclasts through two different mechanisms. After binding to bone, non-N-BPs are metabolized to non-hydrolyzable β,γ-methylene analogs of adenosine triphosphate (ATP) in the osteoclast cytosol that inhibit adenine nucleotide translocase in mitochondrial membranes, affecting mitochondrial

permeability (83,127). Subsequently, caspase activation (an irreversible step in apoptotic cell death) is initiated leading to apoptotic cell death of osteoclasts (83,127).

N-BPs function through inhibition of the mevalonate pathway, which is responsible for the biosynthesis of cholesterol and other sterols. The predominant target for N-BPs in the mevalonate pathway is the peroxisomal enzyme, FPPS, which is inhibited by all N-BPs (83). Inhibition of FPPS blocks the synthesis of farnesyl pyrophosphate (FFP), causing a substrate concentration reduction in FPP required for the production of GGPP (83). FPP and GGPP are both required for the prenylation (lipid modification) of GTPases, which are fundamentally important for the proper function and survival of osteoclasts (83,126). Preventing prenylation of GTPases by inhibition of FPPS causes an accumulation of unprenylated GTPases in osteoclasts, resulting in inactivation of osteoclast function (83,126). Inhibition of FPPS by N-BPs also causes increased concentrations of isopentenyl pyrophosphate (IPP), the metabolite upstream of FPPS (83). Accumulation of IPP forms a metabolite known as ApppI, through the condensation of adenosine monophosphate with IPP. In a similar process as non-N-BPs, ApppI induces osteoclast apoptosis through inhibition of the mitochondrial adenine nucleotide translocase (128).

The level of bone resorption suppression depends on the administered dose and there is no progression of the antiresorptive effect with increasing time, indicating a steady state level of resorption that is dose dependent (129). Burdensome stringent daily dosing requirements of some BPs designed to maximize bioavailability while minimizing gastrointestinal irritation to address has led to development of weekly, quarterly or yearly dosing regimens of variable dosage amounts (130). For instance, a 70 mg once-weekly dose of alendronate vs. a 10 mg daily dose has been shown to provide similar therapeutic effects that may enhance compliance and long-term persistence with therapy (131). Despite alendronate showing a positive dose-related trend with improved lumbar spine BMD gains, dosing regimens must be considerate of the increased risk of adverse events that correspond to increased dosing (132). The frequency and dosage amount are dependent on each BPs relative potency. Dose adjustments may be recommended for some patients that have renal impairment and impaired creatine clearance.
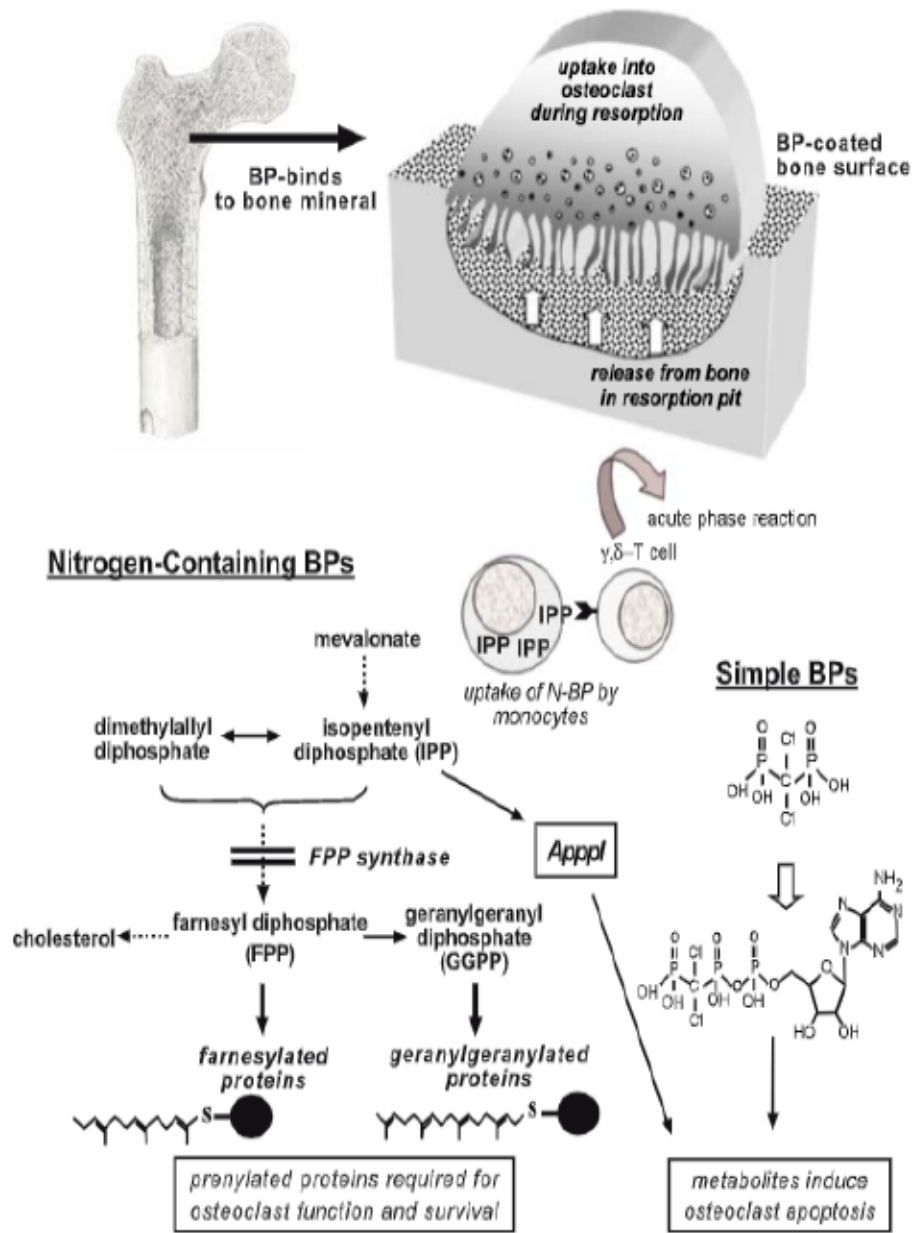
Figure 1.4: Mechanism of action of non-nitrogen bisphosphonates and nitrogen bisphosphonates on osteoclasts. After binding to hydroxyapatite in bone, non-N-BPs cause osteoclast apoptosis through the production of non-hydrolysable ATP analogs causing the activation of caspase. N-BPs disrupt the mevalonate pathway by inhibiting FPPS, leading to accumulation of non-prenylated GTPases that inactivate osteoclasts, or production of IPP that is incorporated into ApppI to promote osteoclast apoptosis. (Reprinted from *Osteoporosis International,* (19):9, Russell RGG, Watts NB, Ebetino FH, Rogers MJ, Mechanisms of action of bisphosphates: similarities and differences and their potential influence on clinical efficacy, Pages 733-59., 2008, with permission from Springer).

1.4.9 Parathyroid Hormone (PTH (1-34)) Mechanism of Action

When administered subcutaneously in intermittent low doses, human PTH (1-34) is able to exert positive effects on BMD and microarchitecture. The N-terminal sequence consisting of amino acids 1-34 have been shown to exert functions identical to the intact hPTH (1-84) hormone, with the first two amino acids (Ser1-Val2) being obligatory for biological activity and bone anabolic properties (106,133). The effects of hPTH (1-34) are mediated through the activation of the PTH/PTH related peptide receptor (PTH1R), which is a member of the B subfamily of G-protein coupled receptors (GPCRs) (133). PTH1R receptors are found in preosteoblasts, osteoblast, lining cells, and osteocytes (134). Activation of PTH1R in osteoblasts triggers the initiation of two parallel signaling pathways as the receptor is coupled to both adenylate cyclase activating G protein-coupled protein (G_s) and the phospholipase C-activating G_q protein (135,136). Activation of G_s leads to the activation of cAMP-dependent protein kinase PK(A), calcium-dependent PKC, and increases intracellular calcium (133,134). The majority of hPTH (1-34)'s anabolic effects on the skeleton can be related to cAMP/protein kinase A activation. The use of *in vivo* studies has concluded that cAMP is responsible for mediating the anabolic response of PTH. Amino-truncated analogs (e.g. hPTH (2-34), hPTH (3-38) or desamino-hPTH (1-34)) failed to produce the full anabolic response of PTH, while non-truncated hPTH (1-34) was able to, indicating that Ser1-Val2 are required for the activation to activate G_s in order to stimulate adenylyl cyclase generating cAMP, leading to full anabolic effects (138,139).

Though the exact molecular mechanisms explaining the anabolic effect of hPTH (1-34) is unknown, it is believed that hPTH (1-34) enhances the activation and number of osteoblasts through four different pathways. The main mechanism is a stimulation in osteoblastogenesis through increases in osteoblast differentiation rather than osteoblast proliferation (134). Additionally, PTH can also promote osteoblast differentiation and osteoblastic lineage commitment from primary calvarial cells, periosteal cells, and bone marrow-derived cells (134). Furthermore, PTH has been shown by *in vivo* and *in vitro* studies to stimulate the expression of genes that signal for bone formation, such as *Osteocalcin, Alkaline Phosphatase, Collagen type I alpha 1 (COL1A1)*, and osteoblast-specific transcription factor *Runx2* (134,140-143).

A second mechanism is PTH's anti-apoptotic actions through phosphorylation and inactivation of *Bad,* which is a pro-apoptotic protein, increasing expression of *Bcl-2* survival

genes, and downregulation of Cell Cycle and Apoptosis Regulatory Protein (CARP-1) (134,143,144). Additionally, treatment of osteoblastic cells with PTH has shown inhibition of the pro-apoptotic effects of etoposide, nutrient deprivation, UV irradiation and a reduction of the negative effects of peroxisome proliferator activator (PPAR)γ receptor (134,137,143). Thirdly, PTH enhances the Wnt-β catenin pathway stimulating bone formation by promoting osteoblast cell lineages by controlling proliferation, differentiation, and maturation (137). Lastly, the activation profile of PTH in bone cells also leads to the synthesis of growth factor genes, IGF-I, IGF-II, transforming growth factor-β and inhibition of growth factor antagonists, like scelrostin (135,137). PTH (1-34) has numerous anabolic effects on bone growth, a better understanding of the exact mechanisms for these effects could lead to improved administration of PTH (1-34) or entirely new treatments for osteoporosis.

A 20 μg /day dose results in a transient increase of serum calcium concentration 2 hours after administration and reaches maximum between 4 and 6 hr. Serum calcium begins to decline approximately 6 hrs after dosing and returns to baseline between 16 and 24 hrs post dose (128). As such, hPTH(1-34) should be taken once-daily, continuous use rather than intermittent use has been shown to lead to increased bone resorption.
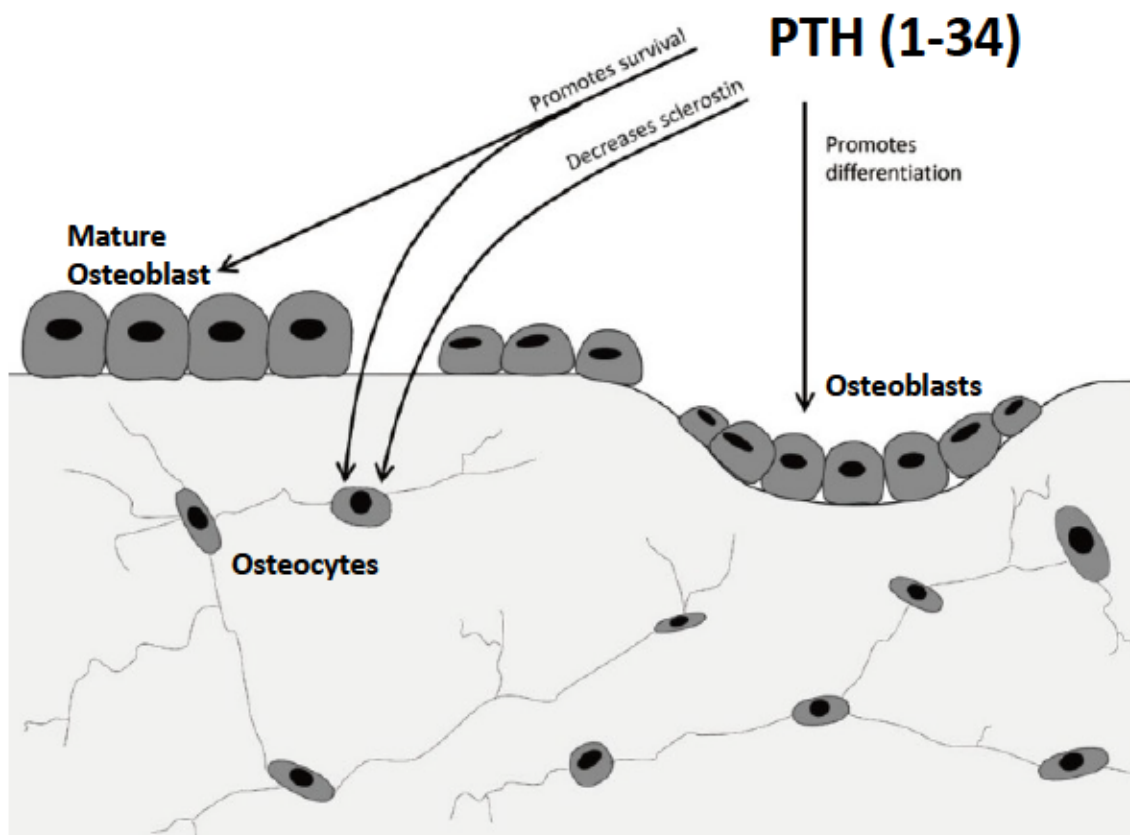
Figure 1.5: Potential mechanisms for the anabolic action of PTH (1-34). Adapted and modified from source 145.

1.4.10 The Need for A Next Generation Therapeutic for Osteoporosis

Though there are currently several classes of compounds being used to treat and prevent OP as mentioned in section 1.4.5 of this thesis, due to patent expirations, companies are moving away from traditional treatment agents (bisphosphonates and SERMs) and moving to new classes of drugs such as scavenging monoclonal antibodies versus PTH and romosozumab as the only approved anabolic agents. The move has largely been made in response to lack of potency and selectivity with systemic calcitonin and hPTH (1-34), adverse events and poor patient compliance with BPs, and patent expiration for calcitonin, BPs and hPTH (1-34). Considering the shortcomings with current treatments for osteoporosis, there is a need to develop improved treatments that are more efficacious, less toxic and more comfortable for patients to use.

1.4.11 The Importance of Targeted Drug Delivery to Treat Bone Disease

Drug delivery strategies offer the benefit of improving delivery of the active pharmaceutical ingredient to the desired site of drug action while minimizing unwanted drug side-effects and lowering systemic exposure. In regards to enhanced drug delivery to bone, the power of targeting drug compounds to remodeling bone surfaces has been known since the mid-1970s when bisphosphonate (BP)-conjugation of radioactive technetium was used as the basis for scintigraphy/diagnostic imaging of bone metabolism (146). Utilizing BP-conjugation as a foundation for enhanced drug delivery of small molecule bone drugs to bone has been explored by several groups to date (81-83). With respect to protein and peptide conjugation strategies, attempts have been less successful due to challenges in controlling the site-directed coupling of bisphosphonate moieties to the polypeptide backbone while continuing to maintain the therapeutic capabilities of the active biologic component (147-149). Our hope is that peptide conjugation to BP moieties would establish a reliable bone-seeking peptide hormone platform, improve bioavailability and usher in a new generation of targeted therapeutics for more effective treatments of bone disease.

1.4.12 A Next Generation Therapeutic for Osteoporosis (BP-PTH)

As mentioned in section 1.4.9, the N-terminal fragment of parathyroid hormone has been proven to clinically stimulate bone formation and improve bone mineral density, bone structure, strength, and quality (150,151). Synthetic PTH (1-34) (teriparatide; FORTEO®, Eli Lilly) is an effective bone-forming (anabolic) FDA approved treatment for osteoporosis that is administered once-daily by a subcutaneous injection. However, due to rapid enzymatic degradation, treatment efficacy of PTH (1-34) is severely restricted by its short *in vivo* half-life of 2-3 minutes in humans when administered intravenously and 1 hr with subcutaneous administration (152). Another negative factor that impacts PTH efficacy is the presence of parathyroid hormone receptors in kidneys (PTHR1), central nervous system, pancreas, testis, and placenta (PTHR2) (47), necessitating relatively high dosages of PTH for clinical efficacy to compete with absorption of PTH by other tissues and organs in the body. Despite never being demonstrated in human clinical trials, there is still significant concern as animal experiments have shown that

prolonged exposure to high dosages of teriparatide resulted in an increased risk of osteosarcoma (112), which limit the duration and efficacy of treatment.

Furthermore, as mentioned in section 1.4.11, previous efforts to conjugate proteins and peptides to BP moieties as a strategy for enhanced drug delivery to remodeling bone surfaces has poised numerous challenges in the synthesis stage. Attaching a BP to PTH serves as a "bone-magnet" which would likely result in the ability to administer lower daily doses, reducing adverse events, toxicity issues and allowing longer duration of treatment.

To address these shortcomings, our laboratory has successfully developed, synthesized and patented a bone targeting variant of parathyroid hormone (1-34) (153) by conjugation to a bisphosphonate (BP) bone-seeking functional group in highly specific reaction conditions and reaction order, known as BP-PTH (Figure 1.8) (154). The goal was to conjugate PTH (1-34) to a bone-seeking non-nitrogenated bisphosphonate (BP) moiety to impart mineral affinity to the attached peptide hormone. Due to the negative charge and structural similarity to naturally occurring inorganic pyrophosphates; BPs are able to localize to positively-charged calcified tissues where they are incorporated into the hydroxyapatite mineral component of bone (154,155). Bisphosphonate-tethered PTH molecules (BP-PTH) by virtue of their affinity to bone, are guided to the surfaces of bone where they interact with their specific receptors on the surface of bone cells. At the cellular level, the anabolic action of PTH on bone cells is effective at stopping bone resorption and promoting new bone formation. Bisphosphonate-targeted delivery of parathyroid hormone to bone will increase its concentration to bone cell receptors at the site of its desired antiresorptive or anabolic actions, relative to its presentation to competing receptors in other organs and cells. BP-PTH offers improved anabolic action at the desired site, reduced off-site side effects, and clearance as harmless amino acids and trace amounts of non-metabolized bisphosphonate residues cleared by the kidneys. Our lab is the first to successfully conjugate and target small peptide hormones to bone surface and prove pharmacodynamic efficacy in two models of bone disease; rat osteoporosis model and inflammatory arthritis.

BP-PTH represents a new class of bone-targeting biologic drug compounds that offers significant potential in the reduction of side-effects experienced with current bone drugs and can further improve the management of bone diseases, such as osteoporosis.

1.4.13 Synthesis and Chemical Structure of BP-PTH

Synthesis was conducted by CPC Scientific Inc. (Sunnyvale, California, USA) using an Fmoc solid phase scheme with lysine-13 N-Boc protection-deprotection was used to construct PTH (1-34) with a bisphosphonate residue tethered via a 27 residue PEG (polyethylene glycol) linkage to Lys-13 (e.g., [BP-PEG27-PTH]. For simplicity sake, the generic "BP" moiety will be referred to as BP. Due to existing patents on treatment approved bisphosphonate drugs, patenting our unique bone-seeking peptide hormone conjugate was only possible if a generic bisphosphonate like moiety was used. The "BP" moiety of the conjugate has the following chemical structure: $C_{14}H_{25}N_2O_9S_2P_2$. This is a generic structure and is not currently an approved BP for the treatment of bone diseases or disorders. No pharmacodynamic or pharmacokinetic information is currently available for this portion of the conjugate. Our hope is that the phosphate groups present in this generic structure will impart mineral affinity.

Identity was confirmed by CPC Scientific Inc. using an AB SCIEX API 4000 LC/MS/MS system equipped with an electrospray (ESI) source used for the mass analysis and detection of PTH (1-34), PTH (1-38) as internal standard, and BP-PTH bone-seeking conjugate. The molecular weight was determined to be 5869.9 Da with a peptide purity of 90.5% determined by reverse-phase high performance liquid chromatography (RP-HPLC). Appearance of BP-PTH is a white lyophilized powder with a solubility of 1mg/ml in water. The conjugate sequence is as follows:

Ser-Val-Ser-Glu-Ile-Gln-Leu-Met-His-Asn-Leu-Gly-Lys (CH$_2$CO-PEG27-2,5-Pyrrolidinedione-3-mercapto-C$_3$H$_6$-SCH$_2$-CH(PO$_3$H$_2$)$_2$)-His-Leu-Asn-Ser-Met-Glu-Arg Val-Glu-Trp-Leu-Arg-Lys-Lys-Leu-Gln-Asp-Val-His-Asn-Phe

A)

Maleimidopropionyl-PEG NHS

R=

B)
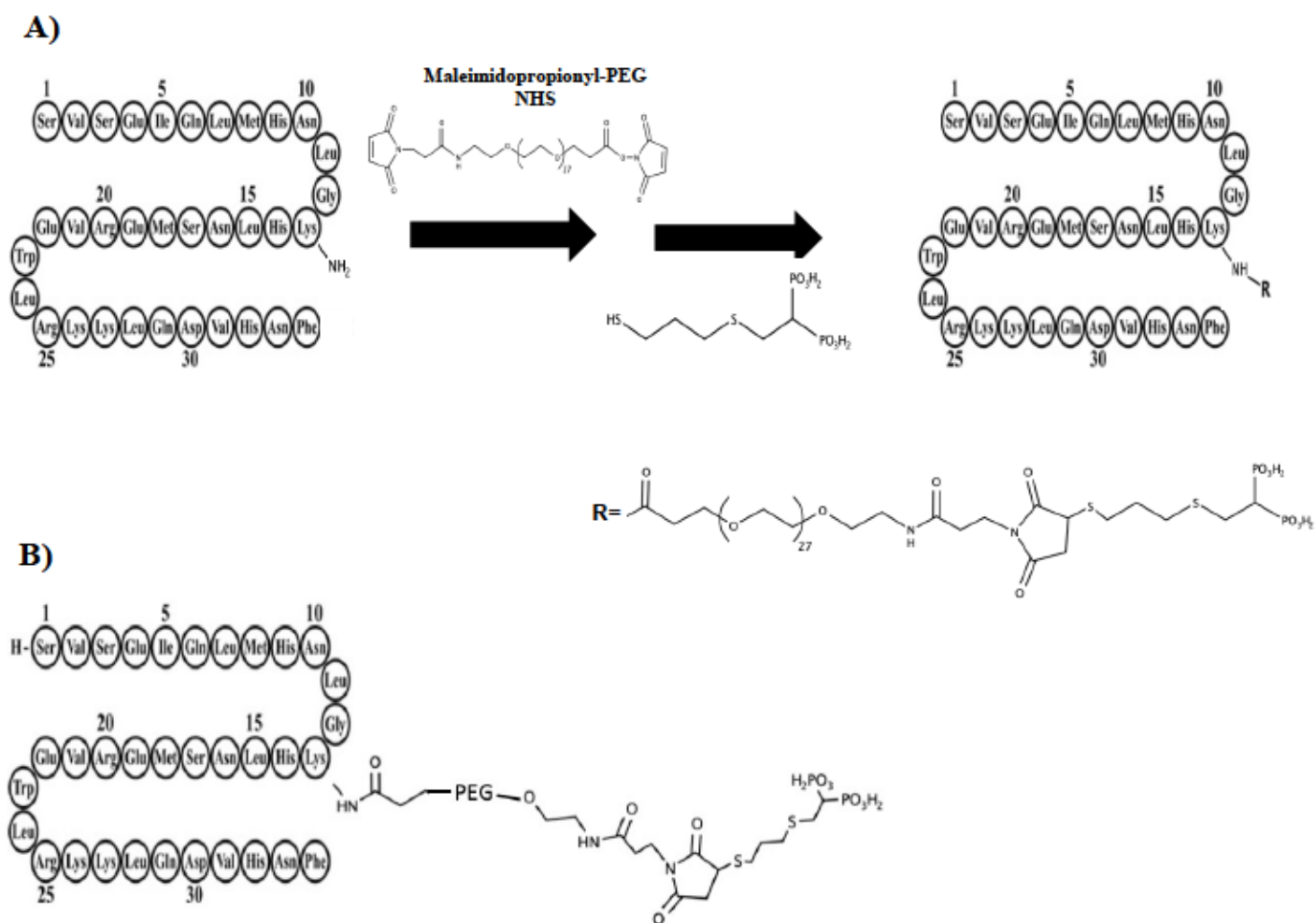
Figure 1.6: Schematic diagram of the synthesis of a novel bone-targeting parathyroid hormone drug conjugate, BP-PTH. A) Fmoc solid phase peptide synthesis with lysine-13 N-Boc protection-deprotection was used to construct PTH (1-34) with a bisphosphonate residue tethered via a 27 residue PEG linkage to Lys-13 (i.e., [BP-PEG27-PTH (1-34)]). B) Chemical structure of BP-PTH.

Chapter Two

Using metal-free LC-MS/MS for the detection of a novel bone targeting
parathyroid hormone conjugate

2.1 Solid-phase Extraction

Solid-phase extraction (SPE) is one of the most common extraction techniques to isolate desired analytes from biological matrixes such as serum or plasma for HPLC or LC-MS/MS analysis (156). SPE can also be used to clean up samples prior to enzyme-linked immunosorbent assays (ELISA). SPE utilizes the chemical and physical properties of the desired analyte to allow for separation of desired analytes or removal of undesired impurities. In addition to sample preparation, SPE can also be used for sample cleanup, analyte concentration, and analyte derivatization. SPE is crucial step in analytical analysis as it allows for cleaner extracts (selectivity), improved sensitivity and reproducibility, less ion suppression, and improved instrument and column lifetimes. Analyte extraction is achieved through the use of a particulate or monolithic sorbent (stationary phase) that is packed in the bottom of plastic columns (often referred to as "cartridges").

Samples containing the analyte of interest are loaded onto the column and the desired analyte(s) of interest or undesired impurities in the sample are retained on the stationary phase. The flow through can then be collected or discarded, depending if it contains the desired analyte or impurities. If the desired analyte(s) is retained on the stationary phase, they can be eluted using appropriate solvents suitable for instrumental analysis. Sorbent selection depends on the SPE strategy that is being employed and the chemical and physical properties of the analyte of interest. Common SPE sorbents can be made from silica-based, alumina-based, polymer-based or graphitized carbon-based materials and can be divided into four main classes; 1) hydrophobic sorbents (reverse phase), 2) hydrophilic sorbents (normal phase), 3) ion-exchange sorbents, and 4) mixed mode sorbents. Certain functional groups are chemically bonded to the silica gel sorbent to impart the desired mode of action. Proper sorbent selection and class of SPE cartridge is determined by the analyte of interest's chemical and physical properties.

Analytes are classified in four major categories: acidic, basic, neutral, and amphoteric compounds. Amphoteric compounds contain both acidic and basic functional groups and can act as anions, cations or zwitterions, depending on the pH environment (157). Therefore, when developing an SPE procedure, the sorbent selected must be able to retain and elute the analyte efficiently. If the analyte of interest is a neutral compound, proper pH environments are needed to shift the analyte between ionic and uncharged state.

Almost all types of SPE procedures regardless of sorbent class consist of 5 basic steps, conditioning, equilibration, sample loading, washing, and elution. Conditioning and equilibrating the column is necessary to wet and settle the sorbent, activate the packing material and remove any residual process materials. Solutions used to condition, equilibrate, wash and elute are determined based off the type of sorbent being used. These solutions will vary in concentration, pH, and polarity depending on the desired extraction protocol. Though SPE is one of the best options available for sample preparation to extract desired analytes from complex matrixes, it does have some drawbacks. SPE is known to be time consuming, costly and may be initially complicated for inexperienced laboratory personnel. Despite these drawbacks, the ability of SPE to provide low matrix factors and reduced matrix interference, clean samples, and concentration of low-level analytes is a substantial benefit for bioanalytical methods.
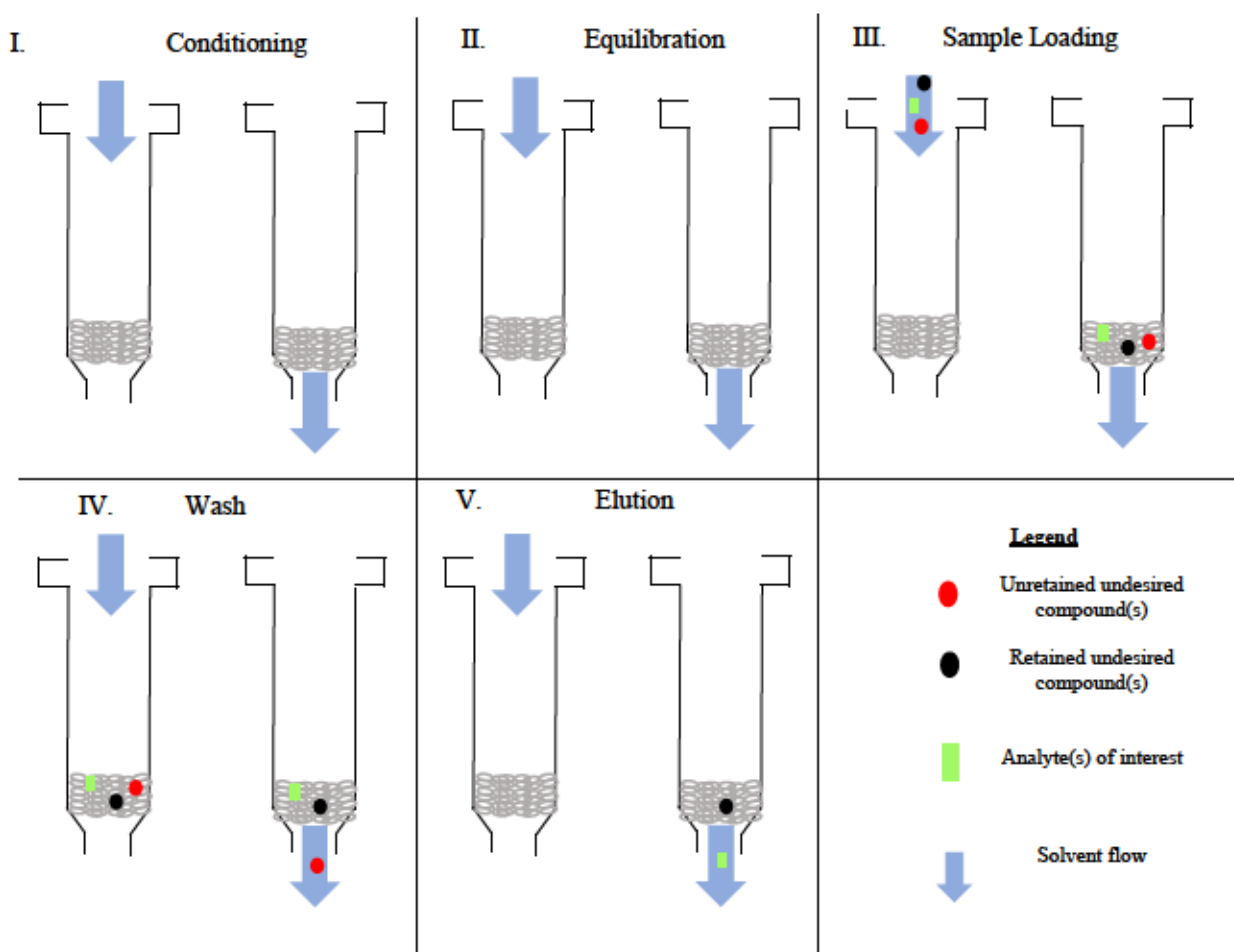
Figure 2.1: Diagram of the 5 basic steps of SPE procedures. Adapted and modified from source 156.

2.1.1 Polymeric reversed phase SPE

Reverse phase polymeric sorbents are designed for the retention of neutral, acidic or basic compounds. The relatively new introduction of polymeric sorbents has improved retention for polar compounds by allowing for a wider pH range of tolerable solvents and buffers that would normally destroy older silica-based sorbents (158). Polymeric sorbents rely on three primary mechanisms of retention: pi-pi bonding, hydrogen bonding, and hydrophobic interaction (158). These sorbents contain a balance between hydrophobic and hydrophilic character, allowing for the retention of acidic, basic, and neutral compounds.

2.1.2 Anion exchange SPE

Anion exchange sorbents are derivatized with positively charged functional groups which allow for the interaction with negatively charged analytes. Strong anion exchangers (SAX) possess a stationary phase with quaternary ammonium group bonded to either silica or polymer and are ionized over the full pH range, showing no variation in ion exchange capacity in various pH conditions. Strong anion exchange columns are often used for retaining compounds that are weakly to moderately negatively charged. Weak anion exchangers (WAX) have primary, secondary, or tertiary amine groups bonded to silica or polymer present in the stationary phase that is only ionized over a limited pH range. At low pH, the functional groups on the stationary phase will be positively charged, while at higher pH it will be neutral. Anion exchange is suitable for isolating acidic compounds; carboxylic acids, sulphonic acids, and phosphates.

Due to the bisphosphonate moiety present on the BP-PTH conjugate, the multiple ionic character from the phosphonate groups on the BP moiety make anion exchange SPE a suitable preparation technique. WAX columns were chosen over SAX for the extraction of BP-PTH as the low pKa of the bisphosphonate moiety indicates a strongly acidic compound. Additional benefits of using a WAX column allows for the combination of sample purification and derivatization into one single step.

2.2 High Performance Liquid Chromatography (HPLC)

High performance liquid chromatography (HPLC) is a sophisticated extension of liquid chromatography (LC) that is used to separate, identify and even quantify components present in a sample mixture. The main difference between HPLC and traditional LC is that in LC, the solvent travels through the use of gravity, while in HPLC the solvent travels under high pressure

which is generated by pumps in the chromatographic system. In this thesis, the abbreviations of LC, HPLC and UHPLC will be used interchangeably. HPLC is a common analytical tool for pharmaceutical analysis and is used extensively in the pharmaceutical industry at many steps of the drug manufacturing process. The objectives of using HPLC will depend on the stage of drug development and the nature of the analyte. Ultimately, it is the chemical interaction between the components present in the sample, the mobile phases used and the column stationary phase that determines the analyte of interest's migration rate and separation through the LC column.
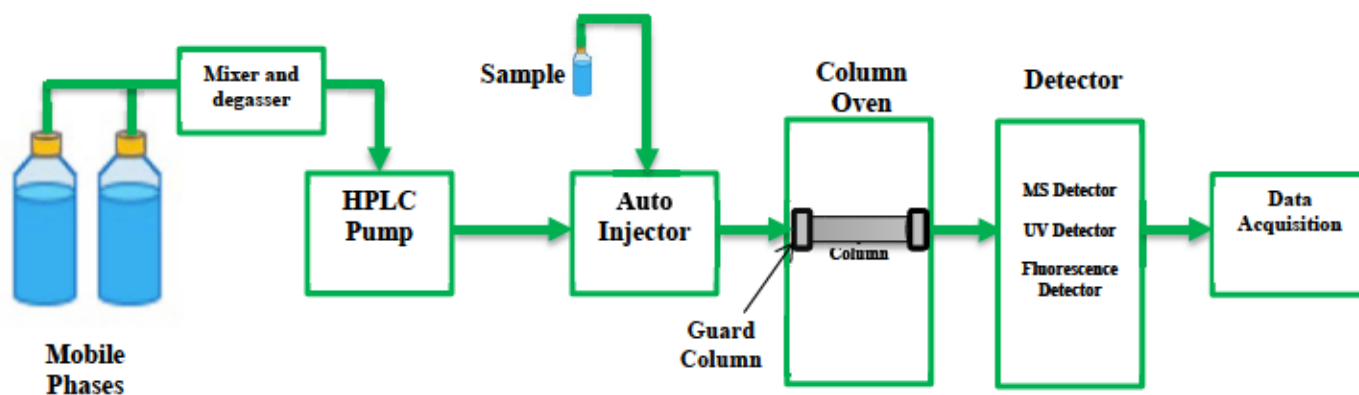
Figure 2.2: Schematic diagram of a traditional HPLC system set-up.

2.2.1 Stationary phase

HPLC utilizes a combination between a stationary phase (known as a column) and mobile phases that allows for the separation of components in a sample mixture. HPLC columns are defined by a few main parameters; column internal diameter (mm), length (mm), pore size (Å), particle size (μm) and their mode of separation (also referred to as phase). The mode of separation of phase is selected based on the chemical characteristics of the analyte of interest or the intended objective of separation. Reverse phase HPLC (RP-HPLC) is the most commonly used liquid chromatography method and utilizes a polar mobile phase and a non-polar stationary phase. Mixture components that are less polar will interact more extensively with the non-polar stationary phase and be retained longer on the column than analytes which are polar. Silica is the most common packing material used in HPLC columns as it is physically robust and chemically stable over a wide range of pH (159). Alkyl chains of either C_4, C_8, C_{18} or any hydrocarbon are covalently bonded to the stationary silica phase, creating the hydrophobic phase that has high

affinity for hydrophobic compounds. Often a metal guard column containing a filter will be attached below the column when running samples from complex mixtures such as serum or plasma in order to remove particulate matter, which may interfere with analysis or contaminate the column.

2.2.2 Mobile phase(s)

The mobile phase(s) flow throughout the entire HPLC system and carry the injected sample. Mobile phases are the second most important parameter (besides column selection) for chromatographic analysis as they have a large effect on analyte retention time (tR). Mobile phases need to be able to interact with the stationary phase and the analytes in the sample. Therefore, it is important that the mobile phases selected are compatible with the HPLC instrument, able to dissolve the analyte and provide the proper pH and ionisation of the analyte (if applicable). Mobile phase optimization is a vital component of proper HPLC method validation. For RP-HPLC, the most common mobile phases are acetonitrile (ACN), methanol and water. Often, a blend of two of these three mobile phases will be used in RP-HPLC. The proportions of the "blend" will alter the polarity of the mobile phase and have effects on the retention time of the analyte of interest. In highly optimized HPLC methods, the blend of mobile phases will be able to separate the range of compounds in the sample mixture and elute them all within a reasonable amount of time (159). Weak acids such as acetic or formic acid are often added in small percentages (i.e. 0.1%) to the mobile phase to increase conductivity and aid in protonation of the analyte. Increased protonation is useful for MS implications as it can increase the sensitivity when operating in electrospray ionisation positive mode (ESI+). However, if the addition of added electrolytes is too high, suppression of analyte signals may result. Since the addition of electrolytes may affect the conductivity and protonation/deprotonation of an analyte, it can also change how the analyte interacts with the column, which may lead to changes in retention times.

2.2.3 Separation of highly polar compounds using HPLC

The separation of polar compounds is usually accomplished using ion-exchange liquid chromatography using ion-exchangers or reversed-phase (RP) liquid chromatography with a silica or polymer stationary phase (160). Conventional HPLC columns often do not provide adequate retention or separation of highly polar compounds. Though separation of highly polar compounds using liquid chromatography is possible, it is not without difficulties. Ion-pairing strategies are useful for obtaining satisfactory retention of mixtures of acids, bases and neutral compounds. Retention is controlled by adjustments in percentage of mobile phases, ion-pairing reagent concentrations, temperature, column stationary phase, sample pH, among other variables (161). Developing a successful ion-pairing technique is complex, time-consuming with potential for many problems, but when done correctly is an effective tool for improving the retention of highly charged polar molecules. Due to the complexity of ion-pairing and potential incompatibilities of ion-exchangers with mass spectrometry (MS), reversed-phase separation is often the best starting point to develop a method for the separation of highly polar compounds (162). RP separation offers a more simplistic approach, lower potential for problems, easier troubleshooting and better column performance. In order to retain the most polar compounds and prevent them from eluting with the solvent front (t_0), various parameters can be explored to increase retention of polar compounds. Low pH conditions suppress ionization of acids, making them neutral and more likely to be retained in a RP column (161). Addition of 0.1% trifluoroacetic acid (TFA) or 0.1% formic acid in both organic and water mobile phases may improve retention of acidic compounds (161). Phosphate buffer (~10-25mM) adjusted to pH 2.5 is an additional alternative to TFA or formic acid, but is not MS compatible. Retainment of basic compounds generally require a mobile phase with pH greater than 8. Mobile phases with pH greater than 8 are not recommended for silica-based RP column use as the silica backbone is soluble at high pH levels (161). In terms of RP columns, using the most non-polar column available can allow for maximum retention of polar analytes. Silica-based C_{18} bonded phases are more non-polar than silica-based C_8 or C_4 columns and should be selected over a C_8 or C_4 bonded phase (161). If the analyte of interest is eluting at t_0 with an organic solvent concentration of 5%, reducing the organic solvent concentration to 2-3% may allow for reliable separations (161). Caution needs to be used when using organic phase percentages lower than 5% as the bonded phase in the column may collapse in the 97-98% aqueous region (162). If using less than

2% organic solvent in the mobile phase is desirable, a column designed for this purpose should be selected.

2.2.4 Separation challenges with bisphosphonates and bisphosphonate-conjugated compounds

The phosphonate groups present in bisphosphonate and bisphosphonate-conjugated compounds are a large hurdle for analytical detection. The following are the major difficulties encountered with BPs and BP-conjugated compounds: 1) the phosphonate groups are highly polar and strongly ionic, therefore it is difficult to retain on non-polar stationary phases such as a C_{18} or C_8 column; 2) BPs have several pK_a values that span the entire pH range, resulting in difficulties maintaining a single species in solution for consistent separation; 3) phosphonate groups have metal chelating abilities, resulting in chromatographic peak tailing and sample carryover (163-165). Ultimately, retention of BPs and BP-conjugated compounds is poor and inconsistent using regular reverse-phase chromatography. Separation gets even more complicated when simultaneous detection of different BPs is required as the chemical structure of BPs are similar, differing only in the variable R_1 chain (164). In general, non-derivatized bisphosphonates have been regarded as either being inconsistent or unsuitable for analysis using conventional HPLC or LC-MS/MS methods (166). Despite the many analytical and chromatographic challenges that BPs and BP-conjugated compounds pose, some direct detection and indirect detection methods have been successfully employed for detection (164). The vast majority of indirect methods for BP detection have involved derivatization or metal-free HPLC, while direct detection methods do not.

Direct detection methods have predominantly utilized ion-exchange chromatography (IEC) using an anion-exchange column for separation and either conductive detection (167), refractive index detection (168), electrochemical detection (169), or mass spectrometry (164,166). Ion-pair RP-HPLC methods have also been reported for direct detection of chromophore containing BPs including, zoledronic acid (170,171) and tiludronate (172,173), though detection of non-chromophore containing compounds has been much less successful (164). Replacing metal hardware (e.g. sample needle, injection valves, column and tubing) with metal free alternatives in LC-MS/MS systems has been reported to address issues with chromatographic peak tailing and reduce carryover when analyzing BPs (166).

Indirect methods for the separation and determination of BPs and BP-conjugated compounds are based on derivatization. Of the various derivatization methods, they all aim to address at least one troublesome aspect that phosphonic acids pose for traditional detection methods. Derivatization has been used to increase volatility, introduce a chromophore into a BP, or prevent their metal chelating abilities. Numerous methods utilizing gas chromatography (GC) and RP-HPLC for separation and detection using fluorescence or mass spectrometry for derivatized BPs and BP-conjugates have been successfully reported to date (164,165,174,175-181). Isobutylchloroformate and BSTFA have been used as derivatizing agents to increase compound volatility, allowing for the determination of clodronate (180), etidronate (181), and pamidronate (182) using GC. Introduction of fluorogenic labels coupled to the amino groups on several BPs has allowed for fluorescence detection and separation using RP-HPLC to the nanogram level (164,175-177,179,183). Perhaps the most common method for the determination of BPs and BP-conjugated compounds has been the use of the derivatizing agent trimethylsilydiazomethane (TMSD). When used safely, TMSD is able to efficiently methylate the phosphonate groups, effectively neutralizing them and preventing them from binding to metal hardware components during LC separation and improve their sensitivity in mass spectrometry. Numerous groups have reported successful derivatization and detection down to low picogram concentrations for several BP compounds (166, 166, 174, 177,178). To our knowledge, no group has reported the successful derivatization, separation and detection of any peptide-conjugated bisphosphonate compound.

Difficult phosphonic acid groups in BP containing compounds has caused researchers to come up with creative and novel solutions to allow for the determination of these compounds. The use of indirect detection methods has been more widely reported than direct methods for the detection of BPs and BP-conjugated compounds (164). Furthermore, indirect methods have been successfully applied to a larger range of BP compounds while achieving lower limits of detection and greater sensitivity than direct methods have been able to produce.

2.3 Liquid Chromatography Tandem Mass Spectrometry

LC-MS/MS is an analytical chemistry technique that combines the physical separation of analytes using liquid chromatography (HPLC or UHPLC) with mass analysis from tandem mass

spectrometry detectors for the quantitation or identification of analytes. In short, liquid chromatography is able to separate mixtures with multiple components and allowing the analyte of interest to flow to the mass spectrometry portion which is able to provide mass identity of the individual components in the analyte mixture with high specificity and sensitivity. LC-MS/MS is popular and powerful instrument for chemical analysis as the combination of the capabilities between LC and MS are enhanced synergistically. Tandem mass spectrometry (MS/MS) further increases the sensitivity of mass analysis by attaching an additional mass spectrometer into the flow path. Mass spectrometry creates ions which are to be detected. Compounds are separated by molecular weight of the first mass spectrometer and undergo fragmentation due to collision with gas molecules. These fragments exit into the second mass spectrometer and are identified based on their fragmentation patterns. Coupling HPLC or UHPLC to an MS/MS creates a versatile, high-throughput and rapid analytical instrument capable of identifying or quantifying most organic compounds, ranging from small metabolites, pharmaceutical formulations to large proteins and protein complexes. LC-MS/MS is suitable for analysis of compounds with various polarities, small or large molecules, ionic, thermally labile and involatile compounds (184).

2.3.1 Analysis using LC-MS/MS

As mentioned previously, the LC-MS/MS instrument is the combination of a LC instrument (either HPLC or UHPLC) coupled to a tandem mass spectrometer. Analysis using LC-MS/MS begins with the LC component. Samples containing the analyte of interest will be loaded into a sample tray where an autosampler will withdraw the specified volume of sample and push the sample into the sample loop. The mobile phases used for chromatographic separation in the system push the sample through the sample loop from the injection port into the column oven. An analytical column is placed in the column oven, which is where chromatographic separation of the analyte of interest occurs. Depending on run conditions, the column oven can be used to maintain a desired consistent temperature for the duration of the analytical run. After elution from the analytical column, the eluent is diverted to the mass spectrometer (MS) ionisation source where the eluent is then nebulized, desolvated and ionized to create charged particles for detection in the MS (185).

2.3.2 Components of a tandem mass spectrometry system

A tandem mass spectrometry (MS/MS or MS^2) system is the coupling of two mass analyzers together for enhanced sensitivity and selectivity. An MS/MS system is composed of three major components; an ion source, mass analyzer and a detector. The work described in this thesis uses an ESI+ ion source and a quadrupole mass analyzer detector. Other components of a MS/MS system include a vacuum system, nitrogen gas flow generator, and a computer system with software capable of MS/MS data analysis. When ions are created in the ion source, they may collide with residual gas (air, water, nitrogen) and as such they may be removed before having the opportunity to reach the detector (186). A vacuum system reduces the likelihood of these collisions and ensures that ions can reach the detector. A rotatory pump and turbomolecular pump are responsible for creating the vacuum space. The turbomolecular pump rotates with high speed (e.g. 60,000 rpm) to hit gas molecules down and remove gas from the vacuum chamber (186). A nitrogen gas flow generator in ESI applications is used to generate nitrogen gas on site to create the nebulizer gas that flows from outside the capillary to spray the sample to create a fine mist of charged droplets that aids in solvent separation from the ionized sample (185).

2.3.3 Electrospray ionisation (ESI)

Electrospray ionisation (ESI) is a soft ionisation technique that is able to transition the analyte of interest into the gas phase without fragmentation (voltage changes can allow for fragmentation, if desired) (185). Rather than compounds undergoing fragmentation into smaller charged particles, intact compounds are instead ionized into small droplets. ESI is a desorptive ionisation technique, meaning it can be performed on solid or liquid samples that are non-volatile or thermally unstable. Further advantages include the ability to analyze intact non-covalent complexes (e.g. ligand and protein binding) and the production of multiply-charged ions for large analyte molecules, enabling analysis of large proteins or complexes (185). Due to these advantages, ESI is typically used for the analysis of peptides, proteins, protein complexes and other biological macromolecules.

The transfer of compounds from solution into the gas phase occurs in three major processes: 1) production of charged droplets from electrolyte dissolved in solvent, 2) shrinkage of charged droplets by solvent evaporation and then fission of the droplets and 3) desorption of gaseous ions (186-188). A continuous stream of sample from the analytical column is passed through a stainless steel fine capillary tube, which has an applied positive voltage of 2.5-6.0 kV

(187). The high electrostatic force in the capillary tube leads to charge separation in the solution. In positive-ion mode, the cations in solution migrate towards the counter-electrode while the anions in the solution migrate away from the counter-electrode towards the capillary tip (189). Migration of the cations towards the counter-electrode is countered by the surface tension of the liquid and the meniscus forms into a cone (known as a Taylor cone) at the capillary tip (185,188). A fine stream of highly charged fine droplets form with the same polarity as which the capillary voltage is generated and is ejected from the tip and accelerated towards the counter electrode (185,186,191). The applied potential, solvent flow rate, solvent characteristics and capillary diameter are all factors which influence the size of the droplets formed (186). In positive ion mode each droplet contains a large excess of positive charge and in negative ion mode the droplets contain an excess of negative charge. The charged droplets traverse down a pressure gradient toward the analyser region of the mass spectrometer where the droplets shrink in diameter by droplet desolvation, which is aided by the high ESI-source temperature and nitrogen drying gas (185,188,189). Droplet fission ("Coulomb explosion") occurs when the charge repulsion exceeds the surface tension holding the droplet together, this instability limit is known as the "Rayleigh limit" (185,188). Continued solvent evaporation and fission occurs resulting in continuous depletion of droplet size and are known as second-generation droplets (185,187,188). These droplets may result in a final formation of containing a singular ion and being only 10 to 20nm in size.
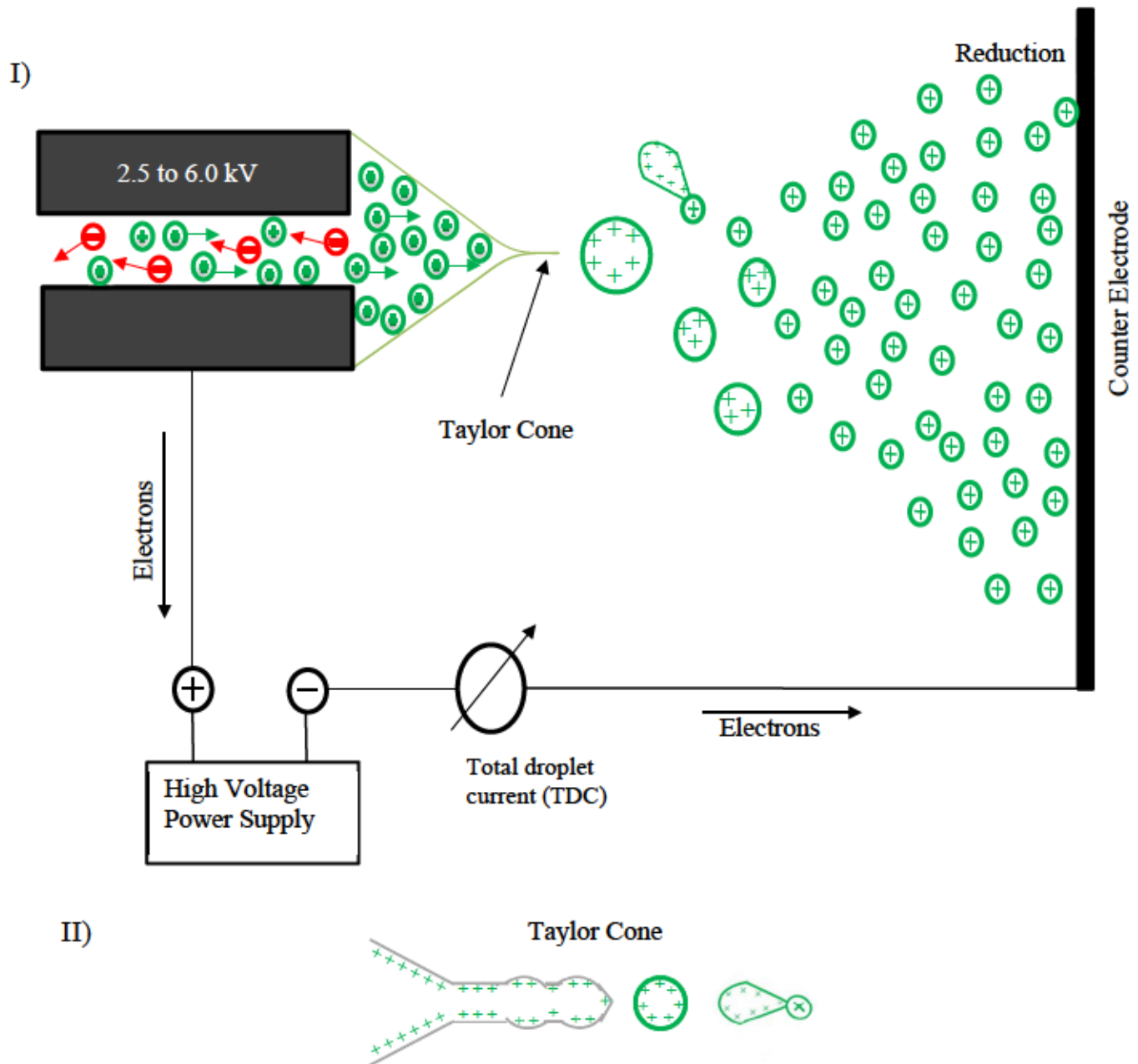
Figure 2.3: Depiction of the ESI interface
A) Diagram of electrochemical processes and Taylor cone formation in the ESI source of an MS instrument. In positive-ion mode, oxidation occurs at the metal capillary while reduction occurs at the counter electrode. At the electrospray needle, there is an accumulation of positive ions that will expand into the Taylor cone when electric field strength overcomes the solvent surface tension to form droplets. The droplets shrink through solvent evaporation and fission to form gaseous ions. B) Diagram of a Taylor cone. Adapted and modified from source 189.

There are two mechanisms of gas-phase ion production that attempt to explain ion production from the droplets: the charge-residue model (CRM) and the ion-evaporation model (IEM) (185,190). The IEM postulates that ions are desorbed directly to the gas phase from the very small (10 to 20nm) droplets. In order for an ion to undergo expulsion, the electric field strength (E) needs to exceed the solvation energy (ΔG_{sol}) of the compound but remain less than the Rayleigh limit (185,189). Analyte ions are able to overcome the solvation energy more efficiently than neutral compounds, increasing their ability to become an ion in the gas phase. The IEM method works well to explain ion production for compounds up to ~3500 MW (185). The CRM postulates that droplet fission and solvent evaporation is repeated numerous times, until the droplet decreases to a size so small (~1 nm radius) that it contains only one solute molecule with a singular charged ion (185). Upon total evaporation of solvent, the molecule is a bare gas-phase ion and is released into the ambient gas while retaining the charge (189). CRM is used to explain the ionisation of proteins with a MW > 3500 as large molecules have a large solvation energy (ΔG_{sol}) that exceeds the electric field strength (E). Due to the inability for the electric field to exceed solvation energy, IEM would predict that no protein ion should be observed. CRM states that large molecules are able to be ionized as continuous droplet shrinkage forms a salt cluster and an ion signal is generated for large molecules by utilizing the front-end voltage of the MS to knock off residual anions from the salt cluster (185).
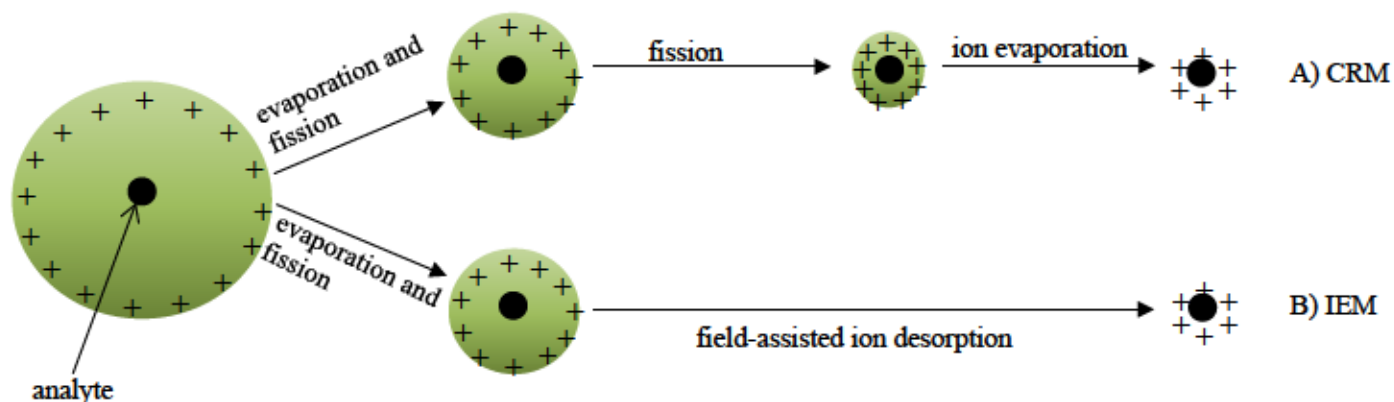
Figure 2.4: Overview of the IEM and CRM models that explain the desorption of ions from charged droplets into the gas phase. A) charge-residue model; b) ion-desorption model. Adapted and modified from source 188.

As stated in the previous section, IEM can explain the ionization of peptides up to ~3500 MW, while the CRM model explains the ionization of peptides and proteins with an MW > 3500. Furthermore, it is believed that the IEM model applies to ions with significant surface activity (i.e. hydrophobic molecules) and the CRM model applies to hydrophilic species (190). This is largely explained by the solvation energy of hydrophilic species being larger than the solvation energy of hydrophobic species (ΔG_{sol} hydrophilic > ΔG_{sol} hydrophobic). Proteins in solution are highly charged with the number of charges per protein molecule increasing with increased MW. The number of charges on a protein molecule is roughly equal to the number of charges on a droplet at the Rayleigh limit (185). At the Rayleigh limit, Coulombic explosion results when the surface tension of the droplet is exceeded and the droplet explodes. A protein cannot explode as it is a single entity, rather the protein can only change conformation in solution to accommodate more charges (185). However, the maximum number of charges cannot be greater than the Rayleigh limit, therefore the ion evaporation model cannot explain the generation of protein ions in ESI (185).

In MS analysis, the ion m/z will not be the same as the theoretical molar mass of the analyte. This is because as analytes become charged they can gain or lose protons slightly changing their mass (m) by +/- 1 (for a singly charged analyte). One of the major advantages of ESI mode is that it can produce multiply-charged ions for large molecules (z > 1), enabling the analysis of large proteins or complexes. Multiply charged species will have different charge states (z) corresponding to their charged state (i.e. z=1,2,3,4, etc.). The number of protons gained corresponds to the number of charges acquired on the analyte.

2.3.5 Mobile phase considerations for mass spectrometry applications

If an MS experiment is to be conducted, there are special considerations that must be considered when selecting and optimizing mobile phases to achieve sensitive MS detection of analytes. For ESI applications, the solvent should support ions in solution. Solvents with increasing levels of viscosity and less volatile and will reduce sensitivity (191). Solvent modifiers (i.e. solvent additives to alter pH) with increasing organic percentage gives better sensitivity due to decreased surface tension and lower solvation energies for polar analytes (191).

Commonly used RP solvents are suitable for ESI applications (e.g. water, acetonitrile and methanol), however some common solvent modifiers used in RP chromatography are not compatible for MS application (185). All solvent modifiers must be volatile and not form ion pairs. Compatible salts and acids include ammonium acetate, ammonium formate and acetic acid and formic acid, respectively (185). Incompatible solvent modifiers include sodium salts, potassium salts, trifluoroacetic acid (TFA), and trichloroacetic acid (TCA) (185). These solvent modifiers have been shown to either be involatile, produce strong ion pairing compounds that contaminate the interface, suppress ionization, or a combination of these issues. Transitioning an HPLC method for MS applications may pose challenges, as many peptide/protein separation HPLC methods require the use of TFA or TCA to improve peak shape, though these additives result in ion-pairing causing ionisation suppression in ESI (low to no signal in MS). Ionisation suppression results due to additives inhibiting the charged separation step during droplet shrinkage and fission through ion-pairing, causing ions to become neutral and reside in the droplet bulk, rather than on the surface of the droplet (185). A larger percentage of ion-paired neutral compounds in the droplet bulk rather than at the surface results in a lower likelihood of forming an ionized offspring droplet. Transitioning from a TFA additive to a MS compatible additive like formic acid may reduce the retention of some peptides but formic acid has become the standard for MS peptide applications as it is still able to provide a low pH to promote analyte ionization and offers significantly enhanced MS signal over TFA (167,185).

2.3.6 Quadrupole mass analyzers in a tandem mass spectrometer system

In order to obtain structural, mass, and/or quantification information, the precursor ion of interest is accelerated out of the ion source and into a vacuum where they can be selected on the basis of their mass using a mass analyzer and fragmented in the collision cell (187). A second mass analyzer is then used to analyze the fragments leaving the collision cell. These fragment ions are what is used to obtain structural, mass and/or quantification information from the original sample. The combination of two or more analyzers in sequence is responsible for the high levels of selectivity and resolution in a MS/MS experiment. Analyzers are able to distinguish and separate ions based off their movement through a magnetic or electrical field which is largely determined by their mass-to-charge ratio (m/z ratio). A quadrupole mass analyzer (Figure 2.5) is the most commonly used analyzer in a clinical laboratory setting (184).

A quadrupole analyzer is composed of an assembly of four parallel metal rods assembled in two pairs at an equal distance apart (184,192). The first two rods are subjected to the same applied voltage, which is different from that of the second pair of rods establishing a two-dimensional quadrupole field in the x-y plane (187,192). The resulting electrical field is dependent upon the radio frequency (RF) and the direct current (DC) voltage which are applied to the four rods (192). The RF potential changes in a cyclical manner from positive to negative (188). The electric field causes ions to travel forward in the z direction with oscillatory motion in the x-y plane as ions are attracted by one set of rods and repulsed by the second set (187,192). Changes to the DC and RF voltages can result in stable trajectories that select for desirable m/z ratios that travel along the z-axis to reach the detector while undesirable ions with unstable trajectories will collide with the quadruple rods, become neutralized and fail to reach the detector (187,188,192). Positive rods act as a high-pass filter for heavier ions while the negative rods act as a low-pass filter for lighter ions (Figure 2.6) (188). Ions with a particular m/z ratio that do not collide with the quadruple rods will travel the whole analyzer length and move on to the next steps which can be detection, fragmentation and entry into a second mass analyzer.
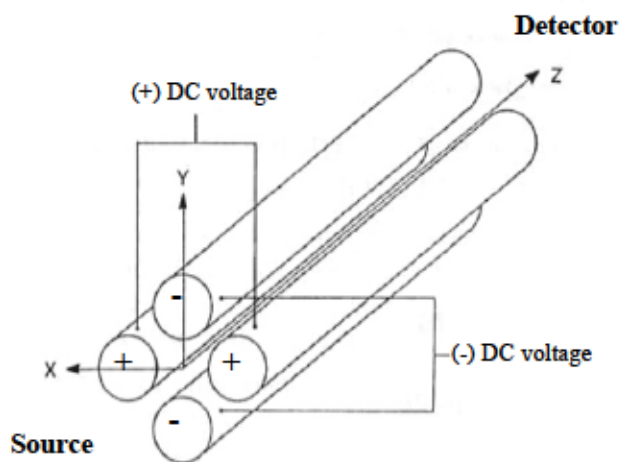
Figure 2.5: Depiction of a quadrupole mass analyser. Ions travel from the source through the two pairs of metal rods in an oscillating trajectory in the *z-axis* towards the detector. Modified from source 185.
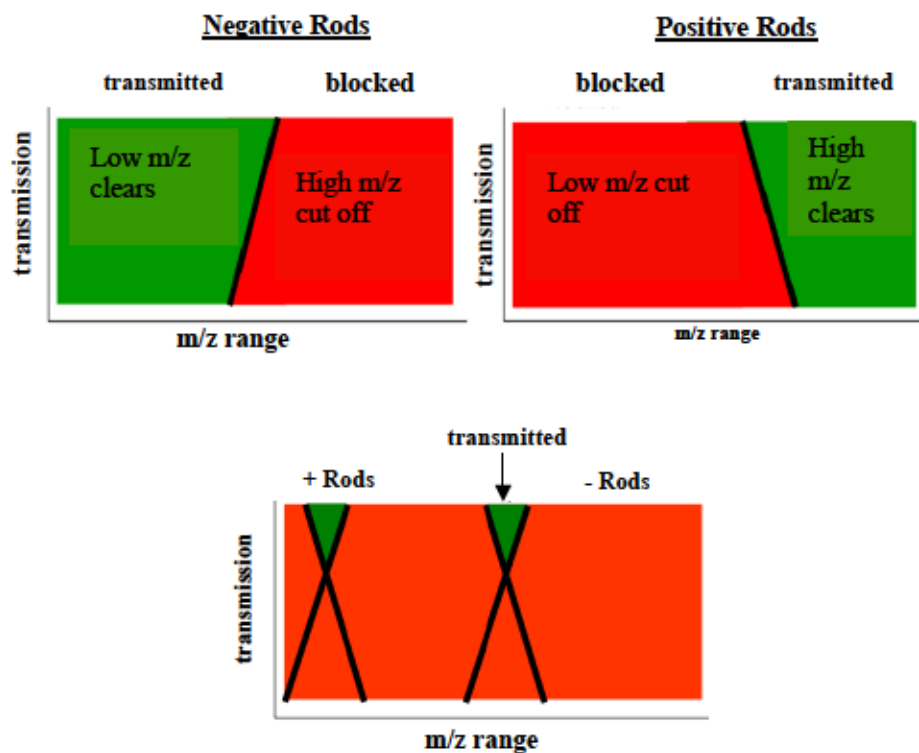
Figure 2.6: Diagram showing how positive rods act as a "high-pass filter" (high masses pass through) and negative rods act as a "low-pass filter" (low masses pass through). Together, the quadrupole is able to act as a mass filter and select for only ions with a desirable m/z ratio. Adapted and modified from source 185.
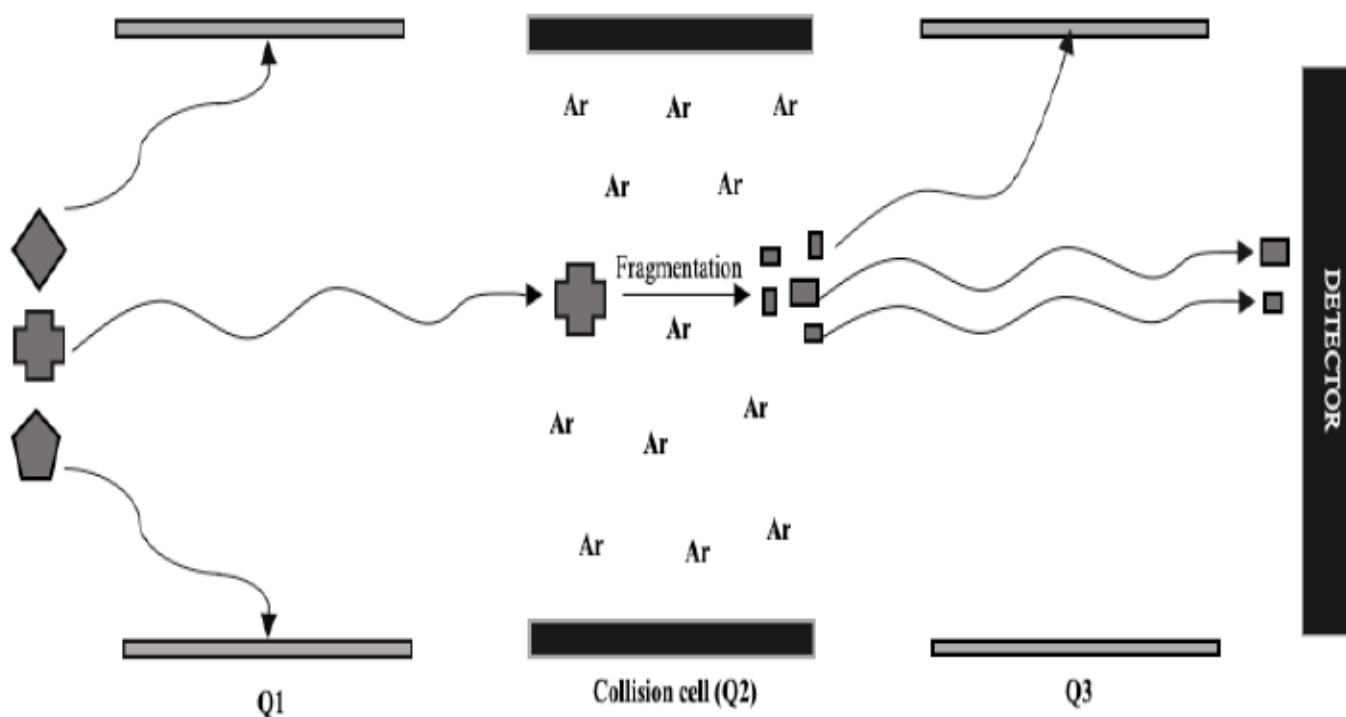
Figure 2.7: Multiple reaction monitoring. In the first quadrupole (Q1), the analyte of interested is selected based off the mass-to-charge ratio and will pass into the collision cell (Q2), while other compounds of differing mass-to-charge ratio will collide with the rods in Q1. In the collision cell, the analyte will collide with an inert gas (e.g. argon or nitrogen) and cause fragmentation. The fragments are then further selected in the third quadrupole (Q3), with the selected mass to charge fragments reaching the detector. Adapted and modified from source 193.

A tandem quadrupole system (known as MS/MS or a "triple quad") contains three quadrupoles set up in a linear arrangement (Figure 2.8). In a triple-quad, only the first and third quadrupoles are mass-selective (194). In a tandem experiment, the analyte of interest (known as the precursor ion) from the ion source is mass-selected in the first quadrupole (Q1 or MS1) and collides with an inert gas (commonly argon or helium) in the second quadrupole collision cell

(Q2). The collision cell is where the precursor ions that passed through Q1 are fragmented by the gas, this process is referred to as collision-induced dissociation (CID) (188). There is no DC voltage in Q2 applied, only RF potential, therefore ions of all m/z values are transmitted (181). Once fragmentation has occurred in Q2, the newly formed fragmented daughter ions from CID are passed into the third and final quadrupole mass analyzer (Q3 or MS2), to provide structural and quantification information (188). The power of the tandem MS/MS system is that when Q1 is set to filter for only one m/z ratio, it filters out all other ions with different m/z ratios. This is effectively a purification step using the MS system which increases system sensitivity, resolution and avoids having to do additional time-consuming and complex sample purification before MS analysis (188).
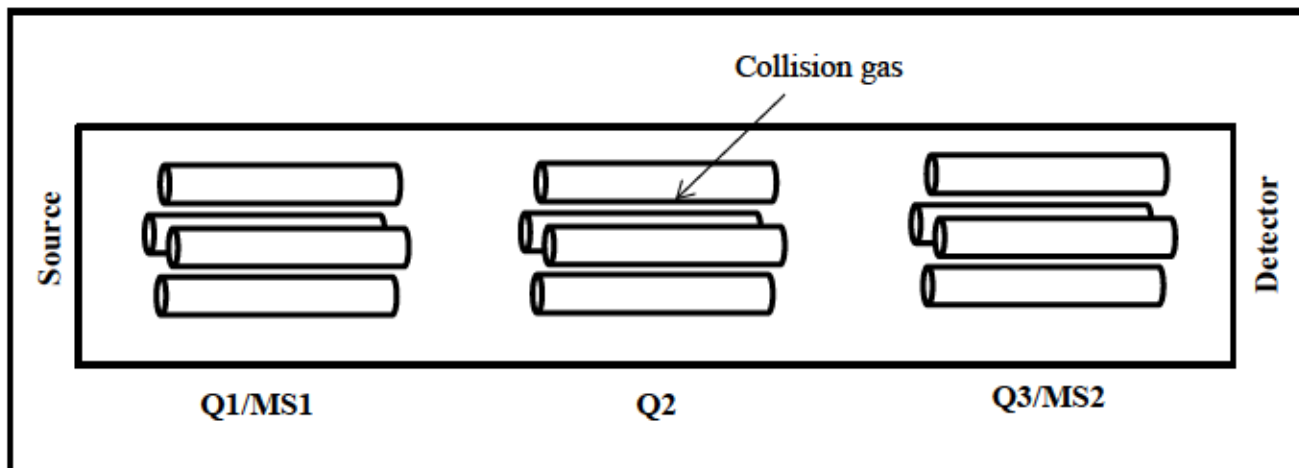
Figure 2.8: Diagram of a triple quadrupole system (MS/MS). Q1 and Q3 are mass analyzers also referred to as MS1 and MS2, respectively. Q2 is the collision cell. Adapted and modified from source 187.

2.3.7 Data Acquisition Modes in Tandem Quadrupole Systems

Tandem quadrupole systems offer a range of modes for data acquisitions, they are described below and summarized in Table 2.1:

Q1 Scan: The first quadrupole scans continuously though a specified m/z ratio range. All ions falling into this range will pass through Q1 and into the detector. A Q1 scan is useful to determine components within a mixture or identifying potential precursor ions for selection for CID and detection in Q3. There is no CID fragmentation in a Q1 scan.

Precursor-ion scan (parent scan): Q1 will scan continuously over a set range of m/z ratios to show potential precursor ions. Q3 is static and will analyze the unique product ions resulting from CID fragmentation. The difference between a precursor scan and a Q1 scan is that fragmentation of ions occurs. Only precursor ions that generate the product ions of interest will appear in the resulting mass spectrum. This is a useful scan mode when attempting to identify compounds with similar polarities and structures (188).

Product-ion scan (daughter scan): Q1 is static allowing for only ions that have been chosen by the MS operator with a specific m/z ratio to pass through Q2 and into Q3 to scan different CID fragmented product ions (187). Q3 is set to scan and analyze all of the fragments from Q2 (known as product ions). This scan mode is useful for identifying amino acid sequences of known or unknown peptides and studying molecular structure (187).

Neutral-loss scan: All precursors that undergo the loss of a common neutral ion fragment from CID are monitored (175). Q1 and Q3 scan simultaneously at a constant difference in m/z ratio that correlates with the mass of the specified neutral (187). This scan has similar uses to the precursor scan for the identification of similarly related compounds in a mixture. An example of this is the neutral loss of 102 Da from most butylated amino acids (187).

Selected-reaction monitoring (SRM): The MS is set to monitor the intensity of specific m/z values rather than scanning over a predefined mass range and recording full mass spectra (189,195). SIM only monitors the masses of interest and alternatively "jumps" between the desired masses (185). Rapid changes between m/z values for which the characteristic ions are expected allows for the SIM mode to be used for quantitative analysis. SIM is used to introduce selectivity into an analysis and improve sensitivity.

Multiple-reaction monitoring (MRM): An MRM experiment is conducted by keeping both Q1 and Q3 static for a selected pair of precursor and product ions (188,189). As the name implies, MRM is able to monitor more than one reaction at a time, meaning multiple precursor and multiple product ions can be selected. This scan mode offers the highest specificity and

sensitivity out of all possible scan modes and is the most commonly used mode for quantitative measurements of analytes in complex samples.

Table 2.1 Summary of MS scan modes capable of being performed on a typical triple quadruple mass spectrometer. Table adapted and modified from source 189.

Scan Mode	Q1 Operation	Q2 Operation	Q3 Operation
Q1 scan	Scans specified range	N/A	N/A
Precursor-ion scan	Scans over specified range for potential precursor ions (m_1)	CID	Static (no scan)
Product-ion scan	Static (no scan)	CID	Scans over specified range for product ions (m_2)
Neutral-loss scan	Scan specified range	CID	Specified scan range shifted by mass charge
Selected-reaction monitoring (SRM)	Monitors only selected precursor (m_1)	CID	Monitors only selected product (m_2)
Multiple-reaction monitoring (MRM)	Static (no scan), select precursor ions (m_1)	CID	Static (no scan), select product ions (m_2)

*Masses before fragmentation = m_1 and masses after CID fragmentation = m_2. This expression can be represented as $m_1=m_2 + n$ where n is equivalent to the difference between m_1 and m_2.

Methodology

2.4 Objective of Method Development

The objective of the work described in Chapter 2 "Method Development" was aimed toward developing a robust, sensitive and reproducible bioanalytical method for the detection of a novel bone-targeting parathyroid hormone conjugate (BP-PTH). The three-part method was optimized in the stages of: 1) Protein precipitation and solid-phase extraction, 2) HPLC chromatographic separation conditions and 3) MS analysis. These three phases are interconnected and optimization in each phase was done carefully to ensure compatibility with subsequent phases. Conditions and parameters were varied between these three phases until a suitable method for detection was developed.

2.5 Validation Experiments and Acceptable Criteria

The method was partially validated according to the European Medicine Agency (EMA) guideline on bioanalytical method validation (195). Method validation was performed in rat plasma. The following sub-sections describe the validation experiments and their acceptable criteria as per the EMA guidelines for chromatographic assays (195).

2.5.1 Quality control (QC) samples

Quality control (QC) samples were prepared in the same biological matrix as the study samples and are used to assess precision and accuracy of the assay and sample stability. QC samples should be prepared fresh and from separate standard solutions for accuracy and precision experiments. Concentrations of QC samples should adequately cover the range determined by the calibration curve. For validation of accuracy and precision runs, four QCs are required; lower limit of quantification (LLOQ), low (L: within three times the LLOQ), mid (M: mid-range) and high (H: high range). For all other validation experiments only a L, M and H are required (195).

2.5.2 Calibration curve

A fresh calibration curve will be prepared on every validation day. The calibration curve consists of a blank (no analyte, no IS), a zero calibrator (blank plus IS), and six, non-zero

calibrator levels that adequately cover the quantification range (including LLOQ) (195). Calibrators will be prepared from plasma solutions. The simplest regression model that demonstrates a suitable concentration-response relationship will be used.

2.5.3 Selectivity

The selectivity of a bioanalytical assay is defined as the capability to differentiate the analyte of interest from endogenous compounds in the biological matrix. Selectivity of the method is assessed by analyzing blank samples (e.g. plasma) from six different sources of plasma. Each batch of matrix was spiked with a different concentration for the analyte of interest and the IS that both exceeded 20% of the LLOQ. The selectivity of the method is deemed acceptable if blank and zero calibrators are free of interfering or co-eluting peaks at the retention times (tR) of the target analyte and the IS. The IS response in the blank cannot exceed 5% of the average IS responses of the calibrators and QCs (195).

2.5.4 Specificity

Specificity is the methods ability not to detect potential interfering compounds from the biological matrix. Specificity can be determined by analyzing drug-free plasma from at least six different plasma batches with addition of IS and without. The specificity of the assay is deemed acceptable if there are no co-eluting peaks with areas of more than 20% of the analyte peak area the LLOQ (195).

2.5.5 Matrix effect

In addition to selectivity and specificity experiments to determine any potential matrix interference, matrix components may affect the analyte signal in MS analysis through suppression or enhancement. Matrix effects can significantly influence analysis performance for both identification and quantification of the analyte of interest (184). Calculating the Matrix Effect (ME) can determine if the matrix has no ionization effect or suggest if matrix components are causing ion enhancement or ion suppression. Post-extraction addition involves spiking the analyte at L and H QC levels and the IS in triplicate into processed blank matrix (to exclude

extraction recovery) and the same QC levels of analyte and IS into pure solution. The ME is calculated by the following equation (198):

$$\text{Matrix Effect (ME)} = \frac{(A-B)}{A} \times 100 \qquad\qquad \textbf{Equation 1}$$

A: peak area of analyte in pure solution.
B: peak area of analyte spiked into processed blank matrix

A ME ~0% indicates that there is no matrix effect. An ME>0% demonstrates an ion-suppression effect and an ME <0% means ion-enhancement is occurring (198).

2.5.6 Sensitivity and linearity

To determine linearity and sensitivity of the method, a calibration curve of at least six concentration levels needs to be freshly prepared on every validation day. The calibration curves should cover the concentration range that is expected in the bioanalytical study and be prepared in the same biological matrix as study samples. The simplest model that is able to describe the concentration-response relationship should be applied to the curve, as well as an appropriate weighting scheme (if required) and regression equation. A blank (no analyte, no IS), a zero-calibrator (blank plus IS) and six, non-zero calibrator levels (including the LLOQ) will be used. If non-zero calibrators are ±15% of the theoretical concentrations and the LLOQ is ±20% of the theoretical concentration in each run, then the calibration curve is deemed acceptable (195).

The lower limit of quantification (LLOQ) is the lowest nonzero concentration on the calibration curve that can be measured with acceptable accuracy (±20% of nominal concentration) and precision (±20% coefficient of variation (CV)) from ≥ five replicates in at least three runs. The LLOQ determines the sensitivity of the assay. The analyte response at the LLOQ should be ≥ five times the analyte response of the zero calibrator (signal-to-noise ratio). Signal-to-noise ratio at the LLOQ is determined by the peak signal divided by the upper noise level (195).

2.5.7 Accuracy and precision

Intra-day and inter-day accuracy and precision should be determined at each concentration level using the percent error and coefficient of variation (CV) of four QC samples (LLOQ, L, M, H) from three separate analytical batches on each validation day (five replicates per QC level). Concentrations were calculated from the freshly prepared calibration curve during each validation day. Accuracy and precision were calculated for each concentration level using the following equations:

$$\text{Accuracy (\%)} = \frac{\text{Measured concentration}}{\text{Nominal concentration}} \times 100 \qquad \textbf{Equation 2}$$

$$\text{Precision (\%)} = \frac{\text{SD of measured concentrations}}{\text{Mean of measured concentrations}} \times 100 \qquad \textbf{Equation 3}$$

Intra-day and inter-day accuracy and precision are deemed acceptable if the accuracy within-run and between runs are ±15% of nominal concentration (except ±20% at LLOQ) and within-run and between run precision is ±15% CV (except ±20% at LLOQ) (195).

2.5.8 Recovery

Recovery should be assessed by determining the extraction recovery of the analyte and the IS from rat plasma by comparing peak area ratios of extracted QCs (low, medium and high) to the peak areas of the same QC levels spiked into extracted blank plasma solutions. Three replicates of each concentration level are required. Recovery can be below 100% and is acceptable if the extent of recovery of an analyte is consistent and reproducible (195). The following equation was used to determine the extraction recovery:

$$\text{Recovery (\%)} = \frac{\text{Mean peak area in biological matrix}}{\text{Mean peak area of analyte spiked into extracted plasma}} \times 100 \qquad \textbf{Equation 4}$$

2.5.9 Stability

Stability experiments to determine the chemical stability of the analyte need to be performed under a multitude of conditions in differing environments to reflect the conditions experienced during sample collection, handling and preparation (benchtop stability), analysis and

storage. In this validation study, all stability experiments were performed using low and high QC samples in triplicate under various conditions. Immediately after the application of the stability conditions, the stored QC samples are prepared alongside calibration standards to generate a fresh calibration curve and are analyzed together. Stock solution stability was accessed by comparison of peak areas of stock solutions after the specified storage condition to initial measurements. Samples are determined to be stable if the accuracy (% nominal) at each level is ±15% (195). The tested conditions are summarized in Table 2.2 below.

Table 2.2: Summary table of conditions used for stability experiments.

Experiment	Temperature	Time	Condition Mimicked
Short-term stability	25 °C under white light	5 hr	Benchtop conditions (sample handling and preparation)
Long-term stability	-80 °C	30 and 60 days	Storage conditions in freezer
Post-preparative stability	4 °C	48 hr	Storage conditions in fridge between sample preparation and measurement
Auto-sampler stability	15 °C	48 hr	Storage conditions in the autosampler during analysis
Freeze/Thaw stability	-80 °C to RT	3 cycles	Freezing and thawing of samples
Stock solution stability	4 °C	5 days	Storage conditions in fridge

2.6 Internal Standard

Internal standards (IS) are frequently used in HPLC and LC-MS/MS bioanalysis. An internal standard is a chemical substance that is added in a constant amount to the calibration standards, blanks, and study samples. During the sample preparation and analysis of biological samples, variations and/or losses such as, evaporation loss, transfer loss, adsorption loss,

injection variation, and MS variations such as ion suppression or enhancement may occur (199). Differences in matrix effects and extraction efficiency incurred by the analyte between calibrators and samples should be identical to the difference incurred by the IS. By using an IS with similar physiochemical properties as the analyte and using the analyte/IS response ratios for quantitation, these variations and losses that may occur during sample preparation, injection and ionization can be corrected (199). Ultimately, the main purpose of internal standards is to improve the accuracy and precision of quantitation as well as the robustness of the method (199).

In general, the chemical properties of the selected IS should be as close as possible to the target analyte so that variations and losses can be accurately corrected for. Most importantly, the hydrophobicity and ionization properties of the IS should be kept as similar to the analyte of interest as feasible (199). Similar physiochemical properties allow for an IS to be added as early as possible in the bioanalysis procedure, and track the analyte of interest in all three stages of bioanalysis (extraction, chromatographic separation, and MS detection) to provide the most accurate corrections (199).

It is recommended to use a stable-label (isotopic label) with a mass of 4 or 5 Da higher than the analyte whenever possible to reduce isotopic interference (200). When stable-label ISs are not possible, a structural analog can be used that is not exogenous and observed in the samples, but can be resolved from the analyte by MS. If using a structural analog, key chemical structure and functionality (e.g. -COOH, -OH, -NH$_2$) should be the same as the analyte of interest (199). Ideally, a structural analog should be from the same therapeutic class.

2.6.1 hPTH (1-34) as an internal standard

Due to the uniqueness of our custom synthesized BP-PTH, there are no available isotopic labels or other very similar structural analogs on the market for purchase. Our lab is not equipped with the expertise or equipment to synthesize an isotopic label or structural analog to use as an IS for method development. Furthermore, contracting the synthesis of custom peptides to external groups is very expensive and is a lengthy process. The closest compound which could be used as an IS was determined to be the peptide hormone hPTH (1-34) as it shares the same amino acid sequence as the peptide moiety of the BP-PTH conjugate. Due to the similar size and polarity of hPTH (1-34) to the BP-PTH conjugate, it was hypothesized that it should behave similarly in sample extraction, chromatography separations and in MS analysis. hPTH (1-34) would be able

to be added early in the extraction process directly to plasma, improving the accuracy of corrections using the IS. As hPTH (1-34) lacks the BP moiety, it likely will not have the same retention time as BP-PTH. Though not having an isotopically labeled IS is a limitation of this study, hPTH (1-34) is considered a structural analog of BP-PTH and belongs to the same therapeutic class, satisfying the recommendations for an IS.

2.7 Instrumentation and Software

Liquid chromatography (LC) was performed on a Shimadzu LC system consisting of a DGU-20A SR degasser, Nexera X2 LC-30AD binary gradient pump, Nexera X2 SIL-30AC autosampler and a CTO-20AC column oven (Shimadzu, Kyoto, Japan). The LC system was coupled to a LCMS-8050 triple quadrupole mass spectrometer (Shimadzu, Kyoto, Japan). Analytical column was a bioZen PS-C$_{18}$ (150mm x 2.1 mm I.D. 3 µm particle size) with guard column (4 x 2.00 mm I.D.) (Torrance, California, USA). Analytical data was collected and processed using LabSolutions software (ver. 5.91). Solid phase extraction was carried out using a 20 position Promega Vac-Man® vacuum manifold (Madison, Wisconsin, USA) to apply positive pressure. An Eppendorf 5415D benchtop centrifuge was used for all centrifugation (Hamburg, Germany).

2.8 Chemicals

BP-PTH was synthesized by CPC Scientific Inc. (Sunnyvale, California, USA). Teriparatide (human PTH (1-34) acetate salt) was purchased from Bachem (Torrace, California, USA). Water (LC-MS grade), acetonitrile (ACN) (LC-MS grade), methanol (LC-MS grade, and formic acid (99.0+%, LC-MS grade) were purchased from Fisher Scientific (Pittsburgh, PA, USA). Ammonium acetate (≥98%), sodium hydroxide (NaOH), and 1.0 N hydrochloric acid were purchased from Sigma-Aldrich Canada Co. (Oakville, Ontario,Canada). Drug-free Sprague Dawley rat plasma (K$_2$ EDTA) was purchased from Innovative Research Inc. (Novi, MI, USA). Oasis® weak anion exchange (WAX) cartridge (60mg, 3cc) were purchased from Waters Corporation (Massachusetts, USA). Strata-X™ cartridges (60mg, 3cc and 30mg, 1cc) were purchased from Phenomenex (Torrance, California, USA).

2.9 Stock Solutions

2.9.1 Preparation of BP-PTH stock, standard and working solutions

A Stock solution of BP-PTH (90.5% pure) was prepared by dissolving proper amounts of accurately weighed lyophilized BP-PTH (equilibrated to room temperature) in deionized water to create a concentration of 500 μg/mL. The stock solution was subsequently stored at 4 °C and protected from light. The stock solution (500 μg/mL) was further diluted to 500 ng/mL with deionized water using serial dilutions to create three standard stock solutions. Standard stock solutions were then further diluted with deionized to create working standard solutions at 50, 75, 100, 125, 200, and 250 ng/mL to be used for calibrator and QC samples. Solutions were stored in polypropylene tubes and kept at 4 °C until required. See Table 2.3 for a summary of BP-PTH stock, standard and working solutions.

1X PBS and 0.9% saline solution were both tested as potential solvents for BP-PTH. Despite being highly soluble in both solutions, 1X PBS and 0.9% saline solutions caused ion-suppression and reduced sensitivity during MS analysis significantly, with 1X PBS causing greater sensitivity suppression than 0.9% saline solution (data not shown). Therefore, deionized water was chosen as a solvent for BP-PTH.

2.9.2 Preparation of hPTH (1-34) internal standard (IS) stock solutions

hPTH (1-34) 500 μg/mL stock solution (99.01% pure) was prepared in deionized water and stored at 4°C. hPTH (1-34) was allowed to equilibrate to room temperature before being weighed. The stock solution was diluted using serial dilutions to 125 ng/mL (working solution) and 25 μL was added to 250 μL of BP-PTH spiked plasma to create a final concentration of 12.5 ng/mL. The IS working solution was stored at 4 °C in polypropylene tubes. See Table 2.3 for a summary of hPTH (1-34) stock and working solutions.

Table 2.3: Summary of stock, standard, and working solutions for BP-PTH and the internal standard (IS).

Solution Type	Purity [%]	Solvent	Storage Condition	Concentration (ng/mL)
BP-PTH Stock Solution	90.50	Deionized water	4 °C or -80 °C (protected from light)	500,000
BP-PTH Standard Solutions	90.50	Deionized water	4 °C (protected from light)	500
BP-PTH working solutions	90.50	Deionized water	4 °C (protected from light)	50, 75, 100, 125, 200, 250
hPTH(1-34) internal standard stock solution	99.01	Deionized water	4 °C (protected from light)	500,000
hPTH (1-34) internal standard working solution	99.01	Deionized water	4 °C (protected from light)	125

2.9.3 Preparation of calibration standards and quality control (QC) samples

All calibration standards and quality control (QC) samples were prepared from freshly prepared stock standard solutions in deionized water. 25 μL of calibrator or QC level is added to 225 μL of K_2 EDTA treated rat plasma. Four QC levels were used: LLOQ (5 ng/mL), low (2 x LLOQ, 7.5 ng/mL), medium (12.5 ng/mL) and high (20 ng/mL). QC samples were snap frozen using liquid nitrogen and stored at -80 °C until use (approx. 1 week). On each validation day, working standard solutions are used to create the calibration standards in plasma. QC samples used in long-term stability experiments or freeze/thaw experiments were stored at -80 °C, until use. All samples were created with pre-wetted pipette tips (3X before dispensing).

Table 2.4: Summary of quality control (QC) samples and calibration standards.

Calibrator Level	Solvent	Storage Conditions	Concentration (ng/mL)
Blank	K_2 EDTA treated plasma	Freshly prepared	0
Zero calibrator	K_2 EDTA treated plasma	Freshly prepared	12.5 of IS only
1	K_2 EDTA treated plasma	Freshly prepared	5.0
2	K_2 EDTA treated plasma	Freshly prepared	7.5
3	K_2 EDTA treated plasma	Freshly prepared	12.5
4	K_2 EDTA treated plasma	Freshly prepared	15.0
5	K_2 EDTA treated plasma	Freshly prepared	20.0
6	K_2 EDTA treated plasma	Freshly prepared	25.0

QC Level	Solvent	Storage Condition	Concentration (ng/mL)
LLOQ	K_2 EDTA treated plasma	-80°C	5.0
Low	K_2 EDTA treated plasma	-80°C	7.5
Medium	K_2 EDTA treated plasma	-80°C	12.5
High	K_2 EDTA treated plasma	-80°C	20

2.10 Anticoagulant

K_2 EDTA as an anticoagulant was selected over other anticoagulant treated plasma on the basis of Yang et al's recommendations and findings (174). All plasma used in the method development and validation experiments used K_2 EDTA treated plasma. EDTA-treated plasma is preferable over other anticoagulants such as heparin, as it produces cleaner plasma, which is better suited for SPE procedures (174). More importantly, Yang et al. concluded that, EDTA contributes to an increase in derivatization yield and better reproducibility (174). The positive effects of EDTA can be attributed to EDTA helping prevent complexing of BP compounds with endogenous cations, increasing the amount of free analyte capable of interacting with the sorbent during the SPE process (174).

2.11 General sample preparation, derivatization and extraction workflow

The IS working solution is added to an aliquot of spiked plasma samples containing BP-PTH and undergoes protein precipitation using an acetonitrile solution containing ammonium hydroxide. Treated samples are then centrifuged and the supernatant is collected for further purification. Supernatant is diluted with water and loaded onto a pre-conditioned polymer solid phase extraction cartridge that was washed with methanol and conditioned with the water. A vacuum manifold is used to apply positive pressure to create controlled flow rate through the SPE cartridge. After sample loading, the cartridge was further washed with a water/methanol solution to remove impurities. The analyte and IS were eluted with the addition of an acetonitrile/water solution with flow through being collected in a microcentrifuge tube. The eluate is then transferred to a glass vial to be injected onto the LC-MS/MS system.

2.12 Protein Precipitation

Chambers et al. have reported a highly optimized protein precipitation (PPT) strategy for the isolation of hPTH (1-34) with approximately 95% recovery (201). A modified version of their protein precipitation strategy was used to isolate both the IS and BP-PTH. 25 μL of internal standard (125 ng/mL) was added to 250 μL of EDTA treated rat plasma containing BP-PTH (standard curve point, QC or sample) and mixed in a 1.5 mL microcentrifuge tube. The final IS concentration was 12.5 ng/mL. 250 μL of ACN containing 5% ammonium hydroxide (1:1 ratio of plasma:ACN/5% NH_4OH) and centrifuged at 4000 rpm for 15 min. The supernatant was then collected and transferred to another microcentrifuge tube containing 1 mL of water and mixed. The mixed solution was then loaded onto a polymer SPE cartridge for further purification.

2.13 SPE Cartridge Selection

Protein precipitation studies for the isolation of hPTH (1-34) by Chambers et al. have shown that protein precipitation alone is not enough to isolate hPTH (1-34) to quantify down to the sub-ng/mL level (201). Chambers et al. have shown that endogenous proteins remaining after PPT reducing sensitivity, therefore, it is recommended to use a low sorbent bed-mass SPE for further purification. hPTH (1-34) has been successfully extracted using polymeric based SPE

sorbents in published studies before (201-203). The polar nature of hPTH (1-34) allows it to be well retained in the polymeric sorbent.

As BPs and BP-conjugated compounds are classified as strongly acidic compounds due to their phosphonic acid groups, it is recommended to use a weak-anion exchange (WAX) column rather than a polymeric sorbent. As BP-PTH is a conjugate of both a BP and hPTH(1-34), WAX columns and polymeric sorbent columns were compared to determine which sorbent type provided optimal retention of BP-PTH and the IS. A Waters Oasis® WAX cartridge (1cc, 60 mg, 60 μm, 80Å) and a Phenomenex Strata-X™ polymeric cartridge (3cc, 60 mg, 33 μm) were compared. Samples containing either BP-PTH or hPTH (1-34) in plasma were subjected to the protein precipitation procedure described in section 2.12 and then loaded onto both WAX and polymeric cartridges to determine percent recovery of the analytes

2.13.1 SPE using a polymeric Strata-X™ cartridge

A Phenomenex Strata-X™ polymeric reversed phase (3cc, 60mg, 33μm) SPE cartridge was used for further purification after PPT. Solutions of 1000 ng/mL of BP-PTH in plasma and 1000 ng/mL of hPTH (1-34) in plasma were prepared. Samples underwent protein precipitation as described in section 2.12. The supernatant was diluted and loaded onto a pre-conditioned Strata-X™ SPE cartridge that had been conditioned with 2 mL of methanol and 2 mL of deionized water. A vacuum manifold was used to apply positive and consistent pressure for elution. Sorbent beds were washed with 2 mL of 5% methanol in water and eluted with 500 μL of 60/40 (v/v) ACN:H$_2$O with 2% formic acid. Eluent was collected for analysis in LC-MS/MS. Peak areas from MS spectra were used to quantify percent recovery. The experiment was conducted in replicates of 3 (n=3).

2.13.2 SPE using a weak anion exchange Oasis® cartridge

A Waters Oasis® WAX (3cc, 60mg, 60μm, 80Å) SPE cartridge was used for further purification after PPT. Solutions of 500 ng/mL of BP-PTH in plasma and 500 ng/mL of hPTH (1-34) in plasma were prepared. Samples underwent protein precipitation as described in section 2.12. The supernatant was diluted and pH adjusted to 4.0 using 25 μL of 1.0M HCl. The supernatant was loaded onto a pre-conditioned WAX SPE cartridge that had been conditioned

with 2 mL of methanol and 2 mL of deionized water. A vacuum manifold was used to apply positive and consistent pressure for elution. Sorbent beds were washed with 2 mL of 25 mM ammonium acetate (pH 6.0-7.0) and eluted with 500 µL of 5% NH$_4$OH in methanol (pH 9.0). Eluent was collected for analysis in LC-MS/MS. Peak areas from MS spectra were used to quantify percent recovery. The experiment was conducted in replicates of 3 (n=3).

2.13.3 Adjusting SPE cartridge sorbent size

To improve recovery further, the sorbent size of the Strata-X™ polymeric SPE cartridge was reduced from 3cc and 60mg to 1cc and 30mg. The 30mg sorbent is better suited for plasma samples of approximately 250 µL whereas the 60mg sorbent is suited for plasma samples of approximately 500 µL. A smaller sorbent size requires less volume of the elution solvent (250 µL instead of 500 µL), which reduces dilution of the samples allowing for lower quantification limits. Experimental conditions were identical to those described in section 2.13.1, for the 60 mg polymeric cartridges, with the only change being volume of elution for the 30 mg polymeric cartridges being performed with 250 µL of 60/40 (*v/v*) ACN:H$_2$O with 2% formic acid.

2.14 Optimized extraction workflow of BP-PTH and IS

The optimized extraction of BP-PTH and the IS consisted of protein precipitation using a 1:1 ratio of acetonitrile with 5% ammonium hydroxide to plasma. Centrifugation for 15 min at 4000 rpm was performed. The supernatant was collected and diluted with 1 mL of deionized water and loaded in two steps (~750 µL per step) onto a preconditioned Strata-X™ polymeric SPE cartridge. BP-PTH and the IS were eluted using 250 µL of 60/40 (ACN:H$_2$O) with 2% formic acid. Eluent was transferred to a glass vial and 15 µL injected onto the LC-MS/MS. A summary of the workflow is presented in Figure 2.9.

1. Protein Precipitation

Addition of IS
25 μL of IS added to 250 μL of rat plasma (standard curve point, QC or sample).

Protein Precipitation
250 μL of acetonitrile containing 5% ammonium hydroxide was added. A 1:1 ratio of modified acetonitrile to plasma.

Centrifugation
15 min at 4000 rpm.

Dilute Supernatant
Collect supernatant and dilute with 1 mL water

2. Solid Phase Extraction
Phenomenex Strata-X polymeric reversed phase (1cc, 30mg, 33μm)

Condition and Equilibrate
1 mL methanol and 1 mL water

Load Diluted Sample
~1.5 mL in two steps, approximately 750 μL each step

Wash
1 mL of 5% methanol in water

Elute
250 μL of 60/40 (*v/v*) ACN:H₂O with 2% formic acid

3. LC-MS/MS Analysis
Collect eluent and transfer 200 μL to vial for analysis.

Figure 2.9: Summary of analyte and IS plasma extraction workflow.

2.15 Optimization of RP-HPLC Chromatographic Conditions

Chromatographic separation of the IS and analyte of interest (BP-PTH) from the remaining plasma compounds present in the extracted samples is required to improve the accuracy, sensitivity, reproducibility and further purify the sample before MS/MS analysis. The aim of optimizing the chromatographic conditions was to develop a rapid RP-HPLC method that is capable of retaining both derivatized BP-PTH and hPTH (1-34) from rat plasma on a RP-column prior to MS/MS analysis.

2.15.1 Metal-free LC-MS/MS hardware for the detection of BP-containing compounds

Analysis of BP compounds and BP-containing compounds is severely impacted by problems with carryover and low sensitivity due to stainless steel parts present in LC-MS/MS hardware that show a high affinity for phosphonic acid containing compounds. If analyzing non-derivatized BP-containing compounds, it is recommended to use metal-free hardware throughout the entirety of the flow path. To achieve a metal-free flow path, all stainless-steel tubing was replaced with PEEK (polyetheretherketone) polymer tubing and a titanium column (no affinity for phosphonic acid groups) was used. The autosampler needle was unable to be replaced with a metal-free alternative.

2.15.2 Column phase selection

In addition to retaining the analytes of interest, the column chosen should possess a stationary phase that is compatible with the MS. This means that when mobile phases pass through the column, there is a low background signal in the MS as to indicate that there is no "bleeding" of the stationary phase into the MS.

To select a suitable column, the column must be able to produce sharp, symmetrical and tall peaks that are consistent, no sample carryover, efficiently retain the analyte(s) of interest and be reproducible across multiple samples. Furthermore, there should be no "bleeding" of the stationary phase into the MS.

For analysis of BP-containing compounds, a stainless-steel free column is required to address problematic column binding issues. A titanium bioZen™ Peptide PS-C$_{18}$ column was selected for this study.

2.15.3 Initial chromatographic method development

Initial chromatographic method development utilized the "60/60" determination method, which is used as a starting point to determine the retention time and peak shape when chromatographing an unknown. Using a RP-C$_{18}$ column, the majority of peptides should elute when the organic phase reaches ~30%. From the outcomes of the 60/60 determination method, a faster chromatographic method can be achieved once the retention time and the corresponding % organic phase is known. Utilizing the 60/60 determination method allows for rapid optimization of mobile phase composition (mixture of ACN/H$_2$O) where the compounds can be retained on the stationary phase but with minimized elution time. The 60/60 determination method consisted of gradient elution using deionized water with 0.1% formic acid (Mobile phase A) and acetonitrile with 0.1% formic acid (Mobile phase B) with a flow rate of 0.4 mL/min. These mobile phases were selected based on successful retention of BP compounds and hPTH(1-34) with reverse phase columns using ACN and water with 0.1% formic acid. Formic acid was used over TFA as it is compatible with MS. Formic acid has been reported to improve resolution of peptides by acting as a moderate ion pairing agent (204).

Gradient time program was 5% B to 60% B from 0.0 min to 60.0 min. The detector used for the determination of chromatographic conditions was an MS/MS. The MS was set to scan in Q1 and the total ion chromatogram (TIC) plot was used to analyze peak shape and retention times. A TIC plot is a type of Q1 chromatogram that displays the signal intensity over the entire selected m/z range plotted as a function of time. Sensitivity was also analyzed, with higher TIC amounts indicating greater sensitivity. 10 μL of a 25 μg/mL solution of BP-PTH or hPTH (1-34) in deionized water was injected into the LC-MS/MS system separately. The observations are summarized below in Table 2.5.

Table 2.5: Observations of initial method development in an attempt to chromatographically identify BP-PTH and hPTH (1-34).

Analyte	Column	Stationary Phase	Gradient Conditions (%B/min)	Flow rate (mL/min)	Observations
BP-PTH	bioZen PS-C$_{18}$ (150 x 2.1 mm I.D. 3 μm), guard column (4.00 x 2.00mm I.D.).	Alkyl chains on silica surface	5/0.0 min, 60/60 min.	0.4	Appearance of broad peak with tailing of moderate intensity between run time of 36 and 37 min, corresponding with a Mobile Phase B% of ~35%-37%.
hPTH (1-34)	bioZen PS-C$_{18}$ (150 x 2.1 mm I.D. 3 μm), guard column (4.00 x 2.00mm I.D.).	Alkyl chains on silica surface	5/0.0 min, 60/60 min.	0.4	Sharp peak of strong intensity with no tailing at ~35 min, corresponding with a Mobile Phase B% of ~33-35%

To improve chromatographic separation and the efficiency of the method, new gradient methods, different flow rates and column temperatures were explored to achieve optimal separation. Results from the 60/60 method determination were used to improve the gradient method. Method development was focused on improving the peak shape of the BP-PTH peak and significantly decreasing retention time and focusing on an elution. Mobile Phase A consisted of deionized water with 0.1% formic acid and Mobile Phase B consisted of acetonitrile with 0.1% formic acid. The observations are summarized in Table 2.6.

2.15.4 Optimizing an LC method for the separation of plasma extracted BP-PTH and hPTH (1-34)

Due to the slightly different chemical properties and polarity of hPTH (1-34) and BP-PTH, a gradient elution program was explored in an effort to retain both analytes in an efficient manner, to allow for high-throughput during the eventual use of clinical or pharmacokinetic samples. Ideally, the retention factor (capacity factor for the analytes) should be greater than 0.5 and less than 10 (205).

To shorten the elution time, various LC parameters were explored. The column volume of the empty bioZen PS-C_{18} column is 520 µL. The void volume (V_0) of a column is generally 60-70% of the empty column, with the remaining 30-40% being the packing material (206).

$$V_0 = 0.65 \times CV_{empty}$$
Equation 5

$$T_0 = V_0/\text{flow rate}$$
Equation 6

Void time (T_0) can be calculated using Equation 6. It is usually recommended to choose chromatographic conditions where analytes of interest elute with at least 1.5 void volumes in order to provide sufficient time for analytes to interact with the stationary phase (207). To satisfy this recommendation, the recommended minimum time for eluting the least retained analyte with a 0.4 mL/min flow rate is at least 1.3 min.

Retention factor (k') defines how much interaction the analyte of interest (sample peak) has with the column stationary phase. Essentially, it is a factor that demonstrates the relative time interacting with the column versus the mobile phase (208).

$$k' = \frac{t_R - t_0}{t_0}$$
Equation 7

t_R= retention time of analyte

Selectivity factor (a) is the ratio of the retention factors of both analyte peaks. Selectivity is also known as the separation factor and is a way to characterize how well chromatographic peaks are separated/resolved (208).

$$a = \frac{t_{RB} - t_o}{t_{RA} - t_o}$$ **Equation 8**

t_{RB}= retention time of analyte B (eluting after A)

t_{RA}= retention time of analyte A (eluting before B)

Resolution (R_s) describes the separation power of the complete chromatographic system relative to the analytes in the mixture (208). In the past, the FDA required a R_s > 2, but does not currently specify a required R_s value (208).

$$R_s = \frac{t_{RB} - t_{RA}}{(\frac{W_B + W_A}{2})}$$ **Equation 9**

W_B= width of peak at its base for analyte B

W_A= width of peak at its base for analyte A

Table 2.6 summarizes the various parameters and conditions explored to optimize the LC method. A TIC plot of the MRM transitions using Method #1 and #5 for the separation of 500 ng/mL of hPTH (1-34) and BP-PTH in plasma can be seen in Figure 2.10.

Table 2.6: Summary of chromatographic methods and their corresponding parameters used to separate BP-PTH and the IS.

Method	Gradient Conditions (%B/min) of BP-PTH and IS. Flow rate (0.4 mL/min)	tR of BP-PTH and IS (min)	Retention factors (k') of BP-PTH and IS	Selectivity (a)	Resolution (Rs)	Column Temperature (°C)	Observations
#1	25/0.1, 25/0.5, 40/4.50, 40/6.0, 25/6.0, 25/8.50	2.59 1.84 (IS)	2.07 1.18 (IS)	1.75	0.90	40	Extremely broad BP-PTH peak with moderate intensity. Peak tailing on both sides of peak.
#2	25/0.1, 25/0.5, 60/4.50, 60/6.0, 25/6.0, 25/8.50	2.42 1.84 (IS)	1.86 1.18 (IS)	1.23	1.15	40	Broad BP-PTH peak with moderate intensity.
#3	10/0.1, 10/0.5, 95/4.50, 95/9.0, 10/10.0, 10/10.50	2.81 2.58 (IS)	2.33 2.05 (IS)	1.13	3.01	40	Nearly identical peak shape for BP-PTH and IS as in Method 4, but higher pump pressure.
#4	15/0.1, 15/0.5, 95/4.50, 95/9.0 15/10.0, 15/10.50	2.85 2.60 (IS)	2.38 2.08 (IS)	1.14	2.83	40	Symmetrical IS and BP-PTH peaks.
#5	15/0.1, 15/0.5, 95/4.50, 95/9.0 15/10.0, 15/10.50	2.76 2.46 (IS)	2.27 1.91 (IS)	1.19	2.86	60	Symmetrical peaks, but sharper than Method #4.

*15 µL of an extracted plasma sample containing 500 ng/mL of both BP-TPH and the IS was injected into the LC-MS/MS system for all experimental runs.
**Retention factors, selectivity and resolution were calculated using Equations 7, 8 and 9.

As shown in Table 2.6, the most efficient chromatographic methods that satisfied chromatographic recommendations were Method #, M ethod # a nd Method #. M ethod # w as selected over the other two satisfactory methods as it produced the sharpest peak shape. The retention factors (k') for Method # was 2.76 and 2.46 for BP-PTH and the IS, respectively. Both analytes eluted after 1.3 min to allow for adequate interaction with the stationary phase. The resolution value of 2.86 confirms that there is satisfactory separation between the two analyte

peaks of BP-PTH and the IS. Method #5 was used for all subsequent LC-MS/MS experiments involving BP-PTH in this chapter.
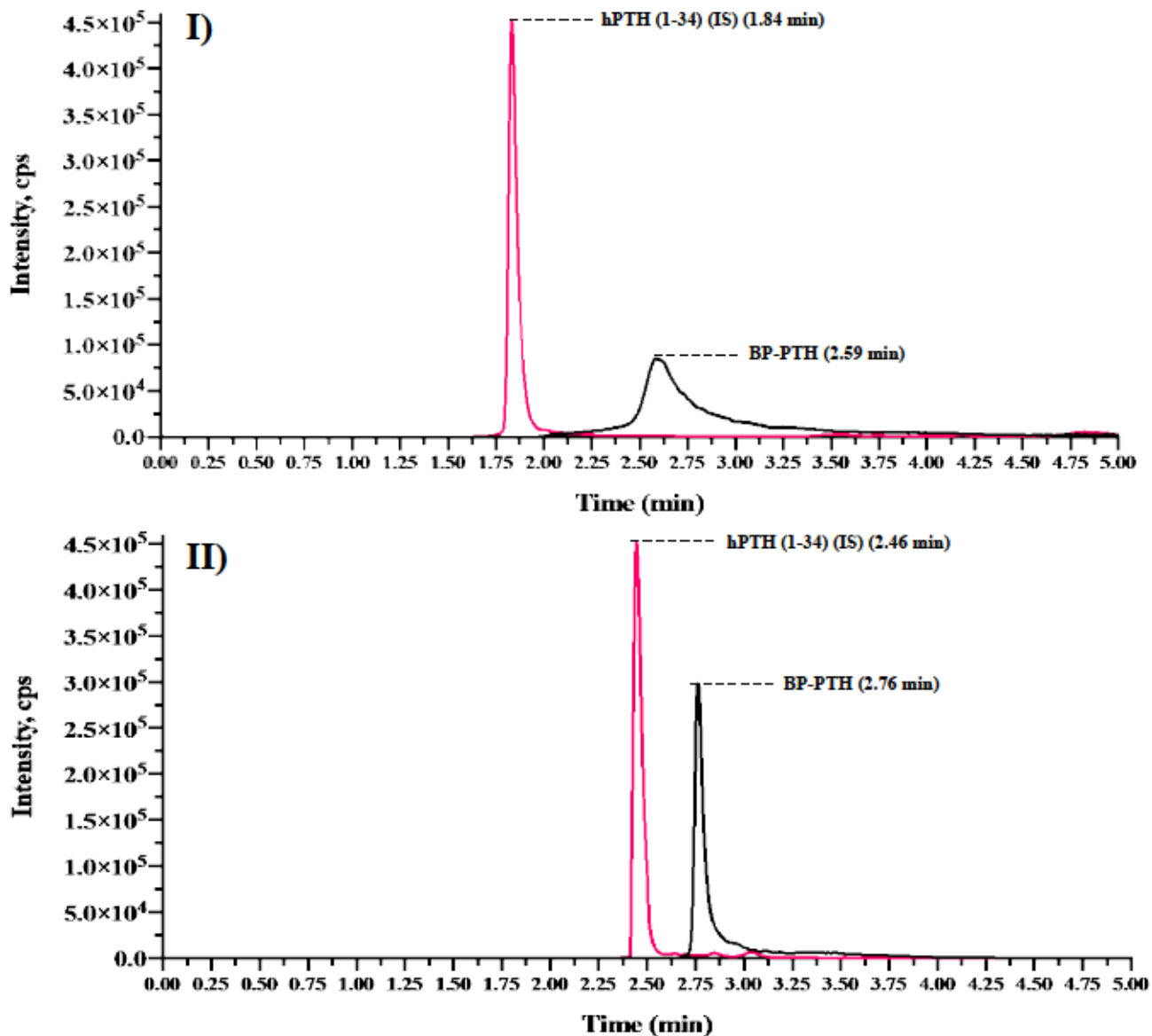
Figure 2.10: HPLC separation of BP-PTH and internal standard. I) Method #1 and II) Method #5, from a 500 ng/mL extracted plasma sample, using a bioZen PS-C18 (150 x 2.1 mm I.D. 3 μm) column.

2.15.5 Optimized LC conditions and parameters

The optimized LC conditions and parameters consisted of using the following gradient program (%B/min): 15/0.1, 15/0.5, 95/4.50, 95/9.0, 15/10.0, 15/10.50. Flow was diverted away from the MS detector from 0.0 to 1.50 min and from 5.00 min to 10.00 min to prevent detector contamination. Mobile phase A consisted of deionized water with 0.1% formic acid and mobile phase B consisted of acetonitrile with 0.1% formic acid. The flow rate was 0.4 mL/min, column temperature was maintained at 60 °C, autosampler temperature was 15 °C, and injection volume for all samples was 15 µL. A bioZen PS-C18 (150 x 2.1 mm I.D. 3 µm) column with guard column (4.00 x 2.00mm I.D.) was used for all runs.

2.16 Optimization of MS/MS for Quantitation

Liquid chromatography (LC) was performed on a Shimadzu LC system consisting of a DGU-20A SR degasser, Nexera X2 LC-30AD binary gradient pump, Nexera X2 SIL-30AC autosampler and a CTO-20AC column oven (Shimadzu, Kyoto, Japan). The LC system was coupled to a LCMS-8050 triple quadrupole mass spectrometer (Shimadzu, Kyoto, Japan). Analytical data was collected and processed using LabSolutions software (ver. 5.91).

2.16.1 Determination of ionization mode for BP-PTH and the IS

Determining which ionization mode and/or the polarity to be used for the detection of the IS and BP-PTH was the first step in developing an MS method. Electrospray ionization (ESI) and atmospheric pressure chemical ionization (APCI) are the most common ionization modes for coupling LC to tandem mass spectrometry (MS/MS) (209). ESI is most appropriately used for analyzing polar and ionizable compounds and is commonly used for the detection of peptides and carbohydrates, while APCI is used for nonpolar molecules with low molecular weights (209). Considering the polarity and size of both BP-PTH and hPTH (1-34), ESI was selected as the ionization mode for MS analysis in this thesis. Furthermore, all reported literature involving the detection of hPTH (1-34) and BP compounds have used ESI mode.

2.16.2 Selecting precursor ions for BP-PTH and the IS

Examining the Q1 fragmentation pattern for BP-PTH and the IS a suitable precursor ion can be selected to be used in developing the MRM transition. The most suitable precursor ion needs to be stable, correspond to the theoretical mass of the analyte of interest and preferably be the most abundant fragment (highest absolute intensity) of all the fragments that may correspond to the analyte of interest.

Direct injections (no column) of 1000 ng/mL solutions of BP-PTH and hPTH (1-34) using an isocratic elution program of 50/50 ACN:H_2O with 0.1% FA at 0.4 mL/min was conducted to determine suitable precursor ions for BP-PTH and hPTH (1-34). The relative intensities of the peaks were measured, with the most intense peak receive an intensity of 100. The most intense ions were selected as precursor ions for further development of the MRM transition method.
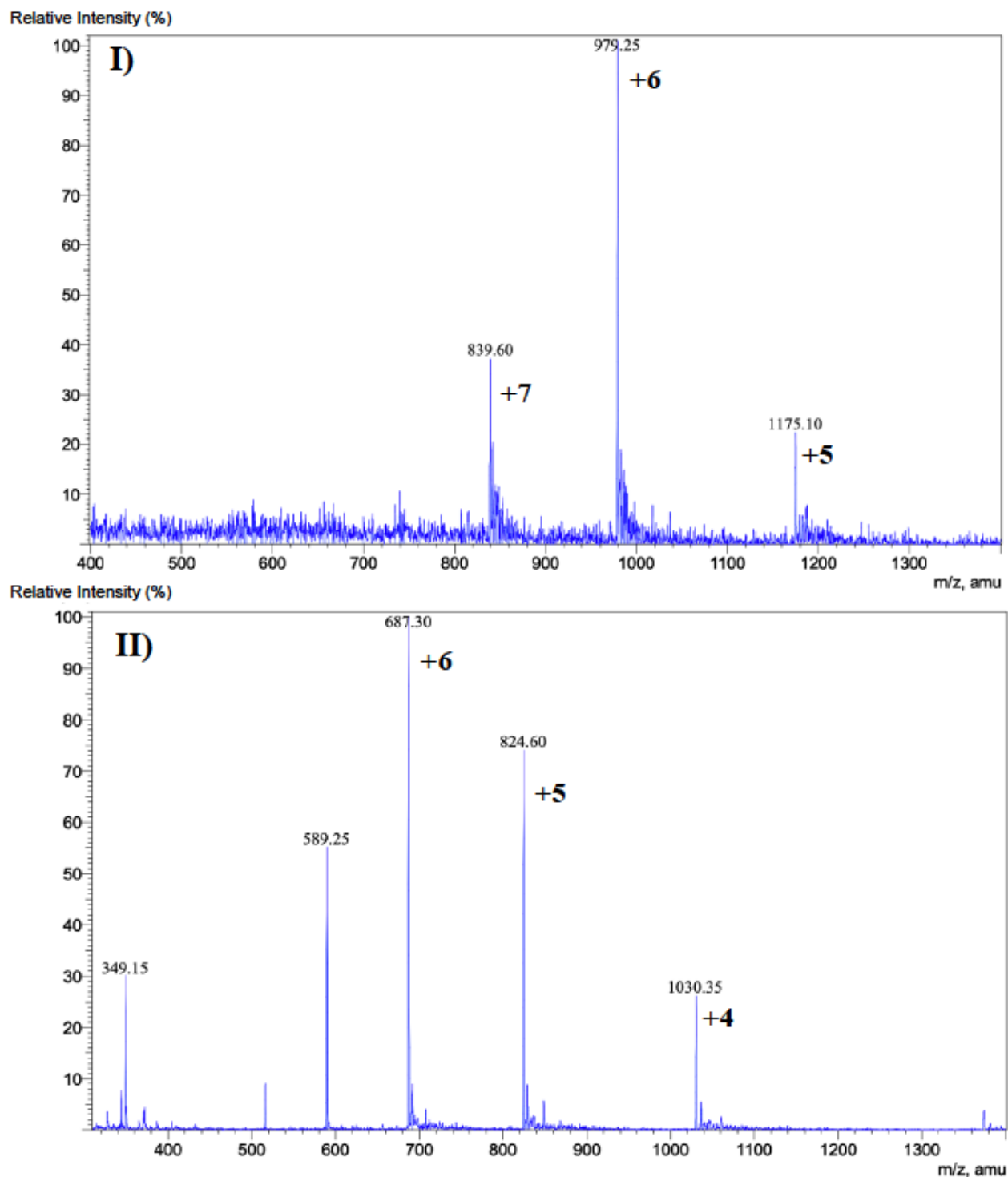
Figure 2.11: MS spectra showing relative intensities of precursor ions for BP-PTH and hPTH (1-34). I) MS spectra of BP-PTH precursor ions. The most intense precursor ion (979.25 m/z) corresponds to +6 charge species of BP-PTH, giving a mass error of -10.21 ppm from the theoretical mass. II) The most intense precursor ion (687.30 m/z) corresponds to the +6-charge species of hPTH (1-34), giving a mass error of -43.65 ppm from the theoretical mass. The 979.25 ion (rounded to 979.30) and the 687.30 m/z precursor ions were selected for further MRM development.

Results

The most intense precursor ion (979.25 m/z) corresponds to +6 charged species of BP-PTH, giving a mass error of -10.21 ppm from the theoretical mass. The most intense precursor ion (687.30 m/z) corresponds to the +6 charged species of hPTH (1-34), resulting in a mass error of -43.65 ppm. The 979.25 (rounded to 979.3) and 687.30 m/z ions were selected as Q1 precursor ions for further MRM development. The Q1 spectra of both analytes is shown in Figure 2.11, the selected precursor ions for further method development are summarized in Table 2.7.

Table 2.7: Q1 scans to select suitable precursor ions of BP-PTH and IS using ESI+ for further MRM method development.

Analyte	Charge (z)	Precursor Ion (m/z)
BP-PTH	+6	979.25
	+5	1175.10 (qualifier ion)
hPTH (1-34)	+6	687.30
		824.60 (qualifier ion)

2.16.3 Establishing and optimizing the MRM transition for BP-PTH and the IS

After selection of suitable precursor ions, suitable product ions (Q3 fragments) need to be determined to establish an MRM transition for BP-PTH and the IS. Fragmentation patterns need to be observed in Q1 (precursor ions) and in Q3 (product ions) in order to select for precursor and product ions to begin the process of optimizing the MRM transitions. Using MRM transitions, the sensitivity of quantification and detection can be vastly improved.

"Fully Automated MRM Optimization" program in LabSolutions software (ver. 5.91) was utilized for rapid and automated optimization to obtain the optimal collision energy (CE) between the range of 10 to 50 eV. Ultra-high purity argon gas is used as the collision gas for the LCMS-8050 triple quadrupole mass spectrometer. The MRM optimizations were conducted at low (50 kPa), medium (125 kPa), and high (270 kPa) CID gas pressure to determine optimal CE

to generate stable and high intensity product ions. This experiment was done to determine if there is any relationship between CID gas pressure and CE.

The automated steps of LabSolutions (ver. 5.91) "Fully Automated MRM Optimization" program is outlined in Figure 2.12. Parameters for the optimized MRM transition for the IS and BP-PTH are summarized in Table 2.10.

Input precursor ion (m/z values) → Search for product ions → CE optimization → Voltage optimization → Optimized MRM method established
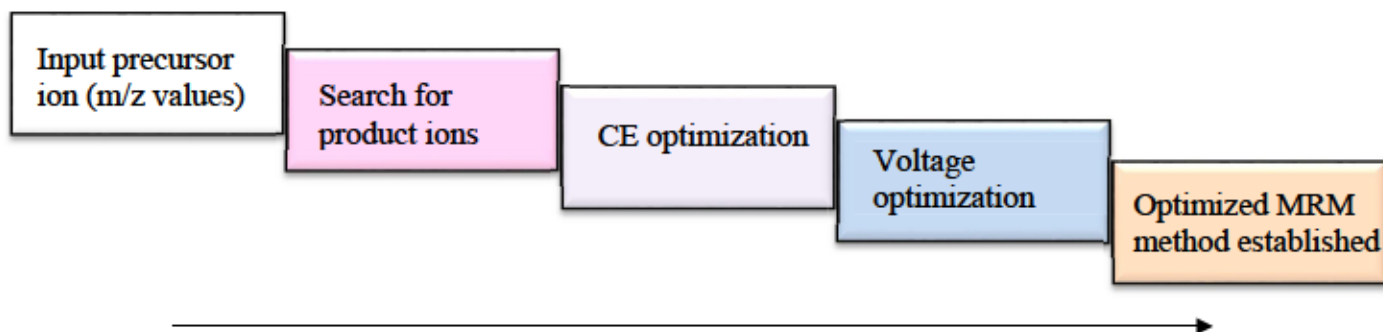
Figure 2.12: Pathway of the operations and sequence performed by LabSolutions "Fully Automated MRM Optimization" program.

Results

MRM optimization at high CID gas pressure (270 kPa) produced the most intense product ion fragments for both the IS and BP-PTH. At low CID pressure (50 kPa), there was no CID induced fragmentation of the 979.25 m/z precursor ion (979.25 → 979.25). Their appeared to be a relationship between CID gas pressure and the intensity of the product ion for both the IS and BP-PTH. As CID gas pressure increased, the intensity of the corresponding product ion also increased. Table 2.8 summarizes the results of the CID gas pressure experiment. No CID gas pressure exceeding 270 kPa was tested as the LC-MS 8050 has a CID gas pressure limit of 270 kPa.

Table 2.8: Summary of MRM optimizations for BP-PTH and IS product ions conducted at low, medium, and high CID gas pressures.

CID gas pressure	MRM transitions	Intensity of product ion (cps)
Low (50 kPa)	979.25 → 979.25	N/A
	687.30 → 675.20	2.53×10^3
Medium (125 kPa)	979.25 → 490.95	7.46×10^4
	687.30 →159.35	5.03×10^4
High (270 kPa)	979.25 → 490.95	5.35×10^5
	687.30 → 159.10	2.36×10^5
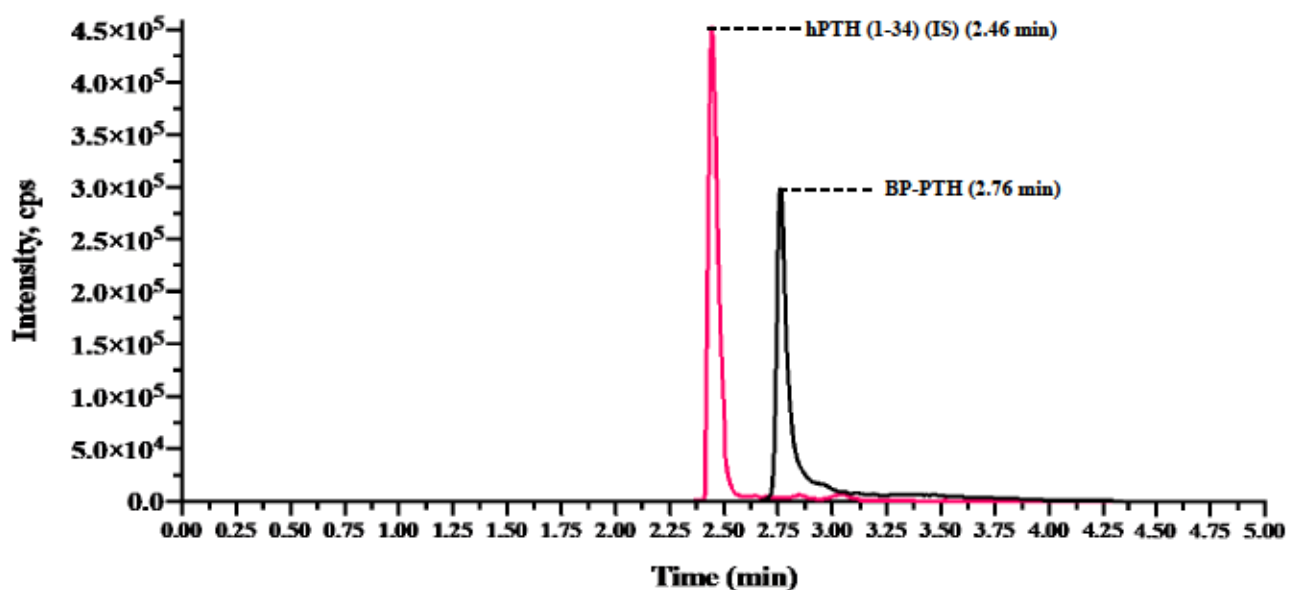
Figure 2.13: Optimized MRM transition of extracted 500 ng/mL of BP-PTH and hPTH (1-34) from rat plasma.

2.16.4 Mass spectrometry of hPTH (1-34)

As the m/z 159.10 product ion of the m/z 687.30 precursor ion was the most intense product ion generated using LabSolutions "Fully Automated MRM Optimization" program, it was used for method validation. Despite achieving suitable linearity ($r^2 > 0.995$) on the first validation run, large background interference was observed using the 687.30 → 159.10 transition after the elution of the IS peak. It is recommended for peptide method developments to avoid using fragments below m/z 200 as these ions usually correspond to immonium ions that result in high background due to endogenous interference and lack of specificity (210). The three most abundant product ions generated for the m/z 687.30 precursor ion by LabSolutions software were m/z 159.10, 110.10 and 86.05. These fragments correspond to the immonium ions of tryptophan, histidine, and isoleucine/leucine amino acid residues, respectively (211).

To improve specificity of the method, the collision energies was optimized using the reported y ion fragments above m/z 700 for hPTH (1-34) by Chambers et al (201). The MRM transitions 687.30 → 787.25 and 824.60 → 983.80 had optimized collision energies of 20 and 28 eV. The 787.25 and 983.60 product ions correspond to 5+ y32 and 4+ y32 ions, respectively. The 824.60 → 983.80 transition was low intensity and produced poor peak shape and was therefore not used in the optimized MRM. Using the y ion fragment (687.30 → 787.25) greatly improved specificity and reduced background signal almost entirely. A comparison between the two tested MRMs can be seen in Figure 2.14.
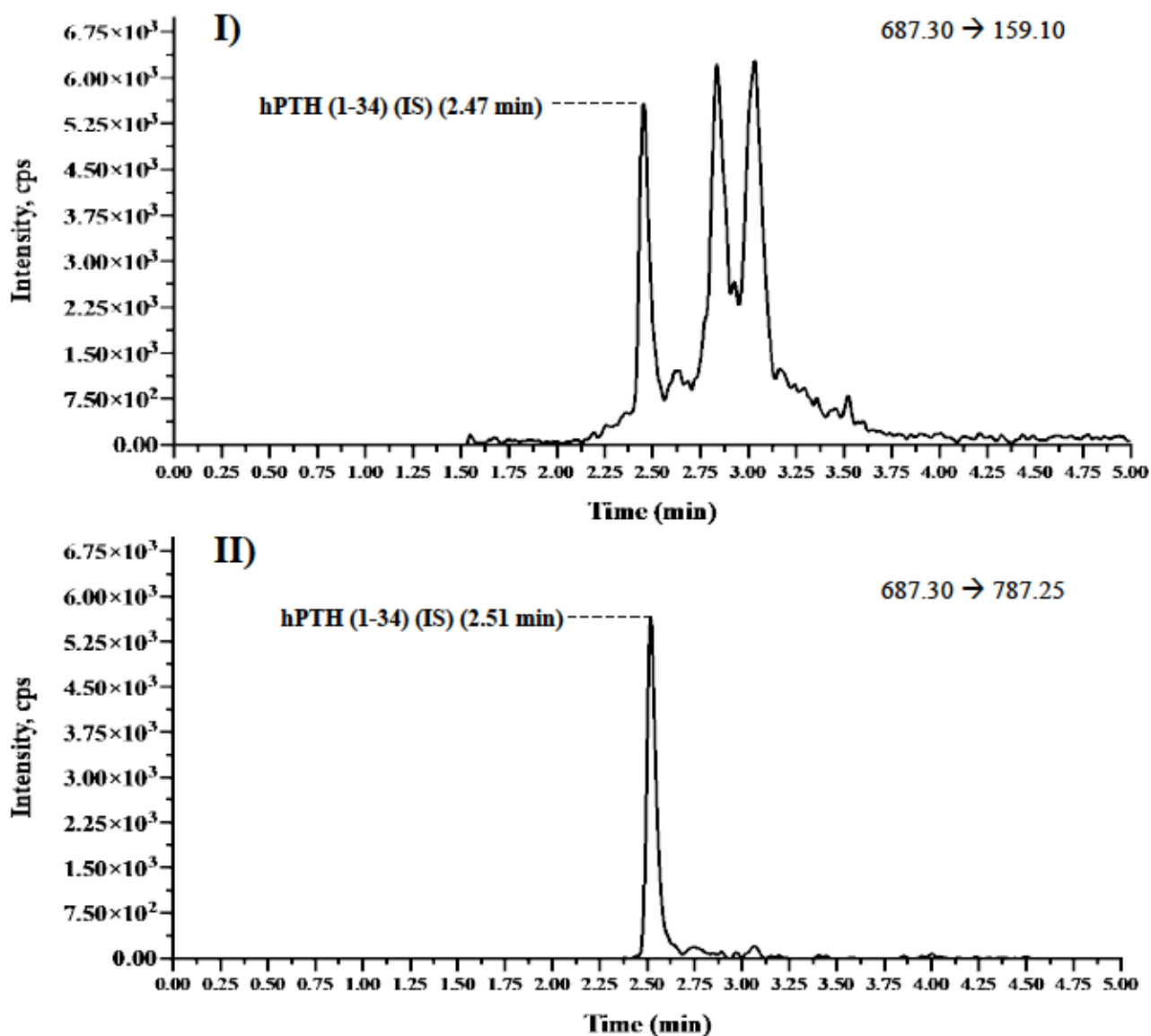
Figure 2.14: Chromatograms of the IS using two different MRM transitions. I) Chromatogram of the MRM transition 687.30 → 159.10. This transition corresponds to the tryptophan immonium ion as a product ion and resulted in high background signal due to interference from endogenous proteins. **II)** Chromatogram of the MRM transition 687.30 → 787.25. This transition corresponds to the 5+ y32 ion of the precursor ion. Background signal was significantly reduced using this transition. IS concentration was 12.5 ng/mL

2.16.5 Optimized MRM method

A multiplexed MRM method was successfully developed and MS parameters were optimized for the detection of BP-PTH and the IS. The transition used for quantification was 979.25 → 490.95 with a qualifier transition of 1175.10 → 490.95 using collision energies of 35 eV and 40 eV respectively. The product ion for these transitions was identified to be the BP moiety of the BP-PTH conjugate ($C_{14}H_{25}N_2O_9S_2P_2^+$ (z=1)). The transition for the IS was 687.30 → 787.25 with a collision energy of 20 eV. The optimized MS parameters are summarized in Table 2.9 and the summary of the multiplexed MRM transitions are summarized in Table 2.10.

Table 2.9: MS parameters of the optimized MRM transitions for BP-PTH and the IS.

MS Parameter	
Ionisation Mode	ESI+
CID gas pressure (kPa)	270.00
CID gas	argon
Interface voltage (kV)	4.00
Nebulizing gas flow (L/min)	2.00
Interface temperature (°C)	300.00
Desolvation line temperature (°C)	250.00
Heat block temperature (°C)	300.00
Drying gas flow (L/min)	10.00
Heating gas flow (L/min)	10.00
Dwell time (msec)	100.00

Table 2.10: Multiplexed MRM summary for BP-PTH and IS

Analyte	MRM Transitions	Collision energy (eV)	Q1 Pre Bias (eV)	Q3 Pre Bias (eV)
BP-PTH	979.25 → 490.95	35	22	26
	1175.10 → 490.95 (qualifier transition)	45	42	18
hPTH (1-34)	687.30 → 787.25	20	20	28

* The 490.95 product ion fragment from BP-PTH corresponds to $C_{14}H_{25}N_2O_9S_2P_2^+$ (z=1) portion of the BP-PTH compound. This portion is the BP moiety of the BP-PTH compound.

**A less intense product fragment of 246.10 was also observed from BP-PTH. This fragment corresponds to $C_{14}H_{25}N_2O_9S_2P_2^{2+}$ (z=2).

2.17 The Optimized Method

The optimized method consisted of using protein precipitation coupled with solid-phase extraction using a polymeric Strata-X™ cartridge. The eluent was collected, and 15 µL was loaded onto the LC-MS/MS system. A titanium-lined reverse-phase C_{18} column (A bioZen PS-C_{18} (150 x 2.1 mm I.D. 3 µm) column with guard column (4.00 x 2.00mm I.D.)) was used for the separation of BP-PTH and the IS. The LC method consisted of gradient elution using the following gradient program (%B/min): 15/0.1, 15/0.5, 95/4.50, 95/9.0, 15/10.0, 15/10.50. Flow was diverted away from the MS detector from 0.0 to 1.50 min and from 5.00 min to 10.50 min to prevent detector contamination. To prevent sample carry-over, after each injection, 40 µL of ACN was injected into the sample loop to remove any BP-PTH that may be on the external portions of the sample needle. Mobile phase A consisted of deionized water with 0.1% formic acid and mobile phase B consisted of acetonitrile with 0.1% formic acid. The flow rate was 0.4 mL/min, column temperature was maintained at 60 °C, autosampler temperature was 10 °C. MRM mode was used for quantification with the following transitions: +6 precursor for BP-PTH 979.25 → 490.95 and using the +5 precursor as a qualifier ion 1175.10 → 490.95. The collision energies for these transitions was 35 and 45 eV, respectively. The MRM transitions for the IS used the +6 precursor of hPTH (1-34) 687.30 → 787.25 with collision energy of 20 eV. The MS/MS system consisted of a LCMS-8050 triple quadrupole mass spectrometer and the interface voltage, interface temperature, desolvation line temperature, drying gas flow and CID gas pressure was 4.0 kV, 300 °C, 250 °C, 10 L/min, and 270 kPa, respectively. Analytical data was collected and processed using LabSolutions software (ver. 5.91).

Results & Discussion

2.18 Results

2.18.1 SPE comparison of a polymeric Strata-X™ cartridge with a weak anion exchange Oasis® cartridge.

The peak area of hPTH(1-34) that underwent extraction using the polymeric Strata-X™ cartridge was arbitrarily defined as 100% recovery as it yielded the largest peak area compared to the other experimental treatments. All other treatment groups were compared to the relative peak area of hPTH (1-34) extracted from plasma using the polymeric cartridge. For both BP-PTH and hPTH (1-34), extraction using polymeric cartridges significantly outperformed extraction using the weak anion exchange cartridges ($p < 0.001$). Findings are summarized in Figure 2.15.
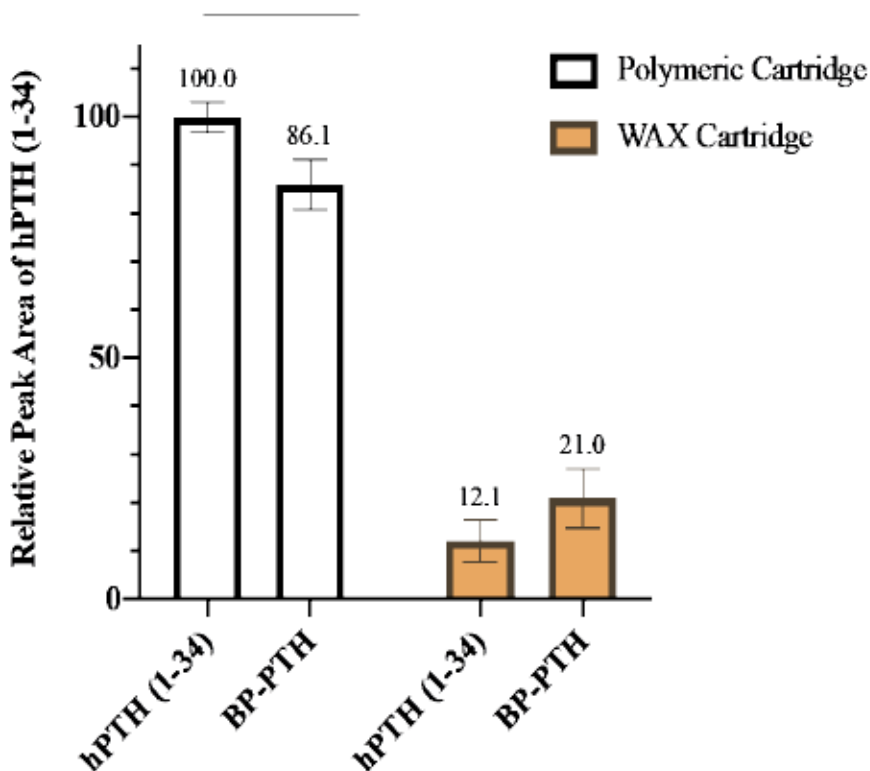
Figure 2.15: Relative peak area of BP-PTH and hPTH (1-34) using two different SPE sorbent types after protein precipitation. Recovery for both analytes was significantly higher ($p < 0.0001$)when using the Strata-X™ polymeric sorbent in comparison to the Oasis® WAX sorbent. Recovery for hPTH (1-34) was the highest (100) and the peak areas of the analytes in both groups were compared to the average peak area of hPTH (1-34) extracted using the polymeric sorbent. Values represent mean ± standard deviation ($n=3$ replicates), *** $p < 0.001$

2.18.2 Adjusting SPE cartridge sorbent size

The peak area of hPTH(1-34) that underwent extraction using the 30 mg polymeric sorbent size was arbitrarily defined as 100% recovery as it yielded the largest peak area compared to the other experimental treatments. All other treatment groups were compared to the relative peak area of hPTH (1-34) extracted from plasma using the 30 mg sorbent size. For both BP-PTH and hPTH (1-34), relative peak areas were significantly larger when using the 30 mg sorbent size compared with the 60 mg sorbent size (p<0.001). As 30 mg sorbent size requires elution with 250 μL of elution agent in comparison to 500 μL, meaning the collected samples from the 30 mg sorbents should have approximately double the concentration. The approximate 50% difference in relative peak areas between the two sorbent sizes is confirmatory of this principle. Findings are summarized in Figure 2.16.
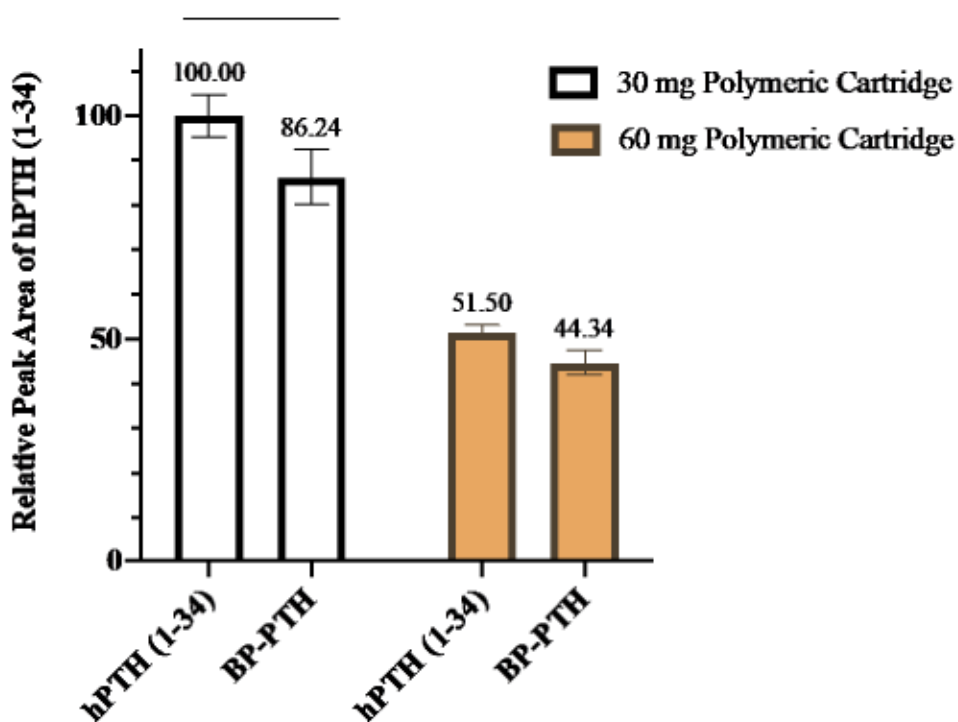
Figure 2.16: Relative peak area of BP-PTH and hPTH (1-34) using two different SPE sorbent bed mass for a polymeric Strata-X™ artridge. Recovery for both analytes was significantly higher (p<0.0001) when using the 30 mg sorbent bed mass in comparison to the 60 mg sorbent bed mass. Recovery for hPTH (1-34) was the highest (100) and the peak areas of the analytes in both groups were compared to the average peak area of hPTH (1-34) extracted using the 30 mg sorbent bed mass. Values represent mean ± standard deviation (*n*=3 replicates), *** p <0.001.

2.18.3 Partial Method Validation

The optimized method outlined in section 2.17 underwent partial method validation to determine if the method is suitable for quantifying BP-PTH in rat plasma for future pharmacokinetic studies. The method was partially validated in accordance to the EMA guideline on bioanalytical method validation to determine acceptability (195). The linearity, accuracy and precision, specificity/selectivity, stability in various conditions, and sensitivity was evaluated.

Complete method validation was prevented due to irreversible clogging of the RP-C18 column which is explained further in section 2.3.12. Full validation will be performed after the publication of this thesis with a new column.
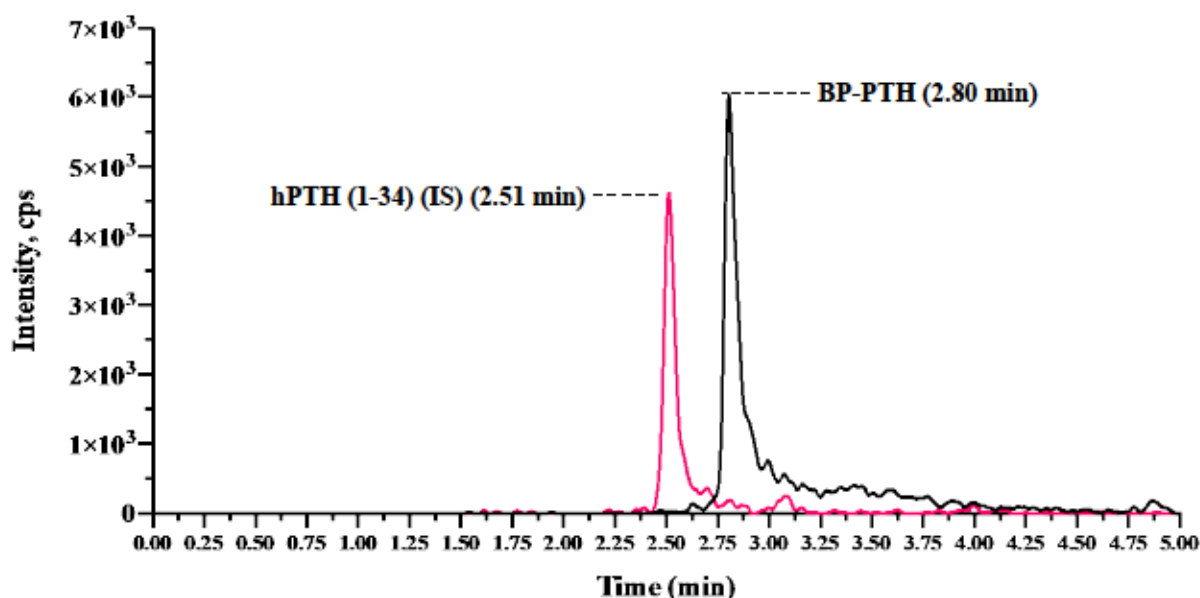
Figure 2.17: HPLC separation of BP-PTH (20 ng/mL) and internal standard (12.5 ng/mL) from an extracted plasma sample using the optimized method conditions. The method ultimately suffered from poor peak shape due to peak tailing that became more significant at the higher concentration levels of BP-PTH. The IS is also susceptible to moderate peak tailing (less extensive than BP-PTH).

94

2.18.4 Selectivity/Specificity

The bioanalytical method is said to be selective if it is capable of differentiating the IS and the analyte of interest from endogenous compounds present in the matrix (195). The method needs to be selective enough to distinguish the analyte at the LLOQ with confidence from endogenous compounds that may coelute at or near the retention time of the analyte. For specificity to be satisfied, the method must be capable of measuring the analyte "unequivocally: in the presence of other compounds (195). It is recommended to assess selectivity by individually evaluating for interference using at least six individual sources of plasma (195). In this study, pooled plasma (100 mL total) from an undisclosed amount of Sprague Dawley rats was used for all experiments. Additional sources state that if the bioanalytical method is capable of maintaining selectivity across all runs, then fewer than six plasma sources may be used (212). However, this is not stated within the guidelines of the EMA.

Results

Over the course of all validation runs, the selectivity of the assay satisfied the EMA requirements for selectivity by successfully differentiating the IS and BP-PTH from endogenous components at the LLOQ. As per EMA guidelines, at the LLOQ, interfering component response is less than 20% of the BP-PTH response and less than 5% for the IS. EMA criteria was also met when analyzing a 2.5 ng/mL sample of BP-PTH, further demonstrating that the developed bioanalytical method is within acceptable EMA criteria. Chromatograms; I) show a blank plasma sample, II) a blank plasma sample with IS, III) a 2.5 ng/mL BP-PTH extracted plasma sample, and IV) an extracted plasma sample of BP-PTH at the LLOQ. The spectra's demonstrated the selectivity/specificity of the bioanalytical method in plasma.
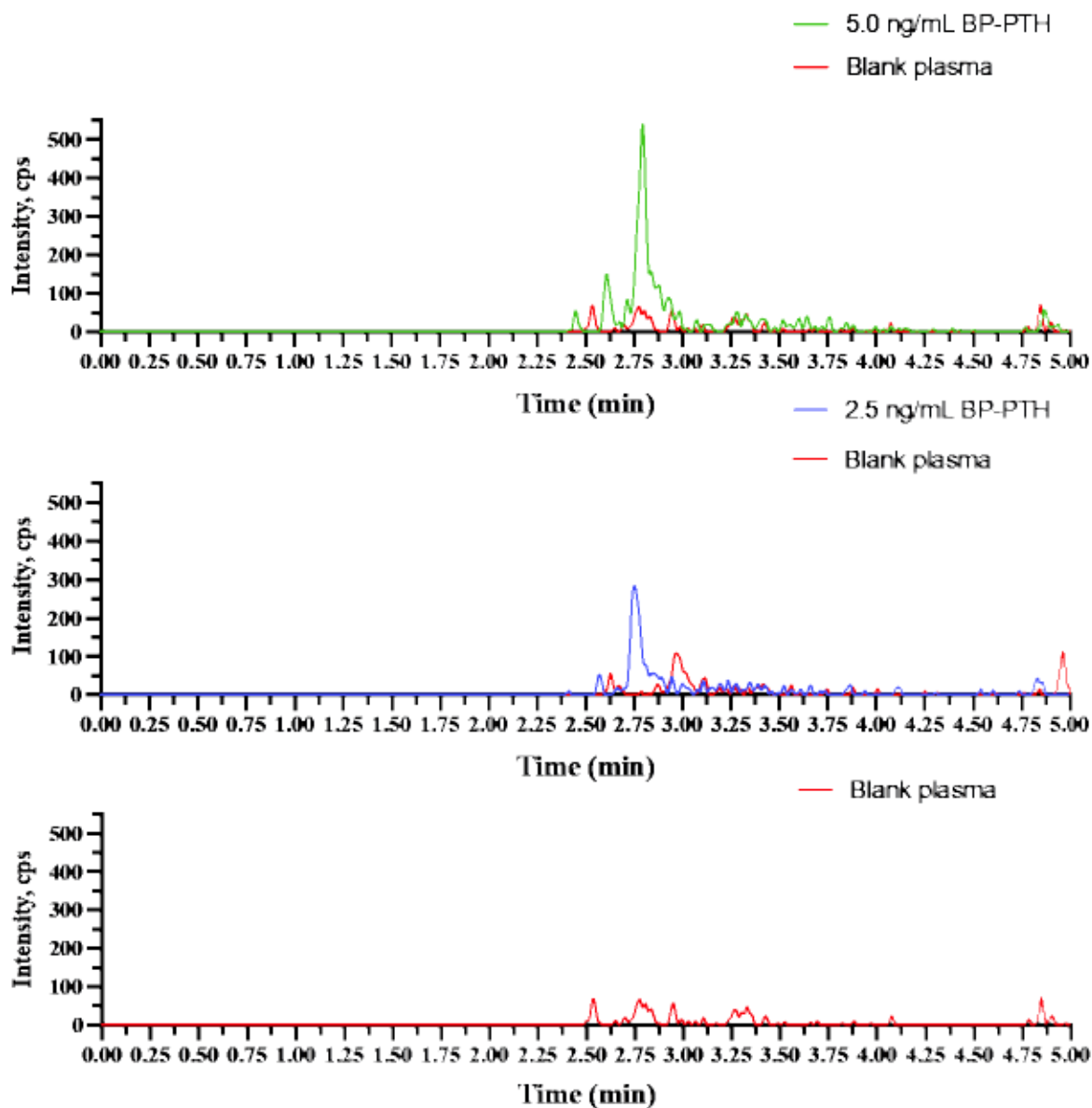
Figure 2.18: Chromatograms of extracted blank rat plasma (I) and BP-PTH extracted from rat plasma at 2.5 (II), and 5.0 ng/mL, superimposed over different blank plasma extracts to show average endogenous interference.

2.18.5 Carry-over

During initial method development when working with high concentrations (500 ng/mL), a large carry-over effect was observed for both BP-PTH and the IS. Though the carry-over effect was much more pronounced at high concentrations well outside of the upper limit of quantification, extensive column wash/equilibration steps and autosampler needle washes were employed. The autosampler needle washes were performed as an extra precaution to reduce BP-PTH carry-over between runs from the autosampler needle, as a bioinert needle was not available for use in this study.

After each analytical run, an injection of 40μL of ACN from a separate wash vial was used to minimize any BP-PTH that may be adhering to the outside of the autosampler needle. The wash method consisted of gradient elution using the following gradient program (%B/min): 95/0.0, 95/3.5, 15/4.5, 15/5.00. Mobile phase A was deionized water with 0.1% FA and mobile phase B was ACN with 0.1% FA.

After extensive column and autosampler needle washes, carry-over was reduced substantially. Carry-over in a blank plasma sample following the highest concentration standard, was determined to be 5.41% of the average LLOQ response. This is in accordance with EMA guidelines that state that carry-over should not exceed 20% of the LLOQ response.

2.18.6 Linearity

The method is deemed to be linear if the analyte response is related to the concentration of the analyte in a proportional manner within the determined calibration curve range. The calibration curve was generated by plotting the ratio of the peak area of the analyte over the ratio of the peak area for the internal standard, against concentration.

Linearity can be assessed visually if the calibration curve forms a linear line increasing away from the LLOQ concentration. Statistically, linearity is determined by calculating the correlation coefficient of regression (r^2) and shows the y-value variance from the linear regression line. The larger the variance from the linear regression line, the lower the r^2 value will be. The r^2 value is between 0 and 1.0, with a r^2 value representing a "perfect" fit with no y-value deviation, indicating that the analyte signals are well correlated with the actual concentration of the analytes.

Results

As the method described in this chapter will eventually be used for pharmacokinetic studies, our goal was to achieve the lowest levels of quantification that we could while generating a linear calibration curve. For extracted plasma samples, the curve was determined to only be linear over a very narrow range (5 ng/mL to 25 ng/mL). Outside of this range, the curve became quadratic. The mean correlation coefficient of regression (r^2) was 0.996. To determine if any weighting was required, the residual errors of the calibration curve were plotted. The residual errors were randomly distributed with no apparent trend, indicating that an unweighted linear regression was appropriate and the data can be modeled with a straight-line relationship.

To evaluate the response-concentration relationship outside of the narrow linear range, a calibration curve from 2.5 ng/mL to 100 ng/mL using three replicates per concentration level in neat solution (without IS) was created. A quadratic fit with 1/x weighting was applied with an r^2=0.998. Chambers et al. performed method validation on hPTH (1-34) using LC-MS/MS and were required to utilize a quadratic fit with 1/x weighting (187). Chambers et al. extensively explored potential reasons for requiring a quadratic fit. They explored sample carry-over, interference at analyte retention time, shift in charge state distribution with increasing analyte concentration and shallowing the gradient and concluded these were not reasons explaining the need for quadratic fit (187). As we are working with a modified variant of hPTH(1-34), their explanations for the quadratic fit cannot be entirely applied to explain the exponential response of BP-PTH. Potential explanations for this trend need to be evaluated in further studies.

The r^2 value greater than 0.99 in both cases suggest that the analyte response is correlated with the actual concentration of BP-PTH. Over the defined range of 5 to 25 ng/mL from extracted plasma samples one can directly predict the concentration of BP-PTH.
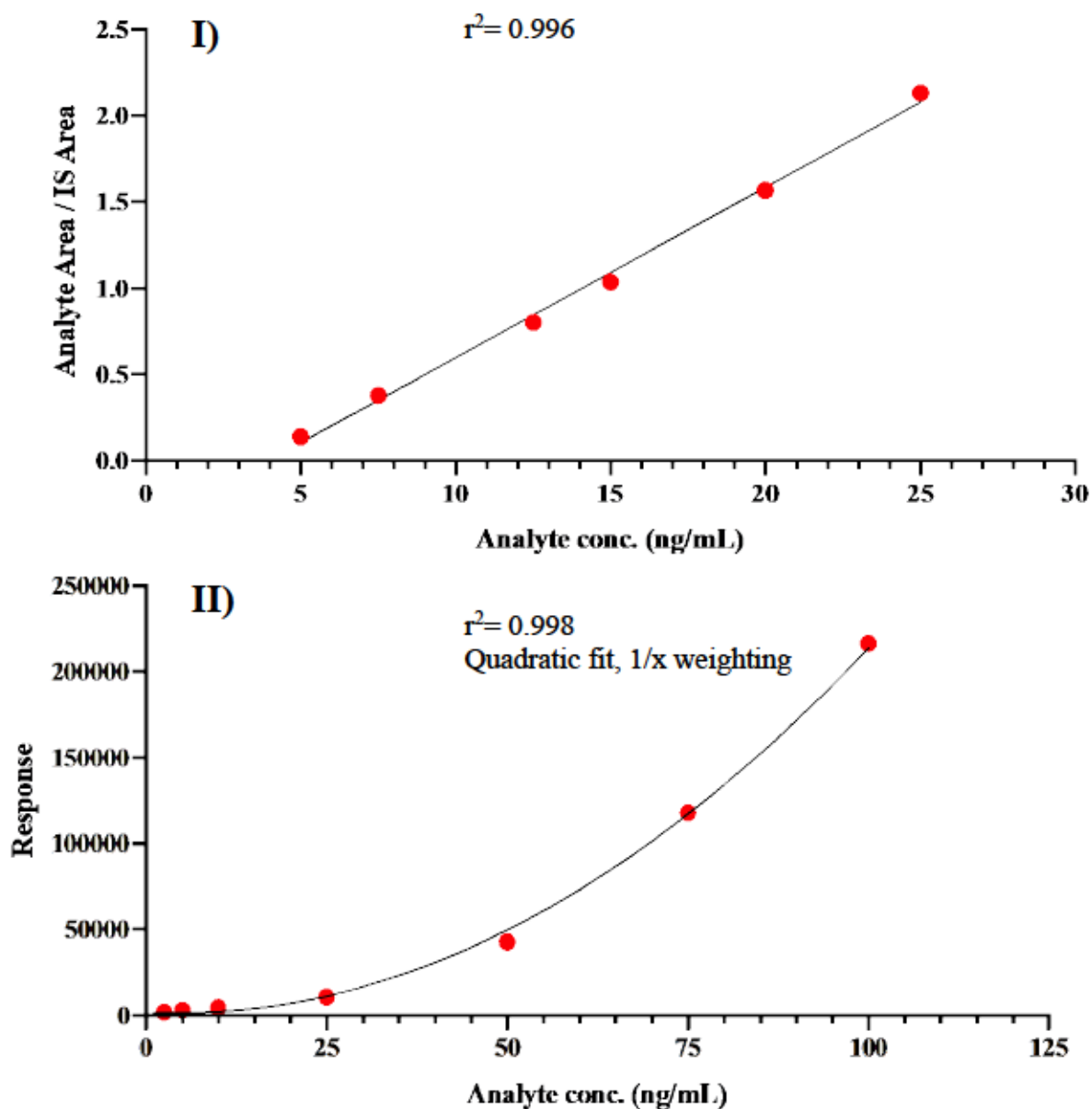
Figure 2.19: Representative standard curve of BP-PTH extracted from rat plasma from 5 to 25 ng/mL (I) and in neat solution (II) from 2.5 to 100 ng/mL.

2.18.7 Accuracy and Precision

Accuracy and precision were determined using the four QC levels in replicates of five, prepared from separate batches over two separate days. A full validation of accuracy and precision is required by EMA guidelines to be completed over three separate days from three separate batches. A partial validation for accuracy and precision was performed due to irreversible column clogging mid-way through the third and final validation run. Alongside the five replicates at each QC level, a fresh calibration curve was also generated. Concentrations, percent error (accuracy) and percent coefficient of variation (precision) for the QC samples were determined by interpolating from the calibration curve. Intraday and inter-day (2 days) accuracy and precision was determined.

2.18.7.1 Intra- and inter-day accuracy and precision

The results of the two analyzed batches on separate days are shown in Table 2.11. The nominal concentration is the theoretical concentration of the prepared QC samples. The mean inter-day error and CV% in rat plasma was less than 2.25% and 4.70%, respectively (Table 2.11). The validation data demonstrates a precise and accurate analytical method with low bias. EMA guidelines state that % accuracy and precision (CV%) for all concentration levels in intra-day and inter-day batches should be within 15% of the nominal concentration, with the exception of the LLOQ being within 20% (195). All replicates (n=5) for each QC level over two separate days confirm to the EMA guidelines. In all cases, intra-day and inter-day error and CV% was less than 10%, well within EMA guidelines. The validation data demonstrates an accurate and reliable bioanalytical method to detect BP-PTH in rat plasma.

As mentioned in section 2.16.5, one validation run was performed using the 687.30 → 159.10 transition for the IS. In this run, error and CV% was below 15% at all QC levels and the correlation coefficient of regression was 0.995. Unfortunately, due to using a different MRM transition, this data cannot be included as the third and final day of validation.

Table 2.11: Validation data for intraday and inter-day accuracy and precision for BP-PTH in rat plasma, n=5

Nominal concentration of BP-PTH (ng/mL)	Intraday		Interday		
	Mean ± SD, ng/mL (CV%)		Mean ± SD, ng/mL	CV (%)	Error (%)
5.0	5.51 ± 0.30 (5.40)	4.66 ± 0.43 (9.33)	5.08 ± 0.37	7.35	1.71
7.5	7.85 ± 0.14 (1.76)	8.35 ± 0.32 (3.79)	8.10 ± 0.23	2.78	8.04
12.5	11.159 ± 0.44 (3.93)	13.46 ± 0.32 (2.40)	12.31 ± 0.38	3.16	-1.52
20	20.35 ± 0.62 (3.05)	19.91 ± 1.56 (7.85)	20.13 ± 1.09	5.45	0.65

2.18.8 Detection and Quantification Limit

2.18.8.1 Limit of detection (LOD)

The LOD is defined as the lowest amount of analyte that can be detected by the assay. At this concentration, the response of the analyte is not required to be quantifiable, only detectable. The limit of detection can be calculated using the residual standard deviation of the regression line (σ) and the calibration curve slope (S) (213). Equation 11 can be used to determine the LOD:

$$LOD = 3.3 \left(\frac{\sigma}{S} \right)$$ **Equation 11**

σ= standard deviation of response

S= calibration curve slope

Though the equation is based on the standard deviation of response and the calibration curve slope, it is also derived from the "signal-to-noise ratio." At the LOD, the signal-to-noise ratio that is deemed acceptable is between 3 or 2:1 (195).

For Equation 11 to be applied, a few assumptions have to be met. The calibration curve needs to show linearity in the range of the anticipated LOD, the response values of the samples are required to be independent and normally distributed and there is variance homogeneity in the range of the calibration curve (213). In many cases, these conditions cannot be perfectly satisfied, so the estimated LOD should be considered with a small degree of error.

Results

Using the calibration curve of extracted plasma samples with 5 replicates per QC level and Equation 11, the LOD for extracted plasma samples was determined to be 1.88 ng/mL.

To test the accuracy of this calculation, five replicates of BP-PTH extracted from rat plasma at 2.5 ng/mL were analyzed. Figure 2.21 shows a chromatogram of BP-PTH extracted from rat plasma at 2.5 ng/mL.
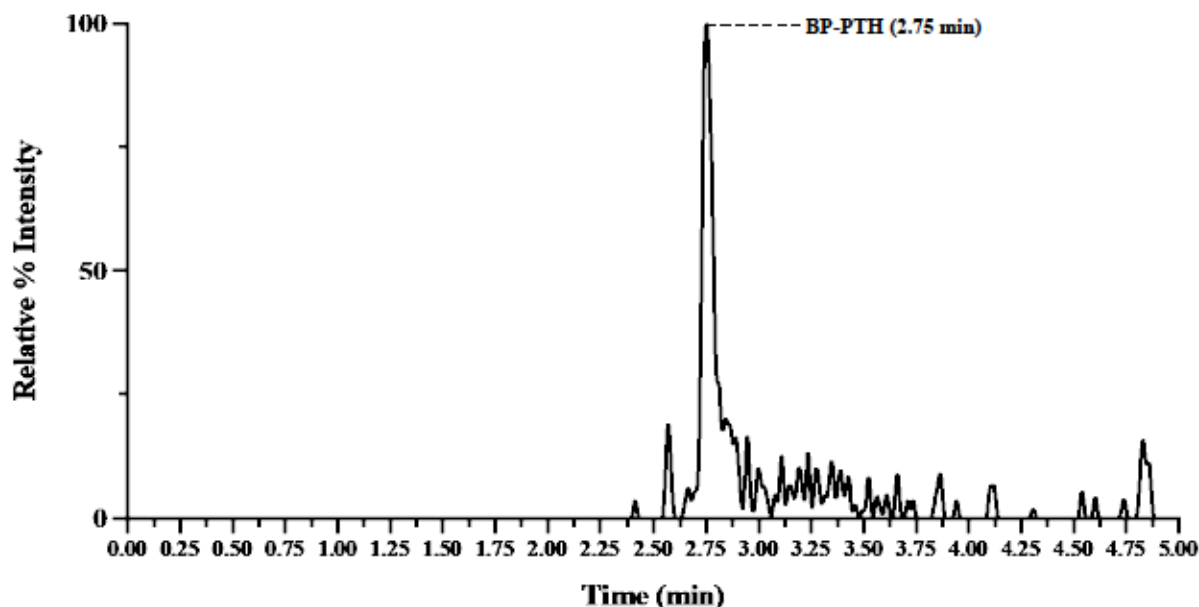
Figure 2.20: Chromatogram of rat plasma extracted BP-PTH at 2.5 ng/mL.

Despite the chromatogram showing an intense peak with acceptable peak shape, the other 4 replicates were similarly intense, but suffered from much worse peak shape. The poor peak shape of the other replicates made integration difficult and inaccurate. In neat solution, concentrations lower than 2.5 ng/mL (1.0 ng/mL, 0.75 ng/mL, and 0.5 ng/mL) were tested and no proportional relationship between analyte response and concentration was found.

2.18.8.2 Limit of quantification (LOQ)

The limit of quantification (LOQ) also referred to as the LLOQ, is defined as the lowest concentration of analyte that can be accurately quantified. The LOQ/LLOQ is the lowest concentration value on the calibration curve. At this concentration, peaks should be able to be unequivocally and demonstrate reproducible precision and accuracy (195). Furthermore, it is required that the response at the LOQ is at least five times larger than the blank response. The typically accepted signal-to-noise ratio is 10:1 (195). A similar equation to the LOD equation can be used to calculate the estimated LOQ.

The LOQ equation requires the same assumptions as the LOD equation and is also based on the standard deviation of response (σ) and the slope of the calibration curve (S). Equation 12 can be used to calculate the LOQ:

$$LOQ = 10.0 \left(\frac{\sigma}{S}\right) \qquad\qquad \textbf{Equation 12}$$

σ= standard deviation of response

S= calibration curve slope

Results:

Using the calibration curve of extracted plasma samples with 5 replicates per QC level and Equation 12, the LOQ for extracted plasma samples was determined to be 5.69 ng/mL. This calculation has slight discrepancies with the actual results obtained in the validation experiments. At 5.0 ng/mL, peaks were reproducible, unambiguous and able to be quantified with confidence. Experimentally, the true LLOQ is likely between 3.0 ng/mL and 5.0 ng/mL.

2.18.9 Recovery

Recovery of the analyte and IS from rat plasma will be assessed by comparing peak area ratios of extracted QCs at L, M and H to the peak areas of the same QC levels spiked into extracted blank plasma solutions. Equation 4 will be used to calculate the percent recovery at the three QC levels. Percent recovery of the internal standard will only be assessed at the internal standard concentration (12.5 ng/mL) and not L, M and H levels. Due to irreversible column

clogging mid-way through validation, recovery was not able to be determined. Recovery for BP-PTH will be determined with a new and more suitable analytical column.

2.3.10 Matrix Effect

Matrix effect is evaluated to determine if the components in the matrix may alter the ionization efficiency of BP-PTH through ion suppression or enhancement. In accordance with EMA guidelines on calculating matrix effect, Equation 1 will be used to calculate matrix effect. To assess matrix effect, the peak area of the analyte in pure solution is compared to the peak area of the analyte spiked into processed blank plasma. Matrix effect will be evaluated at both the L and H QC levels, in replicates of three. Due to irreversible column clogging mid-way through validation, matrix effect was not able to be determined. Matrix effect will be determined with a new and more suitable analytical column.

2.18.11 Stability

Short-term stability experiments were performed at various conditions. These included post-preparative stability (48 hr), autosampler stability (48 hr), freeze thaw stability (three cycles of -80 °C to RT), and stock solution stability (8 hr at RT and 5 days). Determining benchtop (8 hr at RT) stability of processed samples was planned, but was unable to be performed due to the column issues explained in section 2.3.15. Long-term (30 and 60 day) stability was in the process of being conducted as this thesis was published. As previously collected pharmacokinetic samples have been stored at -80 °C, long-term stability samples were stored in -80 °C. All stability experiments were carried out using L and H concentration values in replicates of three (except for IS stability, a 200 ng/mL solution was tested, n=3).

To assess stability of the analyte and the IS in varying storage conditions, the initial peak area response after preparation (T_0) was compared to the response of the same sample that had been subjected to the corresponding storage conditions (T_x). Using Equation 11, a percent ratio was calculated to assess sample stability:

$$\% \ Ratio = \left(\frac{Peak \ Area \ Response \ of \ T_x}{Peak \ Area \ Response \ of \ T_0}\right) \times 100\% \hspace{2cm} \textbf{Equation 13}$$

T_x = Response after storage conditions

T_0 = Response immediately after preparation

2.18.11.1 Post-preparative stability

Post-preparative stability was assessed by re-analysis of freshly prepared and measured L and H QC samples that had been refrigerated at 4 °C for 48 hr. This stability condition was evaluated to determine the stability of the analyte and IS of a post-preparative sample. Suitable stability in post-preparative conditions is desirable for large batch studies, where it may not be feasible to analyze all samples in a working day, but over the course of a few working days instead. It is imperative that if prepared samples are not to be analyzed in a prompt manner, then the post-preparative stability conditions need to be known.

Results

Re-analyzed samples were compared against a freshly generated calibration curve to determine any potential concentration changes between the initial and re-analysis of the samples after 48 hr storage at 4 °C. The mean concentration of the replicates after the treatment conditions were compared to the calibration curve. The accuracy data was within 5% of the nominal concentration for both the L and H QC levels and the mean precision data for both concentrations was less than 3.5%. This data shows that samples are stable for at least 48 hrs in 4 °C conditions. Results are summarized in Table 2.12.

Table 2.12: Post-preparative stability for BP-PTH after 48 hr in 4 °C, n=3

Storage condition	Sample	Nominal concentration (ng/mL)	Mean concentration (ng/mL)	SD	CV (%)	Accuracy (%)
48 hr at 4 °C	L QC	7.50	7.22	0.26	3.53	98.84
48 hr at 4 °C	H QC	20.00	19.04	0.63	3.33	95.44

2.18.11.2. Autosampler stability

Autosampler stability was assessed by re-analysis of freshly prepared and measured L and H QC samples that have been stored on the autosampler for 48 hr. The autosampler temperature was maintained at 15 °C. Evaluating on-instrument stability (autosampler) was performed to determine if any changes may occur to samples over the duration of long analytical runs (large batches). As it is usually most efficient to prepare all analytical samples at once and then run together with no-machine idle time, the stability of samples on the autosampler needs to be determined.

Results:

The mean concentrations after 48 hr in the autosampler at 15 °C for three replicates at both QC levels was determined using a freshly generated calibration curve. The accuracy data was within 5% of the nominal concentration for both the L and H QC levels. The mean precision for both the L and H QC values was larger than the precision values for samples stored at 4 °C for 48 hr. The precision values were 5.25% and 13.78% for L and H QC levels, respectively. The increase in CV% for these samples may indicate that samples are less stable with increasing temperature. As both accuracy and precision are within 15%, the data shows that samples are stable for at least 48 hrs in the autosampler at 15 °C. Results are summarized in Table 2.13.

Table 2.13: Autosampler stability for BP-PTH after 48 hr at 15 °C, n=3

Storage condition	Sample	Nominal concentration (ng/mL)	Mean concentration (ng/mL)	SD	CV (%)	Accuracy (%)
48 hr at 15 °C (autosampler)	L QC	7.50	7.73	0.40	5.25	103.13
48 hr at 15 °C (autosampler)	H QC	20.00	20.9	2.88	13.78	95.68

2.18.11.3 Freeze-thaw stability

The stability of the analyte was determined after three freeze-thaw cycles. Samples were initially stored at -80 °C for approximately one week and then thawed to room temperature. Once thawed, samples were frozen again for at least 12 hr at -80 °C. This process was repeated an additional two times for a total of three freeze-thaw cycles. After the final cycle, the samples were analyzed and compared against a freshly generated calibration curve.

Results

The mean concentration of the replicates at the L and H determined from a freshly generated calibration curve was used to compare stability after three freeze-thaw cycles. The large standard deviation and CV% values for both the L and H QC levels may suggest sample instability after three freeze-thaw cycles. The mean accuracy at the L QC value was determined to be 113.27%, which may also suggest instability. The mean accuracy for the H QC value was 95.5% which is acceptable, but large standard deviation and a high CV% may indicate instability. As BP-PTH is predominantly a peptide molecule, it would be logical that it would suffer instability over repeated freeze-thaw cycles as peptides are susceptible to temperature changes. Another explanation for these results is that this experiment was one of the last experiments to be conducted before the analytical column became irreversibly clogged. Therefore, this experiment should be repeated in the future with a new column. Results are summarized in Table 2.14.

Table 2.14: Freeze-thaw stability of BP-PTH, n=3

Storage condition	Sample	Nominal concentration (ng/mL)	Mean concentration (ng/mL)	SD	CV (%)	Accuracy (%)
3 freeze-thaw cycles (-80 °C to RT)	L QC	7.50	8.49	1.35	15.90	113.27
3 freeze-thaw cycles (-80 °C to RT)	H QC	20.00	19.1	3.91	20.46	95.5

2.18.11.4 Stock solution stability

Stock solution stability at L and H QC concentrations of the analyte and of the IS was assessed at room temperature for 8 hr and 5 days at 4 °C storage. Fresh stock solutions were prepared in deionized water and assess.

Results

Stability was assessed by determining the peak response of the freshly prepared stock solutions using direct injection. The initial peak area response of the stock solution (T_0) was compared to the peak area response corresponding to the tested stability conditions (T_{6hr} and $T_{5\,days}$). Equation 11 was used to calculate a percent ratio between initial response and after treatment response. All of the samples had a deviation of less than 10% from their initial conditions. A deviation of less than 10% suggests that the stock solutions are stable under these conditions. For both the IS and BP-PTH, the largest deviations occurred after 8 hr room temperature exposure. As both of these compounds are proteins, they should be kept on ice or in the fridge when not in use to prevent degradation.

Table 2.15: Stock solutions stability of BP-PTH and the IS at 8 hr RT and 5 days at 4 °C.

Storage condition	Sample	% Peak Area Response
8 hr at RT	L QC	91.73
5 days at 4 °C	L QC	98.41
8 hr at RT	H QC	94.53
5 days at 4 °C	H QC	104.01
8 hr at RT	IS	92.12
5 days at 4 °C	IS	103.93

2.18.12 Long-term stability

Long-term stability using three replicates of L and H QC samples in plasma at -80 °C is currently on-going at the time of this thesis publication. Long-term stability will be assessed for a 30- and 60-day period and compared against a freshly generated calibration curve.

2.18.13 Sensitivity

Mathematically, the sensitivity of the method was determined to be 5.69 ng/mL and 1.88 ng/mL at the LOQ and the LOD, respectively. Experimentally, the LOD is likely ~2.5 ng/mL and the LOQ between 3.0 and 5.0 ng/mL. For this method, the LOQ was set at 5.0 ng/mL.

2.18.14 Column Performance

At the beginning of the third and final validation run, it was observed that column back-pressure was elevated from the normal operating pressure values for this method. Mid-way through the validation run, the back-pressure continued to rise until the max column pressure limit was reached (5000 psi). The LC-MS/MS flow path was inspected for potential blockages but none were found. The batch was unable to be continued as back pressure became so significant that the PEEK tubing connected to the column inlet was falling out due to the high back-pressure from the column.

2.18.14.1 Column washes

The column was extensively washed over the course of two days in consultation with manufacture recommendations. Washes consisted of overnight washes with 95% ACN at 60 °C, 95% H_2O washes, reversal of the column, ~40 column volume washes with 95% ACN and 0.1% TFA (strong wash) and a 5M urea wash to denature and remove all proteins. The guard column was removed and sonicated in IPA and the filter replaced. The column was tested in three separate LC systems with and without guard column to rule out a blockage in the LC-MS/MS flow path or a guard column issue. In all cases, pressure was consistent across all LC systems and the column remained clogged with no drop-in pressure.

2.3.14.2 Irreversible column clogging

It was concluded that the source of the irreversible column clogging was the accumulation of ionic interactions between the positively charged ligands on the surface of the column and the negatively charged phosphate groups of the BP moiety. The accumulation of these interactions slowly built up column back-pressure, leading to an eventual complete blockage.

The PS-C$_{18}$ column was initially purchased for the analysis of derivatized BP-PTH (neutralized phosphonic acid groups) and was suitable for this application. After failing to achieve adequate sensitivity with derivatized BP-PTH, metal-free LC-MS/MS was explored as an option. As low sensitivity, reasonable retention time and adequate peak shape was established, method validation was continued with this column. Though the column phase is C$_{18}$, the phase contained positively charged surface ligands, which were overlooked. Approximately 250-300 injections were performed using derivatized BP-PTH, with no column clogging issues. When switched to non-derivatized BP-PTH, the column became irreversibly clogged only after ~150 injections.

In addition to column clogging, analysis of earlier ran samples appear to have better peak shape with less peak tailing than samples ran later. The worsened peak shape as the number of injections increased could be explained by the accumulation of phosphate groups binding to the positive ligands.

2.18.14.3 Selecting a suitable replacement column

Due to the challenges of analyzing compounds containing phosphonic acid groups, regular C18 columns will not work due to binding of BP-PTH to the metal surfaces in the column. For this reason, the new column replacement needs to be bioinert. As acceptable separation and MS sensitivity was achieved on a PS-C$_{18}$, a column of similar specifications and phase would be a good starting point when selecting a new column. As the positively charged ligands present in the PS-C$_{18}$ column resulted in a short column life due to irreversible clogging, the new column must not have positively charged ligands.

Perhaps a more suitable column to the bioZen PS-C$_{18}$ column is the bioZen XB-C$_{18}$. This column is also titanium lined (bioinert) and contains the exact same phase as the PS-C$_{18}$ column, without the positively charged ligands. Another alternative is PEEK or glassed lined columns from different manufacturers. Absence of the positively charged ligands would significantly improve column lifetime and prevent clogging after only ~150 injections. An important distinction between these two columns is their differences in column packing. The PS-C$_{18}$ is a fully porous column, while the XB-C$_{18}$ column is a core-shell with a solid inner core.

The differences between fully porous and core shell columns will have differing effects on column performance. For LC-MS/MS applications, determining particle choice can often be

analyte specific. Core-shell columns usually improve resolution required to separate isomers or to separate the target analyte from matrix interference (214). The improved retention achieved by a fully porous column often results in significant sensitivity gains, which may be necessary to reach lower levels of detection (214).

Ideally, the most suitable column will be a non-positively charged, bioinert C18 reverse phase column with smaller particle size, internal diameter and length (2.1 mm x 50 mm with 1.7 or 2.6 μm particle size) to the PS-C_{18} column. Using a column of smaller dimensions will also speed up the re-equilibration step.

2.18.15 Limitations

The largest limitation encountered was the column clogging of the PS-C_{18} column after approximately ~150 injections. The irreversible clogging of the column prevented the recovery, matrix effect, benchtop stability and final inter-day accuracy and precision experiments from being conducted to fully validate the method. Furthermore, the build-up of phosphate groups over repeated injections exacerbated the peak tailing of the BP-PTH peak. A more suitable column should reduce peak tailing.

Though all metal tubing was replaced with PEEK tubing and a titanium lined RP-C_{18} column was used for all analytical runs, there was two small portions of the LC-MS/MS flow path that were metal. Unfortunately, a bioinert autosampler needle compatible with the Shimadzu Nexera X2 SIL-30AC autosampler (Kyoto, Japan) was not available. To address this shortcoming and prevent BP-PTH carry-over from the sample needle, extensive needle washes were employed. However, these washes extended analytical run time and it would be more efficient to use a bioinert autosampler needle and forgo the precautionary autosampler washes.

An additional limitation was the unavailability of a titanium lined guard column compatible with the bioZen PS-C_{18} analytical column. Despite the guard column being small in length (4.00 mm), there was likely unwanted binding of BP-PTH to the metal frits. A rough test to determine the extent of binding to the metal frits was employed by running a neat solution of BP-PTH with guard column, cleaning the column and then running the same neat solution without the metal guard column. This process was repeated twice and there was no noticeable difference in peak area response values. Furthermore, during carry-over studies, when the guard

column was removed and a blank injected, the carry-over was still present. This indicated that the guard column was likely not the source of carry-over and rather the column was.

A final limitation encountered was the lack of a more suitable internal standard. The peptide moiety of the conjugate is identical in structure to the internal standard used and therefore there may be a potential "additive" effect on the IS peak response due to metabolism of the conjugate. As there is currently no information regarding the exact metabolites of BP-PTH, to prevent any additive effect, it is more suitable to use an IS that is not a potential metabolite of the parent drug. If hPTH (1-34) is a metabolite of the parent drug, then there would be an uncontrollable "additive" effect on the IS response, which undermines the requirements of an IS to be consistent and of known concentration. Failing to have a consistent IS would greatly impact the accuracy of the detection method. A more suitable IS would be hPTH (1-38), as it is not a potential metabolite of BP-PTH and would behave very similar to hPTH (1-34) during extraction, chromatographic separation and MS analysis.

2.18.16 Future Directions

Testing other titanium or PEEK lined bioinert columns should be the first step towards improving the proposed method. Fully porous vs. core-shell columns should also be compared in an attempt to strike a balance between acceptable MS sensitivity, efficient run time, peak shape and column lifetime.

Though Chambers et al. have reported a highly optimized protein precipitation (~95% recovery) strategy for the recovery of hPTH (1-34) in plasma (187), recovery of BP-PTH and the IS needs to be determined within our laboratory using their protocol. It may also be worthwhile to experiment with acid modified acetonitrile and variations of the amount of organic solvent used to achieve the highest possible recovery of BP-PTH. Though BP-PTH is similar to hPTH (1-34), the presence of the BP moiety may require slight variations to Chambers et al.'s optimized protocol to maximize recovery of BP-PTH.

Increasing the reproducibility and efficiency throughout all method stages (sample preparation, chromatographic separation and MS analysis) can always be performed, and should be performed to further refine and optimize the assay. For studies with large samples, it may be more practical to use a Strata-X™ 96 well SPE plate rather than cartridges. Use of a 96 well

plate for extraction would greatly increase method efficiency. The Strata-X™ SPE plate requires lower elution volumes (200 μL vs. 250 μL) which would increase method sensitivity.

If lower levels of quantification are required for pharmacokinetic studies, transitioning the method to a triple quadrupole MS instrument with higher sensitivity or further concentration of the SPE extract may allow for lower levels of quantification. Performing dry-down or evaporation of the extract for further concentration could be explored. This step should be evaluated with care as evaporation of extracts containing peptides often result in large peptide loss due to inefficient re-solubilization and adsorption to surfaces (210).

A new full method validation will be performed in the coming weeks after this thesis has been published using a new analytical column.

2.18.17 Conclusions

We have developed a LC-MS/MS method for the detection of BP-PTH in rat plasma for future pharmacokinetic experiments. The method had satisfactory accuracy and precision between with acceptable linear response (r^2=0.996) between 5.0 ng/mL and 25.0 ng/mL. The experimentally determined LOD was 2.5 ng/mL. hPTH (1-34) was used as an internal standard during method validation and development. A combination of protein precipitation and solid-phase extraction using a polymeric sorbent resulted in analytical samples with low levels of plasma interference. Sample preparation was relatively efficient, with 30 samples being prepared in under 1 hr. Despite achieving suitable validation parameters, the PS-C$_{18}$ column proved to be unsuitable for large sample batches at it has a short lifetime of 150-200 injections before becoming irreversibly clogged due to ionic interactions between the analyte and positively charged ligands.

Chapter Three

Attempting to enhance BP-PTH sensitivity in MS using trimethylsilyldiazomethane (TMSD) as a derivatization agent.

3.1 Trimethylsilyldiazomethane

Trimethylsilyldiazomethane (TMSD) is an organosilicon compound with the chemical formula $(CH_3)_3SiCHN_2$. TMSD is classified as a diazo compound and is regularly used as a methylation agent for phosphonic acids, carboxylic acids, alcohols, and polyphenols. Chemistry involving TMSD is usually performed in a methanol solution as an instantaneous methylation agent. In comparison to its alternative diazomethane, TMSD is favourable as it commercially available, cost effective, non-explosive and less toxic, while still possessing similar methylation efficiency. An additional advantage of TMSD is stability under recommended storage conditions, whereas diazomethane needs to be prepared fresh for every use. TMSD is a yellow gas that is most commonly dissolved in solvent, such as 2M diethyl ether or hexanes and stored under nitrogen gas. Despite TMSD being a safer alternative to diazomethane, precautions are still required when working with this compound such as a well-ventilated fume hood, a full-face respirator, gloves and eye protection.
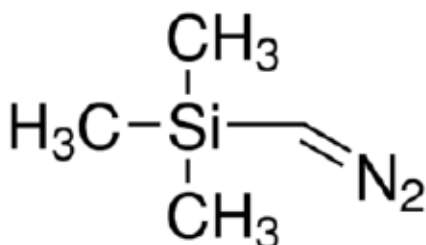
Figure 3.1: Chemical structure of trimethylsilyldiazomethane (TMSD)

3.1.1 Trimethylsilyldiazomethane as a derivatization agent of bisphosphonate-containing compounds

As mentioned in section 2.2.4 of this thesis, bisphosphonates and bisphosphonate containing compounds pose significant challenges for bioanalysis due to numerous factors. To address these challenges, Zhu et al. pioneered a novel approach of performing "on-cartridge" derivatization with diazomethane for the quantitative analysis of bisphosphonates in human plasma using LC-MS/MS (177). Though the original method was applied to only nitrogen

containing BPs (alendronate and risedronate), Zhu et al. postulated that the same method could be applied to non-nitrogen containing BPs as well. Since the methods inception in 2006, numerous groups have utilized their methodology for the successful detection of various different BPs and BP-containing compounds in chromatographic and mass spectrometry systems (164,165,174-180). In recent years, the commercial availability of the safer derivatizing agent TMSD, has resulted in analytical chemists that are following Zhu et. al's methodology, to heavily favour using TMSD over diazomethane prior to chromatographic analysis. Derivatization of the phosphonic acid groups present in BP and BP-containing compounds through methylation essentially "neutralizes" their strong hydrophilic and negatively charged chemical properties and removes their metal chelating abilities. Methylation of the phosphonic acid groups increases hydrophobicity, allowing for improved retention using RP-columns which is necessary for consistent and reliable separation during the LC phase of analysis. Methylation of the negative phosphonic acid groups results in derivatizes with improved volatility that are readily ionized in positive ESI mode, resulting in significantly improved sensitivity of mass spectrometric detection (177).

Using a derivatization agent such as TMSD to methylate BPs or BP-containing compounds successfully addresses the inherent difficulties of performing bioanalysis on these compounds.

Though there are many reports of successful derivatization of phosphonic acid groups, reports on peptide methylation with TMSD are scarce. One group reported that using ethereal diazomethane on small peptides in solution has been shown to produce amino acid artifacts containing *N*-methyl and even *N-N*-dimethyl amino acids (215). Furthermore, trimethylation on the N-terminus of small di- and tri- peptides was achieved with gaseous diazomethane (216), but has not been tested with large peptides yet. Due to the ability of TMSD to methylate carboxylic acids, alcohols and phenols, in theory in addition to N-terminus methylation, serine, threonine, tyrosine, aspartic acid and glutamatic acid could also be methylated as their R groups contain functional groups that could be methylated by TMSD.
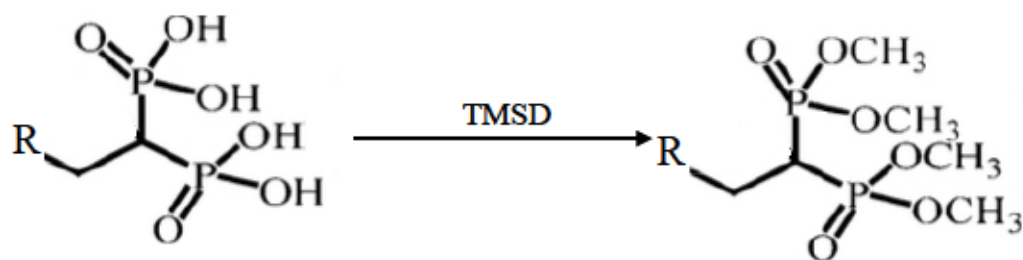
Figure 3.2: Derivatization of phosphonic acid groups using trimethylsilyldiazomethane. Derivatization methylates both phosphonic acid groups to form a tetramethyl derivative.

3.1.2 Trimethylsilyldiazomethane methylation mechanism

Phosphonic acids, carboxylic acids, and alcohols react with trimethylsilyldiazomethane to produce methyl esters in a reaction called methyl esterification. Due to the high reactivity of trimethylsilyldiazomethane, it is produced in-situ as the functional group reacts with TMSD to complete the methyl esterification process. The first step of the mechanism involves an acid-base reaction to deprotonate a phosphonic acid group. The deprotonated phosphonic acid group becomes the nucleophile in an S_N2 reaction with protonated TMSD to produce the methyl ester with nitrogen gas as the leaving group (217). The TMSD reaction is often performed in a methanol solution to suppress the production of acylsilane artifacts (218). Completion of the reaction can be monitored by the disappearance of the yellow colour TMSD and the production of nitrogen gas bubbles. The reaction is relatively quick, with completion being reached around 30 min to 1 hr at room temperature protected from light. Upon completion, acetic acid can be added dropwise to quench unreacted TMSD. Quenching is completed at the complete disappearance of the yellow colored solution and gas evolution ceases (218).

117
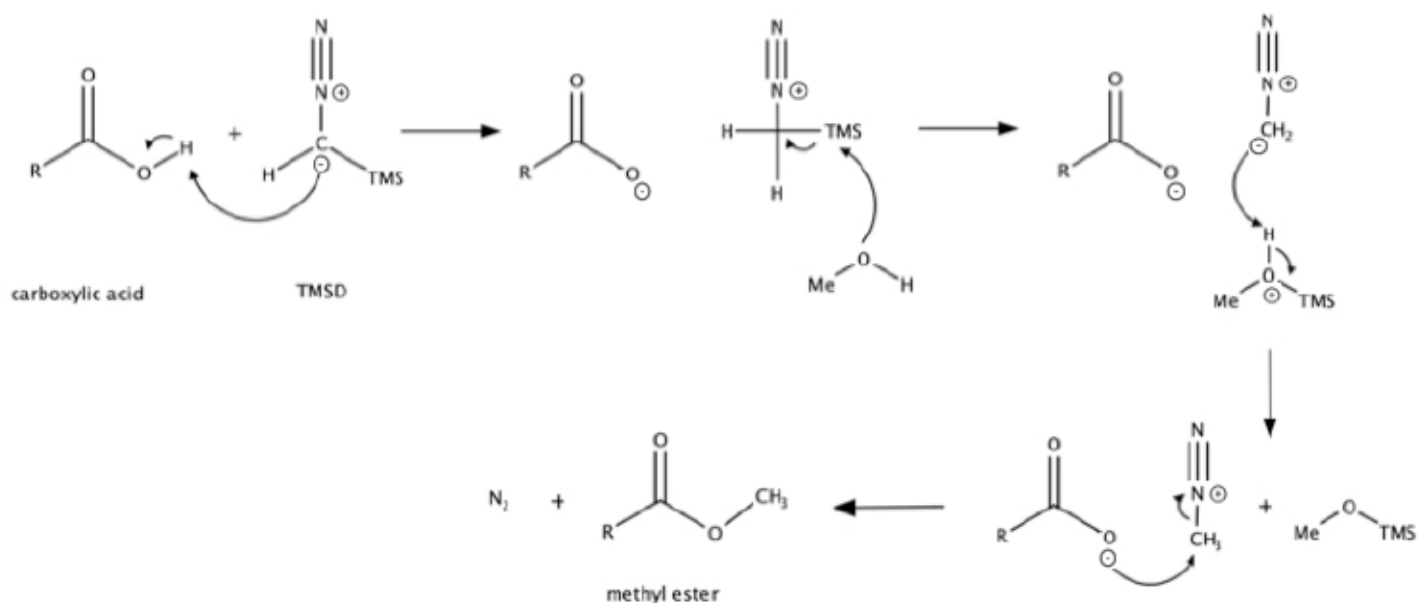
Figure 3.3: Reaction mechanism of the methylation of carboxylic acid functional groups using trimethylsilyldiazomethane (TMSD).

3.1.3 On-cartridge derivatization using trimethylsilyldiazomethane

Performing on-cartridge derivatization offers the benefit of combining derivatization and purification into one single step. Despite some analytical chemists opting for conventional post-extraction derivatization approaches for BPs and reporting satisfactory results (165,177,219), coupling purification and derivatization results in improved derivatization consistency, a reduction in lot-to-lot variability and greater method efficiency. It has been indicated by various reports that a diazomethane or trimethylsilyldiazomethane reaction can be performed efficiently on silica-based solid-phase extraction sorbents (220,221). Underivatized BP-containing compounds bind strongly to the SPE sorbent, isolating the conjugate from the plasma matrix. Methylation of the phosphonic groups with TMSD eliminates the ionic interaction between the sorbent and the conjugate, allowing for the freshly derivatized conjugate to be eluted from the cartridge with methanol. Zhu et al. reported that using an on-cartridge approach

provided much better selectivity and cleaner samples than traditional acidic elution or elution by ionic displacement (177).

Methodology

3.2 Methodology

3.2.1 Objective of Method Development

In an effort to increase MS sensitivity to achieve lower limits of detection (LOD) and quantification (LOQ), on-cartridge derivatization of BP-PTH using trimethylsilyldiazomethane (TMSD) was explored. The objectives of this chapter were to refine the derivatization procedure, determine the most abundant methylation pattern on BP-PTH and establish an MRM method for derivatized BP-PTH.

3.2.2 Using trimethylsilyldiazomethane (TMSD) derivatization to enhance sensitivity in MS Analysis

In an effort to increase MS sensitivity of BP-PTH, derivatization of the phosphonic acid groups was explored. The negative phosphonic acid groups will affect the ionization efficiency of BP-PTH while using ESI+ mode due to their strong negative charges. Methylation of the negative phosphonic acid groups will improve volatility to create derivatives that are readily ionized in ESI+ mode, resulting in significantly improved sensitivity of mass spectrometric detection.

An on-cartridge derivatization approach was explored to potentially enhance the sensitivity of BP-PTH in MS analysis. On-cartridge derivatization combines sample purification and derivatization into one step, increasing the efficiency of the method. Derivatization of the phosphonic acid groups improves column retention during chromatographic separation, reduces sample carryover between runs and enhances sensitivity during MS analysis. The work described by Wong et al. (219) and Zhu et al. (177) for the extraction and on-cartridge derivatization of bisphosphonates from plasma matrix was used as an initial foundation for the development of an extraction method capable of simultaneously extracting and derivatizing BP-PTH. Optimization of the solid-phase extraction and derivatization procedure was performed with 10, 25, and 100 µg/mL concentrations of BP-PTH.

3.2.2.1 Assessing temperature stability of BP-PTH

After BP-PTH extraction from plasma using SPE, the eluent will be evaporated to dryness using a gentle stream of nitrogen gas. Evaporating under elevated temperatures allows for faster and more economical evaporation. Commonly reported evaporation temperatures to prepare BP compounds for LC-MS/MS analysis have been reported at 40°C (165) and 60°C (219). Due to the peptide moiety of BP-PTH, assessing the compounds stability at elevated temperatures will determine if the hPTH (1-34) moiety is susceptible to temperature dependent degradation. Three 1000 ng/mL solutions of BP-PTH were incubated for 60 min at RT, 40°C and 60°C with the intensity of the most abundant precursor ion (979.25 m/z) measured using direct flow injection (0.4 mL/min, 50/50 ACN/water (*v/v*) with 0.1% FA). The experiment was conducted in duplicate. Room temperature evaporation was used for all subsequent evaporation procedures.

Table 3.1: Effect of temperature on average intensity of the BP-PTH 979.25 precursor ion.

Temperature (°C)	Time (min)	Avg intensity of most abundant precursor peak (cps)	Percent change (%)
RT	0	1.33×10^6	0
	30	1.33×10^6	0
	60	1.33×10^6	0
40	0	1.33×10^6	0
	30	6.09×10^5	-54.35
	60	1.24×10^5	-90.71
60	0	1.33×10^6	0
	30	Not observed	N/A
	60	Not observed	N/A

3.2.2.2 Preparation of plasma extracted and non-plasma extracted (neat) samples

BP-PTH stock solution (25 µL) was added to an aliquot of 225 µL of spiked plasma samples to create either 10, 25 or 100 µg/mL solutions. Samples underwent protein precipitation as described in section 2.12. The supernatant was collected and diluted with 1 mL of water

before being loaded onto a pre-conditioned Strata-X™ polymeric cartridge that was washed with methanol (2.0 mL) and conditioned with 2.0 mL of water.

Neat solutions were prepared by addition of 25 μL of BP-PTH stock solution to 225 μL of deionized water creating final concentrations of 1, 25, or 100 μg/mL and diluted with 1 mL of water before being loaded on the Strata-X™ polymeric cartridge (neat solutions did not undergo protein precipitation).

A vacuum manifold was used to apply positive pressure to create consistent and controlled flow-rate through the SPE cartridges. After sample loading, the cartridge was further washed with 2 mL of 5% methanol in water. A methanol:water solution (12:1) was prepared (325 μL) and 175 μL of TMSD was added to the solution and gently shaken. 500 μL of the TMSD:methanol:water mixture was added to the cartridge in a fume hood to perform on-cartridge derivatization in dark conditions. Positive pressure was removed and the eluent was collected in a glass test tube using gravity filtration, evaporated at RT using nitrogen gas and resuspended with 250 μL of H₂O.

3.2.2.3 Optimizing the amount of trimethylsilyldiazomethane for optimal methylation

The amount of TMSD and methanol used to methylate the phosphonic acid groups in BP compounds varies amongst reported methods. Some methods report using a ratio (v/v) of TMSD to methanol as low as 20:80 (165) to as high as 50:50 (219), with the majority of published methods using a ratio between 25:75 to 35:65 of TMSD:methanol. A small amount of water is required as a catalyzer to create diazomethane and nitrogen gas, a commonly used ratio of methanol to water is 12:1 (v/v) (174). To determine which ratio of TMSD to methanol/water during derivatization is most suitable for increasing the yield of methylated hPTH (1-34) and BP-PTH, ratios of 20:80, 25:75, 30:70, and 35:65 (v/v) were tested. The volume of the methanol + water mixture (12:1, methanol:water) was varied between 325 μL and 400 μL. TMSD proportions were adjusted accordingly based on the ratio that was being experimentally tested. 25 μL of 100 μg/mL BP-PTH solution was diluted with 1 mL deionized water and loaded onto a pre-conditioned Strata-X™ cartridge to perform on-cartridge derivatization. The derivatization reaction mixture (TMSD + methanol/water) was prepared by addition of TMSD to the

methanol/water solution and gently shaken. The derivatization reaction consisted of on-cartridge incubation with gravity filtration at RT, with protection from light. Filtrate was collected in a glass test tube. The eluent was injected onto the LC-MS/MS system.

Comparison of peak areas of BP-PTH and hPTH (1-34) under the different ratios (20:80, 25:75, 30:70, 35:65) were used to determine optimal TMSD to methanol/water ratio. Table 3.2 contains a summary of the experimental conditions for the optimization of TMSD to methanol ratio.

Table 3.2: Summary of ratio of TMSD to methanol + water reaction mixture tested to optimize BP-PTH derivatization.

Ratio	TMSD (µL)	Methanol + water reaction mixture (µL)	Total volume (µL)
20:80	100	400	500
25:75	125	375	500
30:70	150	350	500
35:65	175	325	500

*Methanol + water mixture was created using a methanol:water (12:1) *v/v* ratio.

** TMSD was added to the methanol + water reaction mixture to create the derivatization reaction mixture that was added to the SPE cartridges.

3.2.2.4 Incubation time and temperature of TMSD derivatization reaction

After SPE conditioning, sample-loading, washing steps, and addition of the derivatization agent, gravity filtration was used to elute the derivatized BP-PTH from the SPE sorbent under dark conditions at room temperature. It has been previously reported that analytes need to be exposed to the derivatization reagent on the SPE cartridge for 0.5-1 hr for adequate derivatization (174). After ~10-15 min, the 500 µL of reaction mixture was eluted by gravity into a glass test tube, and then re-loaded onto the sorbent bed for additional time to interact with the TMSD reagent. Additional studies show that derivatization also continues in the eluate (174,178), after the second round of elution, the collected eluate was left for an additional 15 mins. The total reaction time was 45 min. Eluate was collected in glass test tubes to prevent plastic leaching from microcentrifuge tubes that may occur as side-reactions to the TMSD

reagent. After 30-45 min, the yellow TMSD solution color disappeared. The disappearance of the yellow TMSD solution indicates that the reaction has gone to completion and no excess TMSD remains. 5 µL of 50% acetic acid in methanol was added to the eluent to quench any remaining TMSD. The eluate was transferred to a vial for LC-MS/MS analysis.

3.2.2.5 Initial chromatographic method development

Initial chromatographic method development utilized the "60/60" determination method as explained in section 2.15.3. The 60/60 determination method consisted of gradient elution using deionized water with 0.1% formic acid (Mobile phase A) and acetonitrile with 0.1% formic acid (Mobile phase B) with a flow rate of 0.3 mL/min. These mobile phases were selected based on successful retention of BP compounds with reverse phase columns using ACN and water with 0.1% formic acid.

Gradient time program was 5% B to 60% B from 0.0 min to 60.0 min. The detector used for the determination of chromatographic conditions was an MS/MS. The MS was set to scan in Q1 and the total ion chromatogram (TIC) plot was used to analyze peak shape and retention times. 5 µL of a 100 µg/mL solution of derivatized BP-PTH (without plasma) was injected into the LC-MS/MS system. Two different columns (Gemini C_{18} and PS-C_{18}) were compared. The observations are summarized below in Table 3.3.

Table 3.3: Observations of initial method development for two different columns in an attempt to chromatographically identify D-BP-PTH.

Column	Stationary Phase	Gradient Conditions (%B/min)	Observations	Remarks
Gemini C18 (250 x 4.60 mm I.D., 5 μm), guard column (4.00 x 3.00 mm I.D.).	Alkyl chains on silica surface	5/0.0 min, 60/60 min.	Appearance of frequently repeating peaks of low intensity between run time of 30 and 35 min, corresponding with a Mobile Phase B% of 30% to 35%. No isolated peak to indicate BP-PTH.	*Not satisfactory.* M/z values of the repeating sharp peaks correspond to theoretical m/z values of D-BP-PTH.
bioZen PS-C18 (150 x 2.1 mm I.D. 3 μm), guard column (4.00 x 2.00mm I.D.).	Alkyl chains on silica surface	5/0.0 min, 60/60 min.	Appearance of frequently repeating peaks of low intensity between run time of 30 and 35 min, corresponding with a Mobile Phase B% of 30% to 35%. No isolated peak to indicate BP-PTH.	*Not satisfactory.* M/z values of the repeating sharp peaks correspond to theoretical m/z values of D-BP-PTH.

Appearance of repeated peaks with m/z values corresponding to theoretical D-BP-PTH m/z values eluting between a Mobile Phase B% between 30% and 35% was further examined to confirm if any of these peaks were D-BP-PTH. A new chromatographic method was established using isocratic flow with 40% Mobile Phase B (acetonitrile with 0.1% formic acid) and a flow rate of 0.3 mL/min with a 5 min run time. Mobile Phase A was 0.1% formic acid in deionized water. The same columns used in the 60/60 determination run were reused. The observations are summarized in Table 3.4.

Background noise is defined as any chemical noise which is generated from all other species other than analytes of interest(s) when being analyzed for the MS detector (222). The average of level of background noise was compared amongst the two columns and determined to

be lower than 1100 cps. When compared to the intensity of the analyte, the average level of background noise was 1625 times lower.

Table 3.4: Observations of initial method development for two different columns in an attempt to chromatographically identify D-BP-PTH using an isocratic gradient.

Column	Isocratic conditions (%B/min)	Flow rate (mL/min)	Retention time (tR) (min)	M aximum levels of background noise (cps)	Intensity of D-BP-PTH (cps)	Observations
Gemini C_{18} (250 x 4.60 mm I.D., 5 μm), guard column (4.00 x 3.00 mm I.D.).	40/5	0.3	3.98	1.1×10^3	1.7×10^5	Peak elution at 3.98 min with predominantly symmetrical peak shape, significant peak tailing.
bioZen PS-C_{18} (150 x 2.1 mm I.D. 3 μm), guard column (4.00 x 2.00mm I.D.).	40/5	0.3	1.44	8.0×10^2	1.3×10^6	Peak elution at 1.44 min with symmetrical peak shape, minimal peak tailing.

*Maximum levels of background noise were measured from 0 to 0.5 min.

The bioZen PS-C18 (150mm x 2.1 mm I.D. 3 μm particle size) column produced better peak shape, minimal peak tailing, shorter retention time, and higher analyte intensity than the Gemini C_{18} column. The maximum levels of background noise were similar for both columns, though was slightly lower for the bioZen PS-C_{18} column. As stated in Chapter 2, the bioZen PS-C_{18} column produced acceptable peak shape when retaining non-derivatized BP-PTH, and was likely to have improved sensitivity than the longer and wider Gemini C18 column. Due to the phosphonic acid groups being neutralized, the Gemini C_{18} was tested to observe how the retention and peak shape of D-BP-PTH would be on a non-titanium lined column.
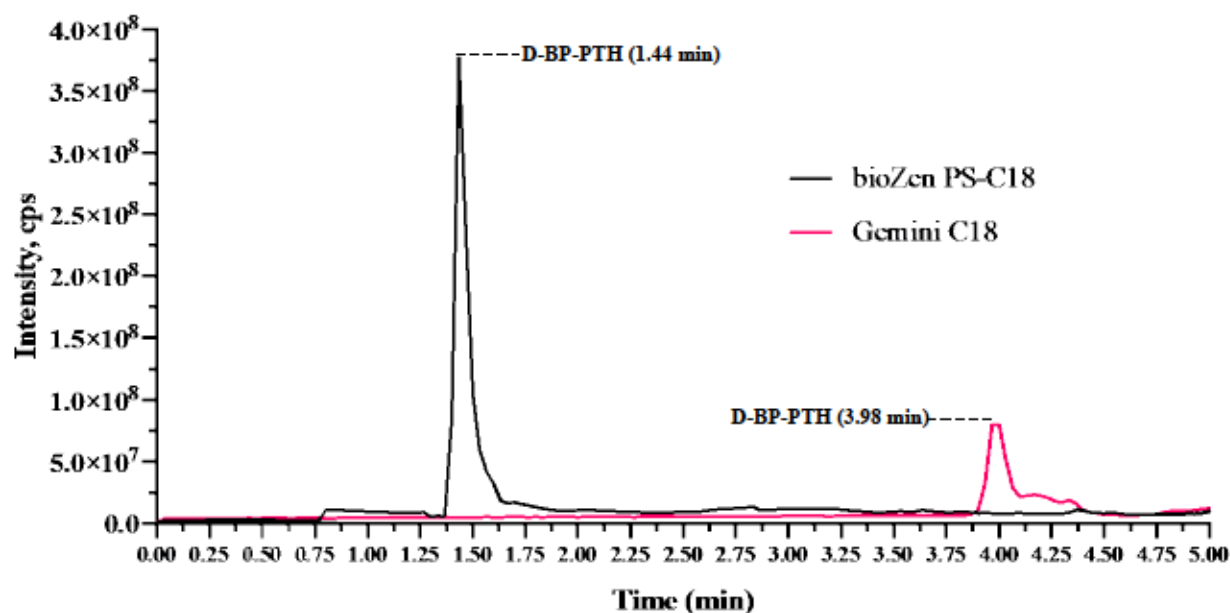
Figure 3.4: Retention of D-BP-PTH on two different reverse-phase C$_{18}$ columns. Concentration of D-BP-PTH was 100 μg/mL with injection volume of 5 μL. Columns used were Phenomenex Gemini C$_{18}$ (250mm x 4.60 mm I.D., 5 μm particle size) with guard column (4 x 3.00 mm I.D.) and Phenomenex bioZen PS-C$_{18}$ (150mm x 2.1 mm I.D. 3 μm particle size) with guard column (4 x 2.00mm I.D.). Flow rate: 0.3 mL/min; isocratic gradient for 5 min using 40% ACN/H$_2$O + 0.1% FA.

3.2.3 Optimization of MS/MS for Quantitation:

3.2.3.1 MS/MS Instrumentation

Liquid chromatography (LC) was performed on a Shimadzu LC system consisting of a DGU-20A SR degasser, Nexera X2 LC-30AD binary gradient pump, Nexera X2 SIL-30AC autosampler and a CTO-20AC column oven (Shimadzu, Kyoto, Japan). The LC system was coupled to a LCMS-8050 triple quadrupole mass spectrometer (Shimadzu, Kyoto, Japan). Analytical data was collected and processed using LabSolutions software (ver. 5.91).

3.2.3.2 Ionisation mode for D-BP-PTH

The ionisation mode selected for quantification of D-BP-PTH was ESI+.

3.2.3.3 Selecting precursor ions for D-BP-PTH

Examining the Q1 fragmentation pattern for D-BP-PTH a suitable precursor ion can be selected to be used in developing the MRM transition. Direct injections of a 1000 ng/mL solution of D-BP-PTH prepared from a neat solution did not produce any suitable precursor peaks as the MS spectra was dominated by peaks in the 300-500 m/z mass range. These peaks are likely contaminants from the on-cartridge derivatization procedure.

A highly concentrated 100 µg/mL and 25 µg/mL sample of D-BP-PTH was prepared using on-cartridge derivatization and the isocratic program for LC separation outlined in section 3.2.2.5. The relative intensities of the peaks were measured, with the most intense peak receive an intensity of 100. The most intense ions were selected as precursor ions for further development of the MRM transition method. A single methylation (-CH$_3$, 14 Da) on BP-PTH is expected to increase the mass of the conjugate by 14 m/z.
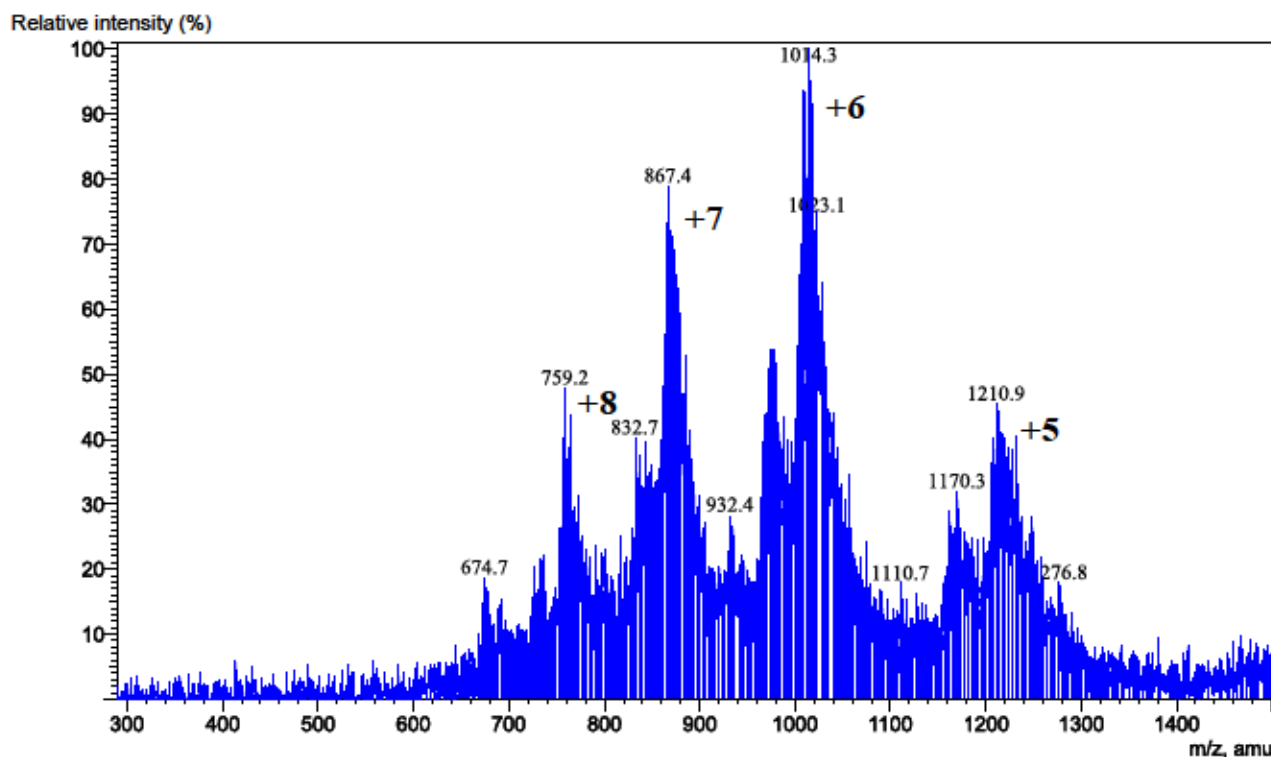
Figure 3.5: MS spectra showing relative intensities of precursor ions for D-BP-PTH. MS spectra of D-BP-PTH precursor ions. The most intense precursor ion (1014.3 m/z) corresponds to +6 charged species of D-BP-PTH that has been methylated 15 times, giving a mass of D-BP-PTH of 6079.6 Da, 210 Da larger than unmodified BP-PTH, corresponding to 15 methylations. The second most abundant precursor ion (867.4 m/z) corresponds to the +7 charged species of D-BP-PTH with 14 methylations, corresponding to a mass of 6064.6 m/z for D-BP-PTH with 14 methylations. The 867.4 m/z precursor ion was selected for further MRM development.

129

Results

The most intense precursor ion (1014.3 m/z) corresponds to +6 charge species of D-BP-PTH that has been methylated 15 times. The addition of 15 methyl groups to BP-PTH increases the mass by 210 Da, resulting in a total conjugate mass of 6079.6 Da in comparison to non-methylated BP-PTH (5869.6 Da). Nearly equally as intense as the 1014.3 m/z ion, was the 1011.7 m/z ion that corresponded to the +6 charged species of D-BP-PTH that had underwent 14 methylations. The second most abundant precursor ion (867.4 m/z) corresponds to the +7 charged species of D-BP-PTH that has undergone 14 methylations. D-BP-PTH that had undergone methylation 14 times was selected as the species to follow in an MRM transition due to the high abundance of both the corresponding +6 and +7 charged ions. The 1011.7 and 867.4 m/z ions were selected as Q1 precursor ions for further MRM development.

The Q1 spectra of both analytes is shown in Figure 3.5, the selected precursor ions for further method development are summarized in Table 3.5.

Table 3.5: Q1 scans to select suitable precursor ions of D-BP-PTH using ESI+ for further MRM method development.

Analyte	Charge (z)	Precursor Ion (m/z)
D-BP-PTH	+7	867.40
	+6	1011.70

3.2.3.5 Establishing and optimizing the MRM transition for BP-PTH and the IS

After selection of suitable precursor ions, suitable product ions (Q3 fragments) need to be determined to establish an MRM transition for D-BP-PTH. The MRM transition conditions were optimized by the same procedure outlined in section 2.16.3 using the "Fully Automated MRM Optimization" program in LabSolutions software (ver. 5.91). The MRM optimization for D-BP-PTH was only conducted at high (270 kPa) CID gas pressure as high CID gas pressure produced the most intense product ions of BP-PTH.

Parameters for the optimized MRM transition for the IS and BP-PTH are summarized in Table 3.6. The MS parameters used can be found in Table 2.9 of section 2.16.5.

Table 3.6: Multiplexed MRM summary for D-BP-PTH.

Analyte	MRM Transitions	Collision energy (eV)	Q1 Pre-Bias (eV)	Q3 Pre-Bias (eV)
D-BP-PTH	867.5 → 738.30	31	20	15
	1011.7 → 1011.7	N/A	N/A	N/A

* The 1011.7 precursor ion did not produce any usable product ions. All product ions generated were under 100 m/z and of very low intensity.

3.2.4 The Optimized Method

The optimized method consisted of using protein precipitation coupled with solid-phase extraction using a polymeric Strata-X™ cartridge. On-cartridge derivatization was performed using 500 μL of reaction mixture (175 μL TMSD and 325 μL of methanol:water (12:1)). The eluate was eluted using gravity filtration and re-loaded onto the Strata-X™ after 15 min for additional time to interact with the derivatization reagent. The derivatization reaction occurred for a total of 45 min in dark conditions and was quenched with 5 μL of 50% acetic acid after 45 min. The eluate was collected, evaporated at RT with nitrogen gas, resuspended in 250 μL of H_2O and 15 μL was loaded onto the LC-MS/MS system. A titanium-lined reverse-phase C_{18} column (A bioZen PS-C_{18} (150 x 2.1 mm I.D. 3 μm) column with guard column (4.00 x 2.00mm I.D.)) was chosen as a suitable stationary phase for the separation of D-BP-PTH. The LC method consisted of gradient elution using the following gradient program (%B/min): 15/0.1, 15/0.5, 95/4.50, 95/6.0, 15/6.0, 15/8.50. Mobile phase A consisted of deionized water with 0.1% formic acid and mobile phase B consisted of acetonitrile with 0.1% formic acid. The flow rate was 0.4 mL/min, column temperature was maintained at 40 °C, autosampler temperature was 15 °C. MRM mode was used for quantification with the following transition: +7 precursor for BP-PTH 867.40 → 738.30. The collision energies for these transitions was 31 eV with a Q1 and Q3 Pre-Bias of 20 and 15 eV, respectively. The MS/MS system consisted of a LCMS-8050 triple quadrupole mass spectrometer and the interface voltage, interface temperature, desolvation line temperature, drying gas flow and CID gas pressure was 4.0 kV, 300 °C, 250 °C, 10 L/min, and 270 kPa, respectively. Analytical data was collected and processed using LabSolutions software (ver. 5.91).

Results & Discussion

3.3 Results and Discussion

3.3.1 Potential methylation sites on BP-PTH

Methylation of the phosphonic acid groups present on BP compounds using TMSD has been widely reported as being an efficient and a consistent reaction that achieves full methylation of the phosphonic groups. The most commonly identified derivatives of BP compounds when reacted with TMSD are tetra- and pentamethyl derivatives. With only four to five potential methylation sites, the methylations on BP compounds are predictable and sites of methylation can easily be identified based off m/z value increases observed in MS spectra.

In comparison to a simple BP compound, BP-PTH has numerous possible sites that can be methylated. There are four possible methylation sites on the BP moiety and a total of nine on the peptide moiety. TMSD is capable of methylation of phosphate groups, carboxylic acids, alcohols and amines. In theory, the amino acids in the peptide moiety: N-terminus, Ser-1, Ser-3, Glu-4, Ser-17, Glu-19, Lys-26, Lys-27, Asp 30 and the C-terminus could all potentially be methylated. In total, there are 16 potential sites for methylation on BP-PTH. It is difficult to predict exactly which sites should be methylated and in which order.

Fei et al. have reported that phosphate groups are alkylated faster than carboxylic acid groups at neutral pH with diazo compounds due to their higher pK_a (6-7 versus 3-4) (223). The pH of the TMSD:methanol/water solution is ~6, it can be stated that phosphate groups will be methylated before carboxylic acid functional groups.

The tertiary structure of the peptide moiety and how the peptide folds in solution plays a large role in determining which amino acid residues would be methylated. Functional groups that are exposed such as the phosphonic acid groups of the BP moiety would likely be methylated first. Functional groups that are buried within the folded protein are less likely to be methylated. The methylation pattern on the peptide portion is further complicated by the lack of literature focused on understanding how TMSD interacts with amino acid residues. It is entirely possible that more or less than 16 methylations can occur on the BP-PTH conjugate, depending on how TMSD interacts with the conjugate.

Modifications of phosphates within large biomolecules using diazo alkylation has been shown to be difficult. Previous work using diazo alkylation of nucleoside monophosphates and nucleic acid oligomers has suffered from poor selectivity; yielding both mono and diester alkylation (223). Ultimately, the lack of specificity of TMSD during the alkylation reaction, the

numerous potential methylation sites on BP-PTH and an unrefined reaction procedure makes it very difficult to achieve consistent and reproducible methylation of BP-PTH.

3.3.2 Using Q1 scans to identify the number of methylations on BP-PTH

The addition of a methyl group ($-CH_3$) to BP-PTH should increase the total conjugates mass by 14 Da. This corresponds to an mass unit increase of 14 in MS spectra. Knowing that the 979.25 and 1175.10 ions correspond to the +6 and +5 charged species of BP-PTH, methylated derivatives of BP-PTH will have larger m/z values that correspond to the +6 and +5 charged species. Direct injections of a 25 µg/mL solution of non-plasma extracted D-BP-PTH did not produce any visible fragments above 500 m/z. It was hypothesized that the spectrum was dominated by contaminates from the derivatization process and therefore LC was used to separate the contaminants and isolate D-BP-PTH. A 100 µg/mL and 25 µg/mL solution of D-BP-PTH were analyzed using isocratic conditions described in Table 3.4 with the bioZen PS-C$_{18}$ column. The spectra generated from Q1 scans of 100 µg/mL and 25 µg/mL solutions of D-BP-PTH shows a large cluster of ion peaks at high relative abundance at the 858 to 869 and 1002 to 1016 m/z range. Abundant ions in the 858 to 869 m/z range correspond to the +7 charged species of D-BP-PTH that has underwent 11 to 15 total methylations. The most abundant ion peaks are in the range of 1002 to 1016 m/z, these ion peaks correspond to the +6 charged species of D-BP-PTH with number of methylations ranging from 10 to 16. Overall, it appears that 14 methylations on the BP-PTH conjugate was the most common methylation pattern. Results are shown in Figure 3.6.
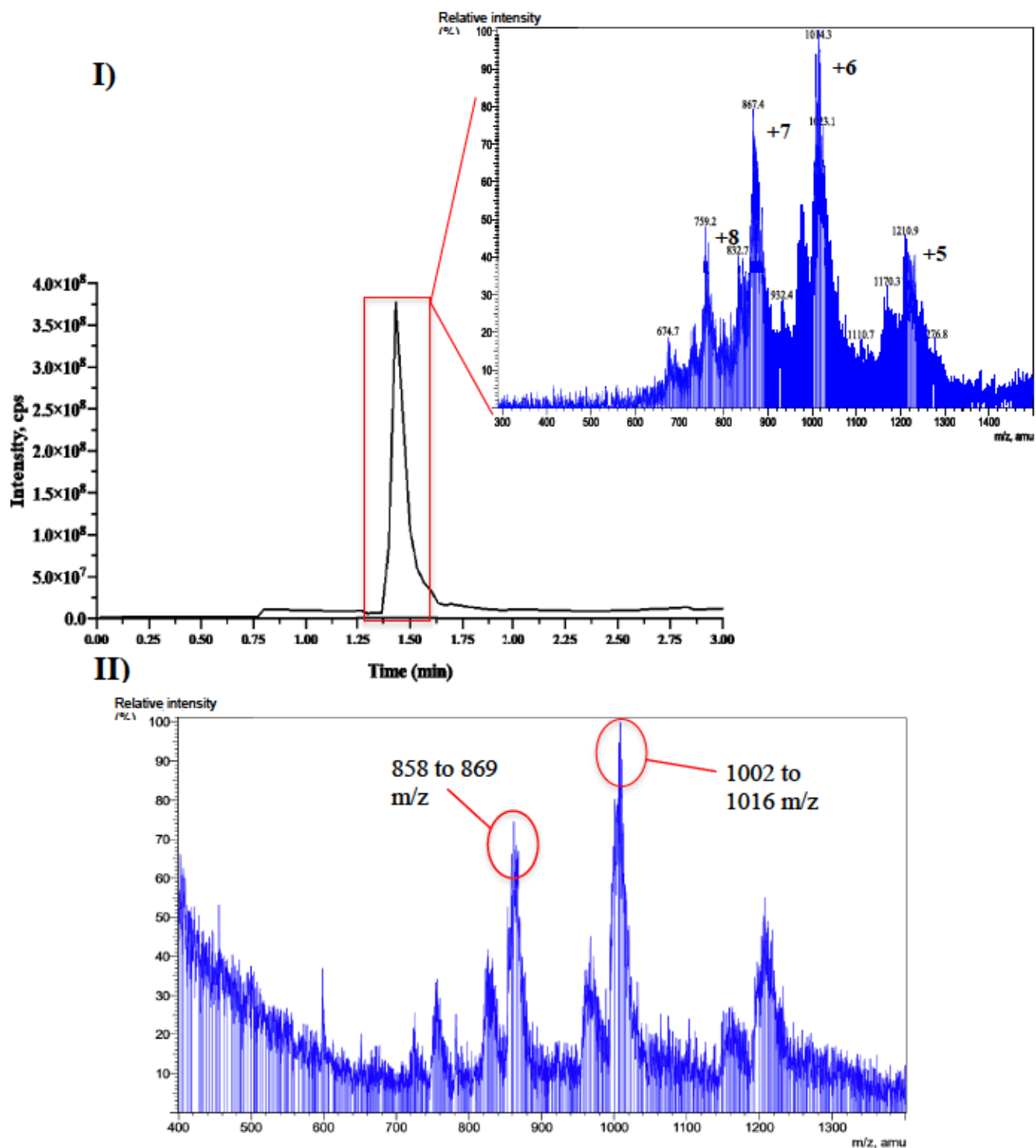
Figure 3.6: MS spectra from Q1 scans showing relative intensities of ions for D-BP-PTH.
I) MS spectra of a 100 µg/mL solution of D-BP-PTH that was separated using LC before MS analysis. The most intense precursor ion (1014.3 m/z) corresponds to +6 charged species of D-BP-PTH that has been methylated 15 times, giving a mass of D-BP-PTH of 6079.6 Da, 210 Da larger than unmodified BP-PTH, corresponding to 15 methylations. The second most abundant precursor ion (867.4 m/z) corresponds to the +7 charged species of D-BP-PTH with 14 methylations. II) MS spectra of a Q1 scan of a 25 µg/mL solution of D-BP-PTH. The cluster of abundant ion peaks corresponds to a m/z range of 858 to 869 and 1002 to 1016 m/z values, respectively.

3.3.3 Determining a sufficient ratio of TMSD to methanol/water for adequate BP-PTH methylation

The ratio of TMSD to the methanol:water (12:1, *v/v*) mixture was varied to evaluate if different ratios could result in more predictable and consistent methylation of BP-PTH. Ideally, if the large majority of all BP-PTH molecules in solution are subjected to the same number of methylations, the "cluster" of ion peaks in the +6 and +7 charged species m/z ranges would decrease and the ion peak corresponding to the dominate methylation pattern would greatly increase in abundancy.

To our knowledge, there is no reported literature for the methylation of BP-conjugated peptides using TMSD. For initial methylation experiments, the published work demonstrating successful methylation of BP compounds was chosen as an initial foundation for method development. Some methods report using a ratio (*v/v*) of TMSD to methanol as low as 20:80 (165) to as high as 50:50 (219), with the majority of published methods using a ratio between 25:75 to 35:65 of TMSD:methanol/water. A small amount of water is required as a catalyzer to create diazomethane and nitrogen gas, a commonly used ratio of methanol to water is 12:1 (*v/v*) (174). In accordance to these established ratios, we tested 20:80, 25:75, 30:70, and 35:65 (TMSD:methanol/water) with a total volume of reaction mixture remaining constant at 500 µL.

To determine the optimal ratio of TMSD:methanol/water, the MRM method established in section 3.2.3.5. All four tested ratios suffered from very poor peak shape and had extremely low product ion peak areas (Figure 3.7). The retention time of these peaks was similar to the retention time of underivatized BP-PTH. A 500 ng/mL solution of D-BP-PTH was also prepared to compare peak area and shape to a 500 ng/mL underivatized BP-PTH sample. Unfortunately, no peaks were observed at all when using MRM mode to analyze the 500 ng/mL sample of D-BP-PTH (data not shown). Failing to observe any successful MRM transitions when analyzing a 500 ng/mL D-BP-PTH sample indicates that the intensity of the precursor ions or product ions was incredibly low and went undetected.

Based on the peak areas and peak shapes of the four different compositions of TMSD reaction mixture used, it was concluded that changing the ratio had very little effect, if any for the derivatization reaction on BP-PTH. All four ratios appeared to generate similar methylation patterns on BP-PTH. A longer retention time for the 20:80 ratio may indicate in-complete methylation.
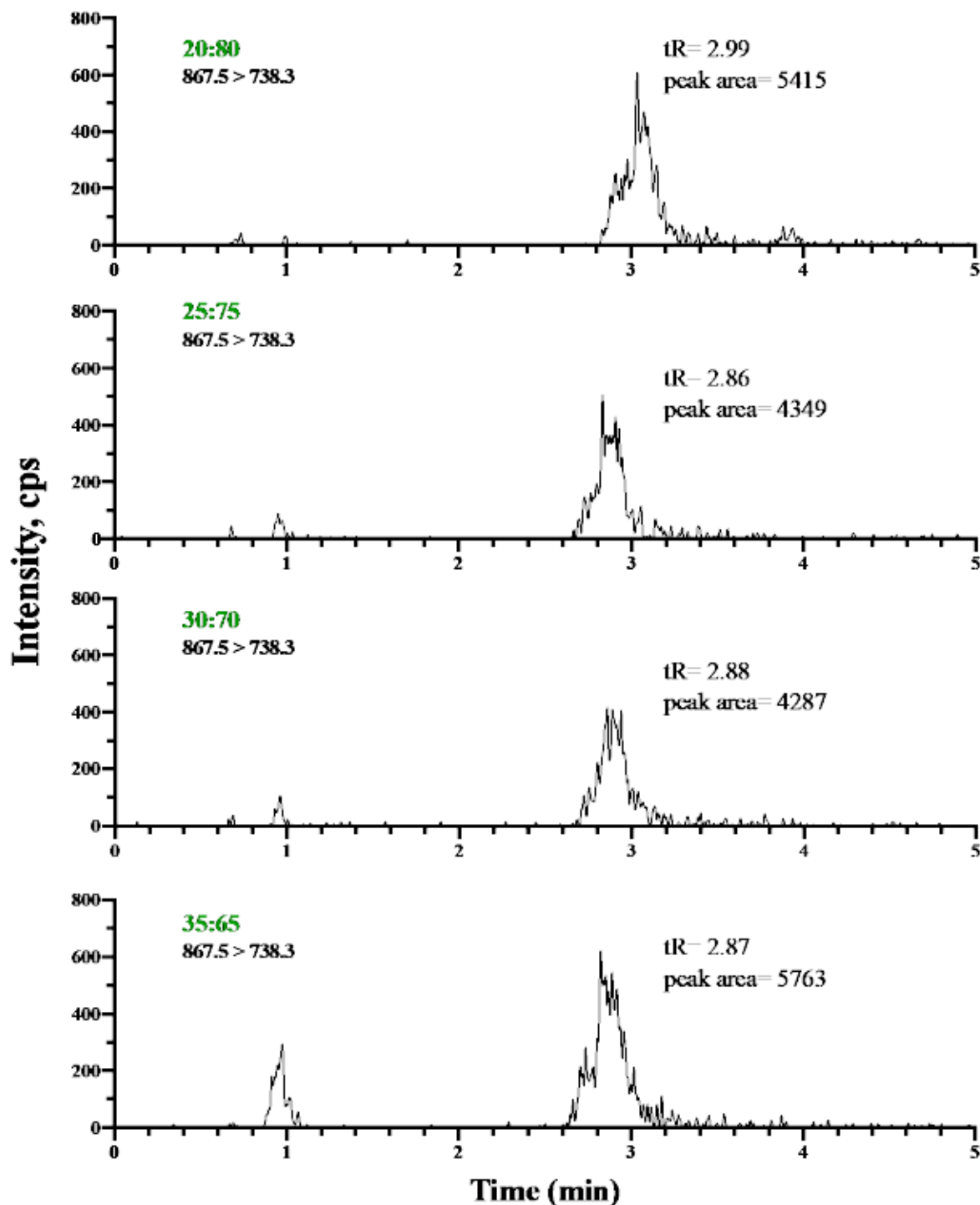
Figure 3.7: Chromatograms of D-BP-PTH using varying amounts of TMSD in MRM mode.
The transition of 867.5 → 738.3 was used for all four samples. A 25 μg/mL D-BP-PTH solution underwent derivatization with a 20:80, 25:75, 30:70, 35:65 TMSD:methanol:water solution. All four conditions suffered from poor peak shape and low sensitivity in MRM mode. Retention times for 25-35:65 ratios are all within 0.02 min and similar to the retention time of non-derivatized BP-PTH. The 20:80 ratio had a longer retention time (2.99 min), which may indicate incomplete methylation. All four ratios suffered from poor peak shape and low intensity.

3.3.4 Liquid chromatography challenges with D-BP-PTH

A substantial analytical hurdle with analysis of D-BP-PTH can be attributed to separation challenges of D-BP-PTH on reverse phase columns. Each methylation and location of methylation that occurs on D-BP-PTH alters the analytes polarity slightly, resulting in a marginal increase or decrease in retention time away from other differing methylated forms of D-BP-PTH, that are also present in the sample. As shown in Figure 3.6, there is no methylated derivative that is significantly more abundant than any other derivative. The lack of an abundant derivative makes it difficult to isolate for only one derivative using LC.

When using a gradient program in an attempt to generate an isolated peak for D-BP-PTH, due to each methylated derivative having slightly differing polarity than the next, each derivative has its own unique retention time. The numerous differing methylated derivatives that have slightly similar retention times, but not identical retention times, prevents the ability to generate a suitable peak shape for analysis when using gradient programs. The appearance of many closely retained peaks of similar intensity (not present in blank plasma samples) when a gradual gradient program was used confirmed this hypothesis. Satisfactory peak shape with high intensity (Figure 3.4) was only achieved when using isocratic program with organic mobile phase compositions (i.e. 40% ACN) above that of which D-BP-PTH elutes from RP columns at (~30-35% ACN). Using organic mobile phase compositions above that of which all D-BP-PTH derivatives elute with, allows all derivatives to be "grouped" to elute together in one single peak. Though an isocratic program generated suitable peak shape in neat solutions, it likely will not be suitable for plasma extracted samples due to large interference/matrix effect from co-eluting endogenous compounds. TIC plots of blank plasma samples show intense peaks both slightly before and after the retention time of D-BP-PTH variants. These endogenous plasma peaks would likely co-elute with D-BP-PTH and cause further analytical difficulties if an isocratic program is used. Complex stepwise gradients could be explored to remove endogenous components while still retaining D-BP-PTH, then eluting the analyte using organic mobile phase compositions of ~40% ACN could address interference.

Figure 3.8 shows a TIC plot of an extracted and TMSD treated blank plasma sample and an extracted and TMSD treated 10 μg/mL BP-PTH solution using a gradual gradient program (%B/min): 25/0, 50,20 with mobile phase A (H_2O + 0.1% FA) and mobile phase B (ACN + 0.1% FA). The repeated sharp peaks between 6 and 10 min in panel II) of Figure 3.8 correspond to the

differing derivatives of D-BP-PTH. The mobile phase composition between 6 and 10 min corresponds to roughly 30/6.0 to35/10 (%B/min). This mobile phase composition is consistent with the mobile phase composition in which non-derivatized BP-PTH elutes.
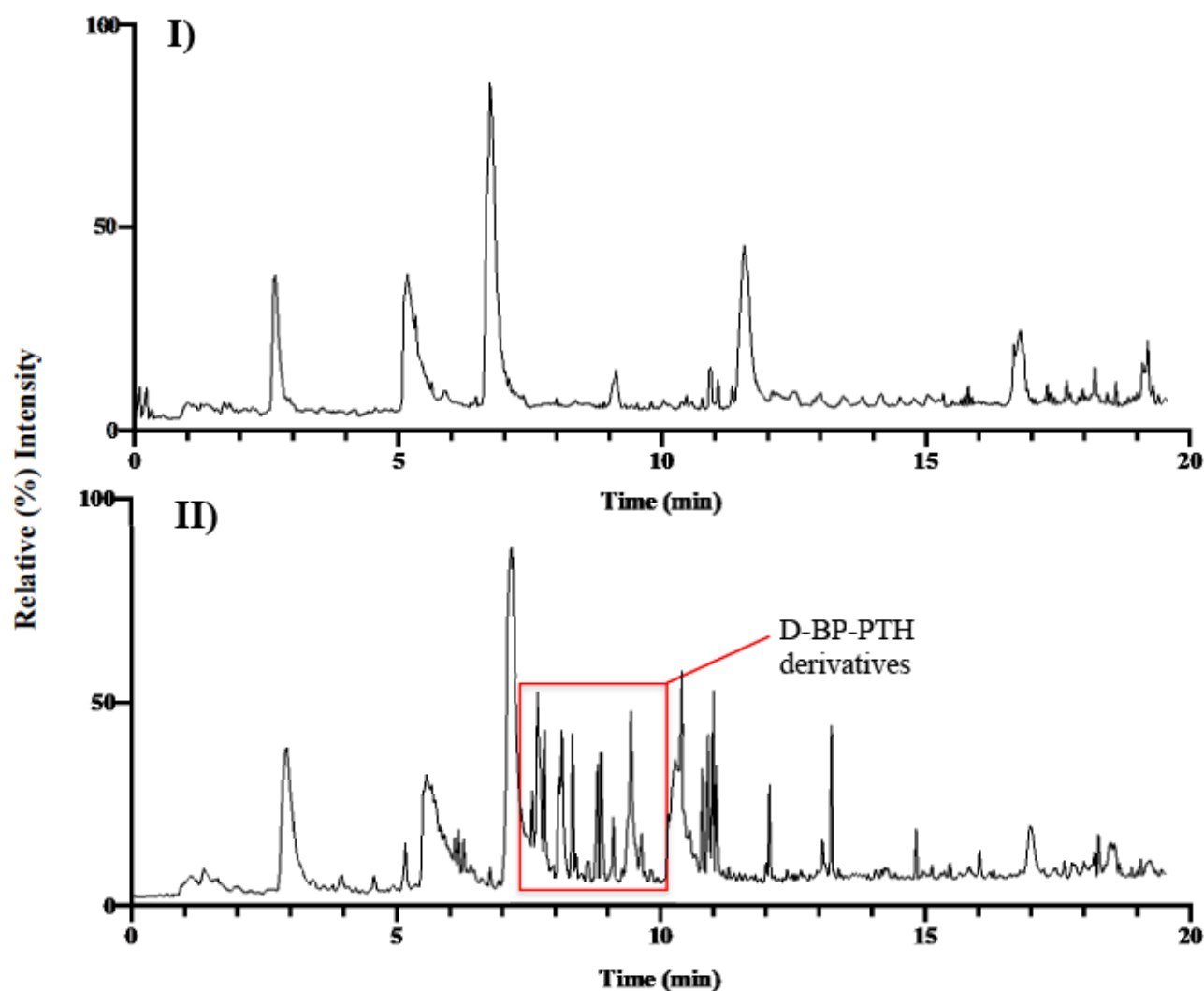
Figure 3.8: Chromatograms of D-BP-PTH and derivatized blank plasma using a gradual gradient program. A gradual gradient program using mobile phase A (H₂O + 0.1% FA) and mobile phase B (ACN + 0.1% FA) from 25/0 to 50/20 (%B/min) was used. I) TIC chromatogram of an extracted plasma sample that underwent derivatization with TMSD. II) TIC chromatogram of a plasma extracted and derivatized BP-PTH solution (10 µg/mL). The repeated peaks that appear in chromatogram II) between 6.0 and 10.0 min represent the BP-PTH derivatives. These peaks elute with similar organic mobile phase composition as BP-PTH (30-35% B).

3.3.5 Summary of challenges encountered with TMSD derivatization of BP-PTH

Two large areas of concern were identified during the course of method development that were hypothesized to have resulted in worse MS sensitivity with derivatization, than without. The combined effect of these two concerns greatly reduced sensitivity and detection of BP-PTH from the nanogram to the microgram level. Our initial hypothesis was that if the phosphonic acid groups present in BP-PTH could be methylated, sensitivity in ESI+ mode would increase and retention on a reverse-phase C_{18} column would also improve, leading to improved peak shape. These improvements would likely allow for sub-ng/mL quantification of BP-PTH.

The first concern that was encountered was the observation of numerous methylation possibilities on D-BP-PTH. Unlike BP compounds that have a maximum of 4-5 possible methylations, BP-PTH has a theoretical maximum of 16, which may very well be exceeded if diester alkylation occurs. With a simpler compound such as a BP, the reaction is consistent, reproducible and generates a more abundant derivative each time (i.e. tetramethyl or pentamethyl derivative). Generation of a significantly abundant and consistent derivative which can be unambiguously identified when selecting a precursor ion is required for MRM method development. When BP-PTH was derivatized, an abundant and unambiguous precursor ion was not observed, rather a cluster of ion peaks that corresponded to 11-15 methylations was seen in Q1 scans. This cluster made it difficult to select a precursor ion, as repeated injections of the same sample would shift the cluster to slightly favour an ion peak that corresponded between 10 to 15 methylations each time. Despite this, over multiple injections and independently prepared samples, D-BP-PTH with 14 methylations appeared to be the most common derivative. The lack of consistent derivative production and poor selectivity with TMSD combined to reduce sensitivity in MS.

In an effort to generate more consistent precursor ions, the ratio of TMSD to methanol/water was varied. Ratios between 20:80 and 35:65 (TMSD:methanol/water) did not show any significant differences or generate a consistent precursor ion. The inconsistent ion peaks observed in Q1 pose a challenge for MRM method development.

The second concern encountered was LC separation of the different derivatives of D-BP-PTH. As the site and number of methylations changes the polarity of the analyte, the corresponding retention time also changes. Due to this, the different derivatives can be separated

using a gradual gradient program, but an isolated high intensity peak of acceptable shape was not observed under gradient conditions. A suitable peak of high intensity was only observed in neat solution when using an isocratic program with an organic mobile phase of approximately 5% above the organic phase that the D-BP-PTH derivative with the greatest retention time elutes (~35% B). Using an isocratic gradient above 35% organic allowed for the derivatives to be "grouped" together and elute within one consolidated peak. However, when analyzing extracted plasma samples, the isocratic gradient program is not suitable as the D-BP-PTH peak experiences large interference from endogenous compounds.

3.4. Limitations

The lack of TMSD selectivity prevented generation of consistent and reproducible BP-PTH derivative ions of sufficient abundance to be used in MRM method development to improve sensitivity in ESI+ mode. Though various ratios of TMSD:methanol/water were explored, additional reaction conditions such as temperature and incubation duration were not explored. Without extensive exploration of the reaction conditions, it may be premature to conclude that derivatization of BP-PTH with TMSD for LC-MS/MS analysis is completely unsuitable.

The resolution of the LCMS-8050 triple quadrupole mass spectrometer (Shimadzu, Kyoto, Japan) was another limitation encountered in this work. MS resolution is defined as the ability to separate ions of one mass from those of another mass. Resolution is defined as the full width of the peak at its half maximum height (FWHM). Peak width is set to 0.7 on the LCMS-8050 instrument. This means, that any masses greater than 0.7 amu will be distinguished as separate ion peaks. Since mass spectrometry is an analytical method of high precision, greater resolution should always be desirable. However, in the case of methylated BP-PTH, if the peak width could be set to 1.0 or 1.5, then some of the clustered derivative peaks could be grouped together as "one mass" creating a more abundant derivative that is the "average" of the some of the methylated derivatives. If this were possible, it may allow for a suitable MRM method to be developed. A drawback of reducing the resolution would be detection of contaminant and other non-analyte peaks which would reduce the accuracy of quantification.

3.5. Future Directions

Though methylation using TMSD to neutralize the phosphonic acid groups on BP-PTH was successful in addressing the problematic metal binding issues when using LC-MS/MS, we failed to achieve improved MS sensitivity due to inconsistent methylation on amino acid residues of the peptide moiety. Further exploration of how TMSD interacts with large peptide molecules such as BP-PTH could be of interest to groups studying phosphopeptides, phospholipids or other phosphonic acid containing biomolecules by LC-MS/MS. As phosphonic groups poise challenges for MS analysis, developing reliable, efficient and economical methods to detect or quantify these compounds would have implications in bioanalysis, proteomics, and metabolomics.

3.6. Conclusions

TMSD derivatization has been proven successful for the methylation of phosphonic acid groups in BP compounds allowing for LC-MS/MS analysis. On-cartridge derivatization of BP-PTH using TMSD was performed in an attempt to neutralize phosphonic acid groups present in BP-PTH to enhance sensitivity in ESI+ mode and improve chromatographic separation. A lack of TMSD specificity prevented methylation of only the phosphonic acid groups and numerous (11-14) methylations were observed over the entire conjugate. Inconsistent and unpredictable methylation sites yielded a range of BP-PTH derivatives that showed significantly reduced sensitivity in ESI+ mode and poor LC performance on a RP-C_{18} column.

Chapter 4

Using an enzyme-linked immunosorbent assay for the detection of a novel none targeting parathyroid hormone conjugate.

4.1 Introduction

As mentioned earlier in this thesis, the need for a sensitive, efficient and accurate bioanalytical method for the detection of BP-PTH in rat plasma is required to move preclinical studies into clinical studies. The work described in this chapter focuses on exploring an alternative to LC-MS/MS quantification, by using a commercially developed high sensitivity enzyme-linked immunosorbent assay (ELISA) for the quantitative determination of hPTH (1-34). As the analyte of interest (BP-PTH) is modified hPTH (1-34), derivatization as a sample treatment strategy was explored to in an effort to improve detectability using a commercially developed hPTH (1-34) ELISA with hopes of improving BP-PTH detection in rat plasma.

4.1.1 Enzyme-linked immunosorbent assay (ELISA)

Enzyme-linked immunosorbent assay (ELISA) is powerful plate-based assay technique for the detection and quantification of soluble substances such as peptides, drugs, antibodies, and hormones. ELISA techniques are often used as a diagnostic tool, quality control checks or to preform pharmacokinetic analysis in various industries.

ELISA is commonly performed in polystyrene 96-well plates that have antigens pre-coated to the surfaces of the microliter wells (224). If an applied sample to the well contains the matching antibody, the antibody will bind to the antigen. The antibody can then be linked to an enzyme (commonly horseradish peroxidase (HRP)), with the final step involving the addition of the enzyme's substrate to the microliter well (224). Addition of the substrate will result in an enzymatic reaction and produce a color change. This color change often directly or inversely correlates with the concentration of the analyte of interest in the well and can be read using a spectrophotometric microtiter plate reader. Using high-affinity antibodies allows for non-specifically bound materials to be washed away, making ELISA a powerful quantification tool.

There are several different ELISA formats that can be used to detect or quantify an analyte of interest. These include direct, indirect or sandwich capture methods (225). These formats are classified accordingly by the method in which they are able to immobilize the antigen of interest; either direct adsorption to the microliter well or indirectly, using a capture antibody that has been immobilized to the microliter well (225). If the antigen is detected directly, it is referred to as a primary antibody, and if it is detected indirectly it is labeled as a secondary antibody (225). The sandwich ELISA assay is referred as "sandwich" assay because

the analyte of interest is bound between two primary antibodies (225). Each primary antibody (the capture antibody and the detection antibody) binds to a different region (epitope) of the antigen- forming a sandwich (225). The sandwich ELISA assay is the most common type of ELISA format used due to its high specificity and sensitivity.

Quantification is achieved by generating a standard curve from standard solutions of the analyte of interest. A standard curve is done by plotting the absorbance values (determined by the spectrophotometric plate reader) versus the respective concentration of the standard on linear or logarithmic scales.
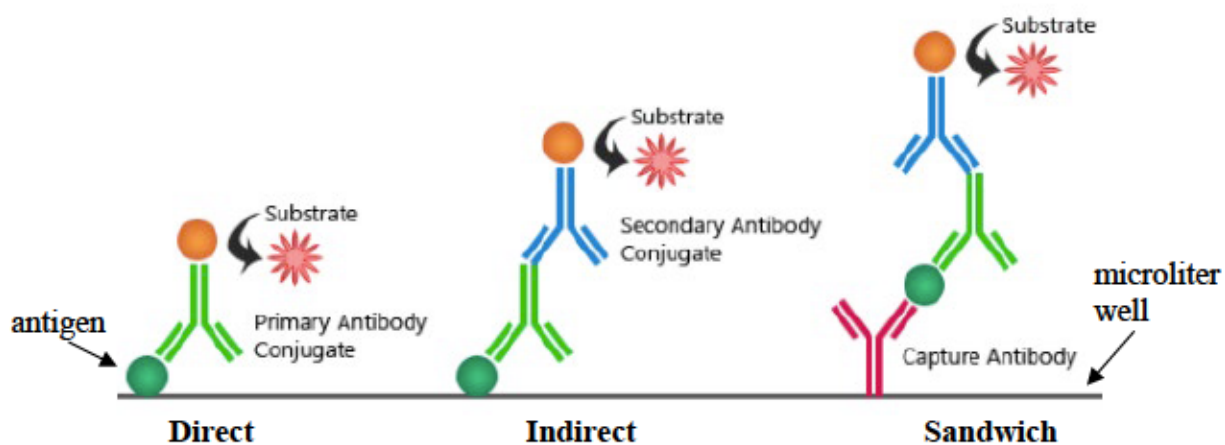
Figure 4.1: Schematic of the three main types of ELISA formats.
Adapted and modified from source 226.

4.1.2 High sensitivity ELISA for the quantitative determination of human parathyroid hormone 1-34 in plasma

Immutopics, Inc. (San Clemente, California, USA), has developed and validated a commercial high sensitivity ELISA kit for the quantitative determination of human parathyroid hormone 1-34 (hPTH (1-34)) levels in plasma for laboratory use. The high sensitivity human PTH (1-34) kit utilizes the sandwich ELISA format with two antibodies that have been prepared for optimal recognition of human PTH (1-34) while minimizing binding to endogenous PTH (1-84). Immutopics states that an affinity purified goat polyclonal antibody which is optimized to bind a region of hPTH (1-34) is biotinylated for capture (capture antibody). An additional affinity purified goat polyclonal antibody that recognizes and binds a second region of hPTH (1-34) is conjugated with the enzyme HRP to allow for detection (detection antibody). Samples

145

containing hPTH (1-34) are incubated alongside the biotinylated capture antibody, the HRP conjugated detection antibody in the microliter well that is coated with streptavidin (Immutopics). After incubation, the well is washed to remove unbound compounds and excess detection antibody. Addition of the substrate solution (HRP substrate) results in colour change that can be measured using a spectrophotometric plate reader. In this high sensitivity hPTH (1-34), the amount of enzymatic activity of the detection antibody is directly proportional to the amount of hPTH (1-34) in the sample. The sandwich ELISA format is summarized below:

Streptavidin coated well --- Biotin Anti-h PTH --- hPTH (1-34) --- HRP Anti-h PTH

4.1.3 Shortcomings of using a hPTH (1-34) ELISA to detect BP-PTH

The most obvious shortcoming of using a commercial ELISA kit to detect and quantify BP-PTH is that the commercial kit only has proven specificity and high sensitivity for hPTH (1-34), and not BP-PTH. Since BP-PTH is a custom peptide conjugate, there are no commercially available kits for the detection of BP-PTH. Furthermore, our laboratory is not equipped with the expertise or resources to develop and validate an ELISA for the detection of BP-PTH in rat plasma. As our bone-seeking peptide conjugate contains a hPTH (1-34) moiety, we hypothesized that the Immutopics high sensitivity hPTH (1-34) ELISA may be able to detect BP-PTH. The hPTH (1-34) moiety in the conjugate shares the identical amino acid sequence as hPTH (1-34) that is recognized by the ELISA. A 27 residue PEG linkage to Lys-13 was used to tether the bisphosphonate moiety to hPTH (1-34). If neither the capture nor detection antibody requires Lys-13 for recognition and binding, the commercial ELISA may be able to detect the BP-PTH conjugate. In cases where either antibody requires Lys-13, it is highly likely that the PEG modification to Lys-13 would prevent antibody binding. Furthermore, even if Lys-13 is not required for antibody recognition, the addition of a PEG and BP moiety creates an extremely bulky Lys-13 "side-chain" which may reduce possibilities of antibody binding due to steric difficulties. Conversely, as the specific binding between the antigen (epitope) and the antibody (paratope) site usually involves portions comprised of just a few amino acids (227), it may also be likely that a Lys-13 modification would not pose binding difficulties. Unfortunately, Immutopics was unwilling to disclose which amino acid sequences of hPTH (1-34) are used for recognition and binding of the capture and detection antibodies.

A second shortcoming of using an ELISA to detect BP-PTH is the presence of the negatively charged phosphonic acid groups present on the BP portion of the conjugate. The forces that join the antigen (target analyte) to the antibody to form the antigen-antibody complex are not covalent bonds, but rather weak interactions like van der Waals forces, hydrophobic and hydrophilic interactions, and electrostatic forces (227,228). The hydrophobic interactions (attractive forces) and hydrophilic interactions (repulsive forces) are reported to play a considerable role in the phenomena of antigen-antibody binding (227). Van der Waals and electrostatic forces (long-range non-covalent forces) determine the epitope-paratope interactions at the molecular level, while also acting between whole antigen and antibody molecules (227). A protein antigen and its corresponding antibody typically repel each other, until the attraction between their epitopic and paratopic sites at the molecular level exceeds the overall repulsion (227). The highly negatively charged phosphonic acid groups that are in close proximity to the hPTH (1-34) moiety may interfere with the attraction or repulsion between the epitope and paratope, preventing antibody detection.

Methodology

4.2 Methodology

4.2.1 Objective of using an enzyme-linked immunosorbent assay for the detection of a novel bone targeting parathyroid hormone conjugate

The objective of the work described in Chapter 3 "Using an Enzyme-linked Immunosorbent Assay for the Detection of a Novel Bone Targeting Parathyroid Hormone Conjugate" was aimed toward attempting to use a commercial hPTH (1-34) ELISA to detect the BP-PTH compound in rat plasma. In an effort to address the potential shortcomings of using a hPTH (1-34) specific ELISA to detect a modified variant of hPTH (1-34), a creative approach was explored to address the two biggest shortcomings discussed in section 4.13. The approach was to methylate the phosphonic acid groups of the BP moiety using TMSD to minimize potential repulsion forces between the epitope and the paratope, with the hope to improve ELISA detection of BP-PTH.

4.2.2 Chemicals

Hydroxyapatite (reagent grade powder) and 1.0 N hydrochloric acid was purchased form Sigma-Aldrich Canada Co (Oakville, Ontario, Canada). High sensitivity human PTH (1-34) ELISA kit was purchased from Immutopics, Inc. (San Clemente, California, USA). Trimethylsilyldiazomethane (2M in hexanes) was acquired from Fisher Scientific (Pittsburgh, PA, USA). Oasis® weak anion exchange (WAX) cartridge (60mg, 3cc) were purchased from Waters Corporation (Massachusetts, USA). Slide-A-Lyzer MINI dialysis devices (0.5mL, 3.5K MWCO) and Micro BCA™ protein assay kit was purchased from ThermoFisher Scientific (Burlington, Ontario, Canada).

4.2.3 Instrumentation

Solid phase extraction was carried out using a 20 position Promega Vac-Man® vacuum manifold (Madison, Wisconsin, USA) to apply positive pressure. A 15 position MICROVAP nitrogen dryer (Organomation, Berlin, Massachusetts, USA) was used for solvent evaporation. Eppendorf 5415D benchtop centrifuge was used for all centrifugation (Hamburg, Germany). IKA MS 3 digital plate shaker was used to provide consistent shaking of 96-well plates used in ELISA experiments (Wilmington, North Carolina, USA). Well absorbances were read on a

BioTek SynergyIII hybrid plate reader (Winooski, Vermont, USA). A Wellwash™ microplate washer was used to automate ELISA wash steps (ThermoFisher Scientific, Waltham, Massachusetts, USA).

4.2.4 Determination of bone targeting potential: comparing hydroxyapatite binding of BP-PTH vs hPTH (1-34):

To assess the potential electrostatic covalent interaction between the negative phosphonic acid groups of BP-PTH and the positively charged calcium ions present in HA mineral, percentage binding to HA mineral was compared between BP-PTH and hPTH (1-34). Assessing the relative strength of the electrostatic interaction between BP-PTH and HA mineral will provide insight into the extent that BP-PTH may exert metal chelating abilities in LC-MS/MS analysis. A high level of binding may provide experimental evidence that a WAX SPE column is suitable for extraction. As a benefit, this experiment will show if the novel BP-PTH conjugate can outperform hPTH (1-34) in terms of HA mineral binding. 20 µg of BP-PTH or hPTH (1-34) was added to 10 mg of HA at room temperature with tube inversion for 2 hr. Tubes were centrifuged at 12,000 rpm for 2.5 min. Three binding environments were examined: double distilled water, 10mM phosphate buffered saline (PBS) and 50 mM PBS. We hypothesized that if the interaction between BP-PTH and HA is electrostatic, then we should see lower percentage binding to HA in PBS environments as it will interfere with the electrostatic binding interaction. HA percent binding was determined by the remaining amount of peptide in the supernatant after incubation. A micro-BCA protein assay was used for quantification.

4.2.5 Assessing recovery of BP-PTH using a WAX cartridge

To determine the percent recovery of BP-PTH using a Waters Oasis® WAX cartridge, a micro BCA assay was used to quantify the concentration of BP-PTH before cartridge loading, and after cartridge elution. The WAX cartridges were conditioned using 2.0 mL of methanol, followed by an equilibration step using 2.0 mL of 25 mM ammonium acetate. 100 µL solutions of 60 µg/mL BP-PTH prepared in deionized water were diluted with 1 mL of deionized water and adjusted to pH 4.0 using 25 µL of 1.0 M HCl before being loaded on the WAX cartridge. The remaining 60 µg/mL BP-PTH solution was diluted to 10 µg/mL to be used in the micro

BCA assay as the "pre-extraction" concentration. The cartridges were then washed with 2.0 mL of 25 mM ammonium acetate and 2.0 mL of methanol. BP-PTH was eluted from the WAX cartridge using two washes (2X 500 μL) of 5% NH$_4$OH in methanol (pH 9.0). The eluent was collected and evaporated under a stream of nitrogen at 40°C. Residue was resuspended in 600 μL of deionized water to create a 10 μg/mL solution. Aliquots of 300 μL (post-extraction samples) were collected for micro BCA assay. 150 μL of the pre-extraction and post-extraction were used in the micro BCA assay (two wells using 150 μL per well), absorbances were read at 562nm. The experiment was performed in triplicate (*n=3*).

4.2.6 Sample preparation for use in a high sensitivity hPTH (1-34) ELSIA for the determination of BP-PTH

In an effort to address the potential shortcomings of using a hPTH (1-34) specific ELISA to detect modified hPTH (1-34), two sample preparation routes were explored. The first sample preparation method that was explored was using unmodified BP-PTH extracted from rat plasma. The second preparation method explored was performing on-cartridge derivatization of BP-PTH using a WAX solid phase extraction cartridge. Derivatization using TMSD will effectively "neutralize" the negatively charged phosphonic acid groups of the BP moiety through a methylation reaction. It was hypothesized that neutralization of the phosphonic acid groups should reduce any significant electrostatic interactions that may be preventing antibody binding.

Residue was reconstituted in 200 μL of distilled water. Reconstitution to a sample volume of 200 μL adjusts sample concentrations into the ELISA quantitative range (300 pg/mL, 150 pg/mL, 75 pg/mL, 34.5 pg/mL, 18.75 pg/mL, and 9.375 pg/mL Samples were then subjected to four buffer exchange cycles (three 3 hr exchange and an overnight exchange) using a 3.5K MWCO membrane to remove any excess TMSD.

4.2.6.1 Sample preparation using TMSD as a derivatization agent

Rat plasma (250 μL) was spiked with 100 μL of BP-PTH solution (600 pg/mL, 300 pg/mL, 150 pg/mL, 75 pg/mL, 34.5 pg/mL, and 18.75 pg/mL) prepared in water. Samples were further diluted with 1.0 mL of water and pH adjusted to 4.0 using 25 μL of 1.0 M HCl. Samples were centrifuged for 1.0 min at 3,500 x *g* and the supernatant was loaded onto a preconditioned

(2.0 mL methanol followed by 2.0 mL of water) Waters Oasis® WAX cartridge (3cc, 60mg). Flow was stopped for 5 min to allow for the negative phosphonic acid groups to orient and interact with the WAX sorbent. Flow was resumed without the aid of vacuum pressure to allow for a slow flow rate of ~100 μL/min to 200 μL/min. The WAX sorbent was washed with 2.0 mL of 25 mM ammonium acetate and 2.0 mL methanol. BP-PTH was eluted using 500 μL of a 35:65 (TMSD:MeOH, v/v) ratio as mentioned in section 3.2.4. Filtrate was collected and evaporated under a gentle stream of nitrogen at 40°C. Reconstitution to a sample volume of 200 μL in deionized water adjusts sample concentrations into the ELISA quantitative range (300 pg/mL, 150 pg/mL, 75 pg/mL, 34.5 pg/mL, 18.75 pg/mL, and 9.375 pg/mL. As a precaution, samples underwent dialysis using a 3.5 MWCO membrane (exchanges evert 3 hr for 9 hr and left overnight) to further remove any remaining TMSD which could interfere with the reagents used in the ELISA.

4.2.6.2 hPTH (1-34) ELISA procedure

The high sensitivity human PTH (1-34) ELISA (cat.# 60-3900) procedure was followed as stated in the procedure provided by Immutopics, Inc. (San Clemente, California, USA). All standards, controls and samples were assayed in duplicate. The ELISA has a linear range from 2.5 to 150 pg/mL when absorbances read at 450nm (primary assay) and a linear range of 75 to 300 pg/mL (secondary assay) when absorbances read at 620nm. An automated microtiter plate washer was used to complete all washing steps. As per Immutopics recommendation, the sample volume was altered to 50 μL by reducing the volume of ELISA HRP substrate added to the wells. Reducing the sample volume to 50 μL changes the sensitivity from 5.8 pg/mL to 2.5 pg/mL. Two main experimental groups were analyzed to determine the utility of the commercial hPTH (1-34) ELISA to detect BP-PTH. The two treatment groups were BP-PTH (non-treated), TMSD derivatized BP-PTH (D-BP-PTH). Teriparatide (human PTH (1-34) acetate salt) was used as an additional control.

Table 4.1: Summary of samples and concentration ranges tested using Immutopics high sensitivity hPTH (1-34) ELISA.

Sample	Concentration range (pg/mL)
hPTH (1-34) standard solutions (Immutopics, Inc.)	0, 7.3, 15. 34, 70, 151, 299
Teriparatide (hPTH (1-34))	9.375, 18.75, 34.5, 75, 150, 300
D-BP-PTH	9.375, 18.75, 34.5, 75, 150, 300

Results and Discussion

4.3 Results and Discussion

4.3.1 Determination of bone targeting potential: comparing hydroxyapatite binding of BP-PTH vs hPTH (1-34)

The BP-PTH conjugate significantly (p<0.05) out performs hPTH (1-34) when binding to HA in a distilled water environment. In the distilled water environment, 85.02% of all BP-PTH bound to HA within a 2 hr RT incubation period, in comparison to 21.07% of hPTH (1-34) bound. Reduced binding for the BP-PTH conjugate in PBS environments (24.06% in 10 mM PBS and 19.30% in 50 mM PBS) indicates that BP-PTH appears to bind to HA mineral through an electrostatic covalent interaction. Multiple t-tests were used to evaluate significance amongst treatments (p>0.05). These findings provide insight into the high likelihood that BP-PTH will interact with positively charged metal surfaces in LC-MS/MS instrumentation unless the phosphonic acid groups undergo neutralization through a derivatization reaction or metal-free LC-MS/MS is used.
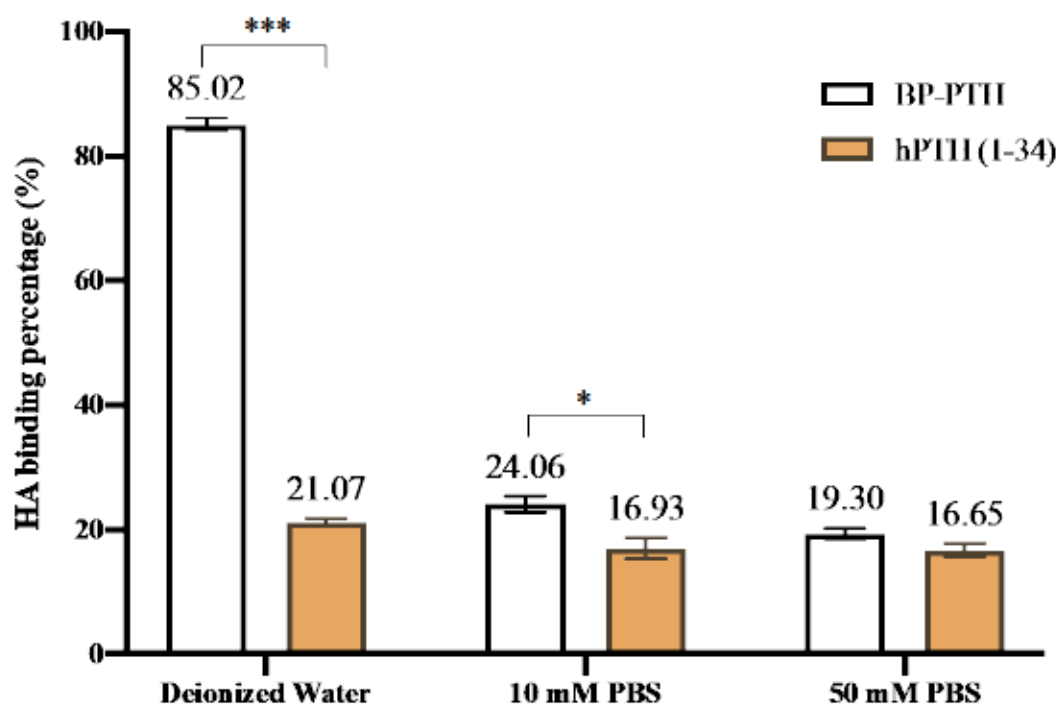
Figure 4.2: In vitro HA binding affinities: BP-PTH vs unmodified hPTH (1-34).
Peptides were incubated for 2 hr with HA in corresponding buffers with inversion. Amount of peptide in the supernatant after centrifugation was quantified using a micro-BCA protein assay. BP-PTH out performs hPTH (1-34) when binding to HA in both deionized water and 10 mM PBS (p<0.05). No statistical difference (p>0.05) was observed between the two groups in 50 mM PBS. Values represent mean ± standard deviation (*n*=2 replicates), * p < 0.5, *** p <0.001.

4.3.2 Assessing recovery of BP-PTH using a WAX cartridge and subsequent dialysis

The percent recovery of a 60 µg/mL solution of BP-PTH that was diluted to 10 µg/mL after elution from the WAX cartridge was determined to be 47.1%. Dialysis was undertaken to determine the overall percent recovery from sample loading to after dialysis. As a precaution, dialysis of any residual TMSD reagent was performed to prevent any potential interfering effects during ELISA analysis. After plasma extraction and dialysis, the percent recovery of BP-PTH was determined to be 45.2%.

A limitation of this experiment is that neat solutions of BP-PTH (non-plasma containing) had to be used. Plasma samples still contain macromolecules, proteins and other plasma components (in small concentrations) after extraction. These residual plasma components lead to an over estimate of protein concentration when using a micro-BCA assay.

However, based on the percent recovery of BP-PTH determined by LC-MS/MS, using the extraction procedure, the percent recovery of a plasma solution (21.0%) is differs significantly to the recovery of a BP-PTH in a neat solution (47.1%) determined by micro BCA assay.
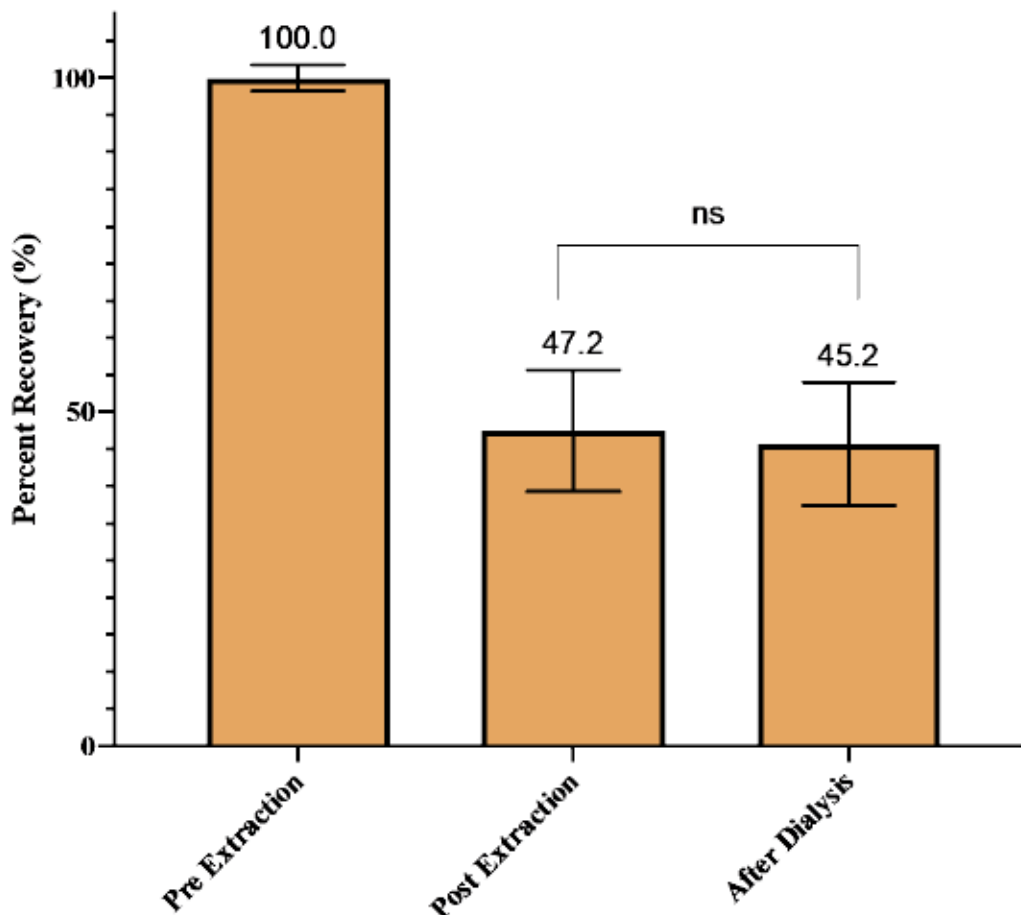
Figure 4.3: Percent recovery of a neat solution of BP-PTH after SPE extraction and dialysis. A 60 µg/mL solution of BP-PTH loaded onto a WAX cartridge and diluted to 10 µg/mL after elution was determined to have a percent recovery of 47.2%. After four buffer exchanges (three for a 3 h period and one overnight) using a 3.5K MWCO membrane, recovery was determined to be 45.2%. Values represent mean ± standard deviation (n=3 replicates).

4.3.3 ELISA Results

As per Immutopics, Inc. recommendations, the primary assay was used to evaluate whether the commercial ELISA specific for hPTH (1-34) is able to detect unmodified BP-PTH and derivatized BP-PTH (D-BP-PTH). Concentration range was 2.5 to 150 pg/mL when absorbances read at 450nm. Non-linear regression (Prism 8 for macOS, ver. 8.4.0) with second order quadratic fit was performed on all four sample types and a p-value of <0.001 was selected to determine if slopes are significantly non-zero. Curve fitting used a second order quadratic fit as recommended by Immutopics.

The hPTH (1-34) standards and controls (provided by Immutopics) appeared to work as expected producing a calibration curve with acceptable goodness of fit from 0 pg/mL to 151

pg/mL (r^2=0.998, p<0.001, y=$4.00^{-5}x^2$+0.007x-0.267). As an additional control, solutions of teriparatide were assessed to determine any potential differences between the Immutopics supplied standards and teriparatide. A similar curve (r^2=0.997, p<0.001, y=$6.50^{-5}x^2$+0.004x-0.03) with similar absorbance values was generated for the teriparatide standards. An unpaired t-test determined that there was no significant difference between the two control calibration curves (p=0.987, p>0.05). No significant differences between the commercial controls and teriparatide indicate that the ELISA is working as intended. Unmodified BP-PTH appears to have been unable to be reliably or accurately detected by the commercial ELISA kit (r^2=0.911, p<0.001, y=$9.39^{-6}x^2$+0.0009x+1.00), producing very high absorbance values (1.23-1.54) at low concentration levels (9.375-34.5 pg/mL) and failing to demonstrate an acceptable relationship between increasing absorbance values and increasing concentration. Failing to detect unmodified BP-PTH underscores the importance of a unique sample preparation/modification procedure of BP-PTH if a commercial hPTH (1-34) ELISA is to be used for quantification.

Derivatization of BP-PTH proved to be an unsuccessful sample approach for the improved detection of BP-PTH. The low and non-linear absorbance values failed to establish any relationship between absorbance and concentration (r^2=0.787, p>0.001, y=$-1.92^{-5}x^2$+0.004x+0.196). Since TMSD is capable of methylation of some of the amino acid groups (Ser, Thr, Tyr, Asp, and Glu) and the C-terminal end of the hPTH (1-34) moiety, it is likely that these methylations prevented antibody recognition and binding. As terminal sequences are often involved in antibody recognition/binding, any methylation to the C-terminus would likely impact antibody binding ability. Methylation of the hPTH (1-34) moiety could explain why this sample preparation step was unsuccessful.

As a general note, the SD values on the standards (Immutopics and teriparatide) were all quite small (average SD= 0.011) while SD values for experimental treatment groups were larger (average SD= 0.058). The larger SD values for the treatment groups is indicative of larger variance between measured values. In summary, the commercial ELISA tested is unsuitable for the detection of BP-PTH, or BP-PTH that has been derivatized using the conditions described in Chapter 3 of this thesis. Summary of the ELISA results are shown in Figure 4.4.
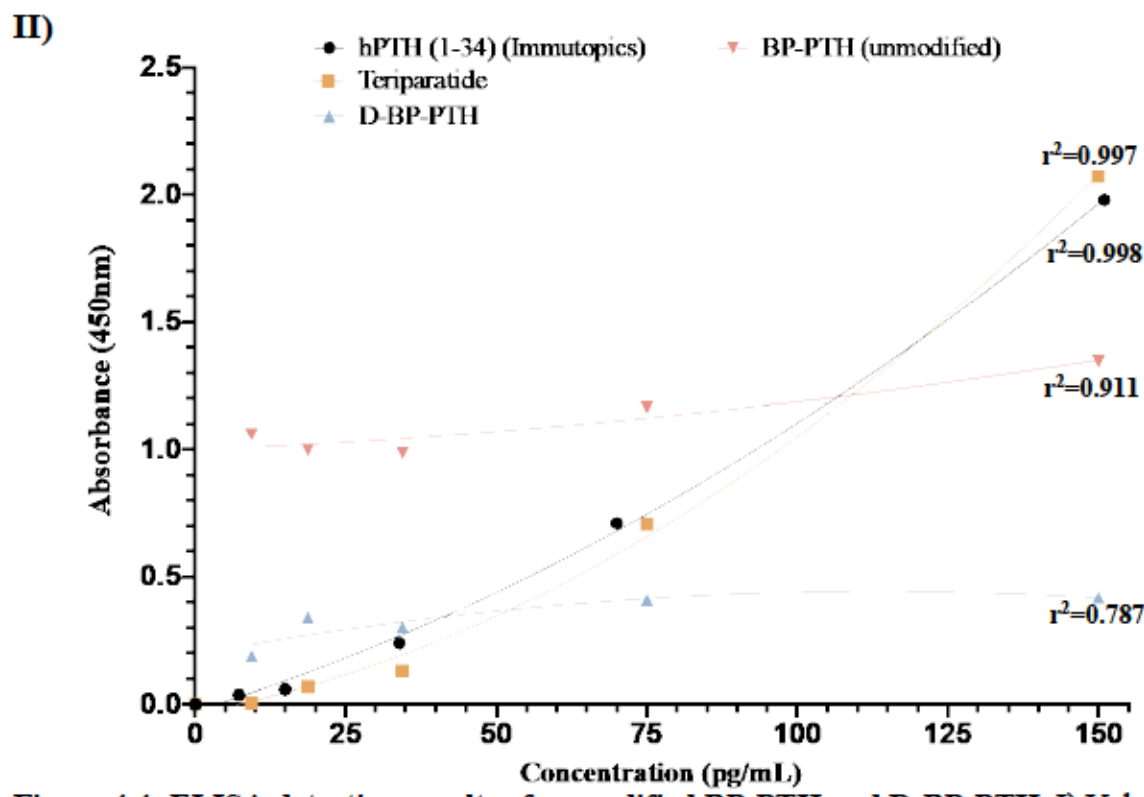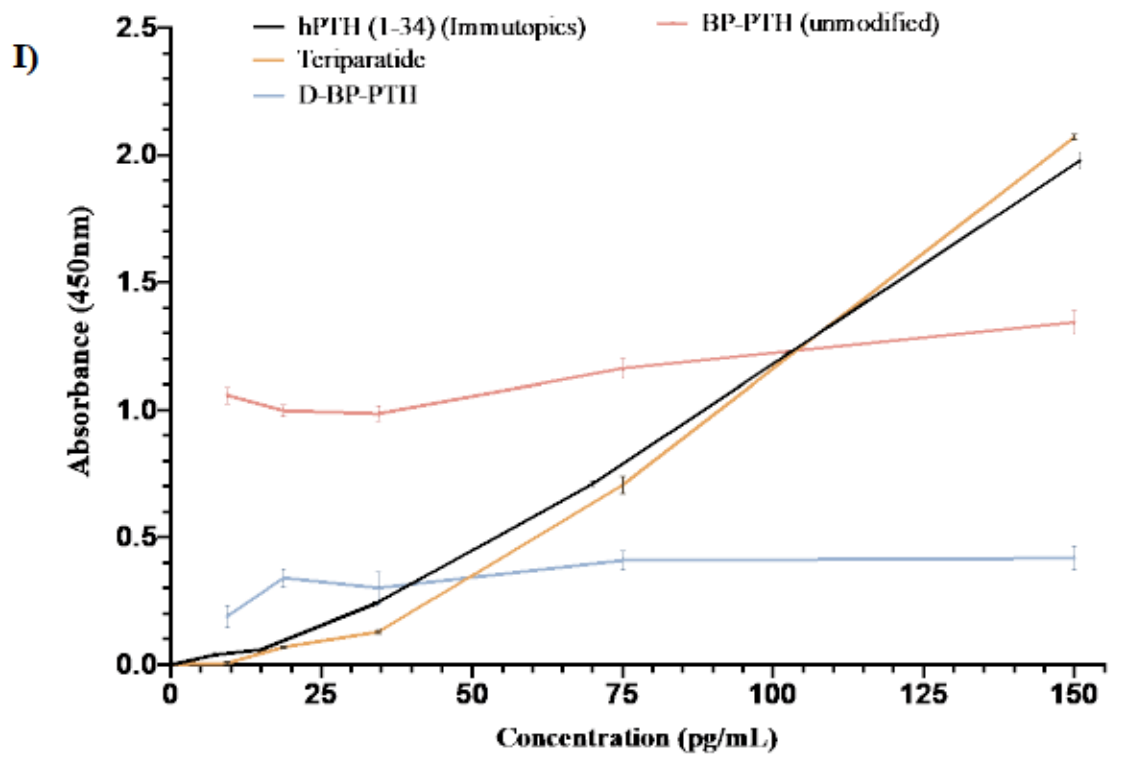
Figure 4.4: ELISA detection results of unmodified BP-PTH and D-BP-PTH. I) Values represent mean $\pm$ SD (n=2). II) hPTH (1-34) (Immutopics): r^2=0.998, p<0.001, y=$4.00^{-5}x^2$+0.007x-0.267. Teriparatide: r^2=0.997, p<0.001, y=$6.50^{-5}x^2$+0.004x-0.03. BP-PTH (unmodified): r^2=0.911, p<0.001, y=$9.39^{-6}x^2$+0.0009x+1.00. D-BP-PTH: r^2=0.787, p>0.001, y=$-1.92^{-5}x^2$+0.004x+0.196.. No significant difference was found between the hPTH (1-34) standards from Immutopics and the teriparatide standards (p=0.987, p>0.05).

4.4 Limitations

The largest limitation encountered with attempting to use a hPTH (1-34) specific ELISA for the detection of BP-PTH is that the ELISA is not specific for BP-PTH. Though the commercial ELISA is specific for half of the BP-PTH conjugate, the tethering of a BP moiety prevents accurate detection. Another significant limitation encountered with the work described in Chapter 3 was the high cost of the high sensitivity hPTH (1-34) ELISA. To properly troubleshoot and explore additional sample preparation/modification conditions requires a substantial amount of ELISA kits. Furthermore, if a suitable method had been developed, additional ELISA kits would be required to properly validate the method in accordance to the EMA guidelines for bioanalytical methods (195).

Another limitation was that the work in this chapter was conducted before the LC-MS/MS work described in chapter 2. Therefore, the use of LC-MS/MS analysis was not available to improve or increase the accuracy of the method development for ELISA analysis. An example of this is the discrepancy between percentage of BP-PTH WAX cartridge binding (Figure 4.3 and Figure 2.15) determined by two different methods, micro BCA assay and LC-MS/MS. Unfortunately, at the time the ELISA experiments were conducted, the Strata-X™ polymeric sorbent as a purification strategy had not been explored yet.

As detection of BP-PTH later using LC-MS/MS analysis had proven to be a more successful and economically feasible method to quantify BP-PTH, attempts to do the same using a commercial ELISA were not explored as extensively.

4.5 Future Directions

If detecting BP-PTH by ELISA is the desired method for bioanalytical detection, then likely it would be most appropriate to develop an in-house ELISA that is specific for the detection of BP-PTH, rather than just hPTH (1-34). This method was not explored by our research groups as we do not have the expertise or facilities to develop and validate an in-house ELISA procedure.

As a future direction, it may be worthwhile investigate cleavage of the PEG linker that tethers the BP moiety to the peptide moiety. If the PEG linker is able to be cleaved to free the hPTH (1-34) portion, then the commercial ELISA may be able to indirectly detect BP-PTH through cleavage. LC-MS/MS may be a viable strategy to assess potential cleavage agents. A

suitable cleavage agent would be required to successfully cleave the PEG linker, while ensuring that the hPTH (1-34) portion remains intact for antibody recognition/binding. Lastly, performing purification using the optimized purification strategy described in section 2.14 to prepare the samples for ELISA analysis may yield improved results.

4.6 Conclusion

In summary, derivatization of BP-PTH appeared to be an unsuccessful (when tested with the experimental conditions mentioned in this chapter) approach to quantify BP-PTH using ELISA. The inability of the commercial ELISA to detect unmodified BP-PTH underscores the importance of using a creative approach for the detection of BP-PTH in rat plasma with an ELISA. This approach may be developing an in-house ELISA with specificity for BP-PTH, or using a unique sample preparation/modification procedure to allow samples to be analyzed using a commercial hPTH (1-34) ELISA.

Chapter 5

General limitations, future directions and conclusions

5.1 Limitations

The largest limitation that is involved with the immediate work conducted in this thesis was the short column lifetime of the PS-C$_{18}$ column which prevented completion of method validation. At the beginning of method development with the PS-C$_{18}$ column, peak shape was suitable with minimal peak tailing and column back pressure was not an issue. As more non-derivatized samples were ran through the column, column performance began to decrease, leading to significant peak tailing and back-pressure. To maintain reproducibility, column performance needs to be maintained over hundreds of analytical runs. Due the limited selection of bioinert RP-C$_{18}$ columns compatible with MS, it may be challenging to find a more suitable column to achieve similar sensitivity levels as to that of the PS-C$_{18}$ column.

Another limitation that was encountered was the lack of an isotopically labelled internal standard. Given the custom nature of our compound, there are no commercially available structural analogs (BP-conjugated peptides) or isotopically labeled compounds. Synthesizing an isotopically labeled variant of BP-PTH or using hPTH (1-38) would address this limitation in our study and further improve accuracy.

Enhancement of MS sensitivity by TMSD derivatization of the phosphonic groups in BP-PTH was greatly limited by the seemingly countless number of possible methylation combinations that arise due to the variable number of methylations and the possible sites of methylation that can occur on the BP-PTH conjugate. The generation of numerous methylated derivatives of BP-PTH prevented an abundant precursor ion from being selected for MRM development, greatly reducing the methods sensitivity.

5.2 Future Directions

The method described in Chapter 2 will undergo complete method validation once a more suitable analytical column is acquired. Optimal chromatographic and MS parameters will be determined for the new analytical column. Furthermore, future method development will be performed using hPTH (1-38) as an internal standard to further improve quantification accuracy. Using rhPTH (1-34) will ensure the IS concentration is consistent across all samples as rhPTH (1-38) is not a possible metabolite of BP-PTH.

As part of a previously conducted Good Laboratory Practice (GLP) study, plasma samples containing BP-PTH were collected at various time points after intravenous and

163

subcutaneous administration in ovariectomized rats (osteoporosis model) and frozen for storage. Pharmacokinetic evaluation will be performed on the previously collected plasma samples to determine biodistribution, clearance, and retention of BP-PTH to correlate serum concentration with pharmacological response. Pharmacokinetic evaluation parameters will be determined using the described LC-MS/MS method from Chapter 2 with a new column. Like any analytical method, there is always room for improvement by further optimizing procedural steps or introducing automation where possible. Further improving sample extraction and chromatographic conditions could lead to lower limits of detection and a more robust and efficient method.

5.3 Conclusions

A reproducible and accurate LC-MS/MS method for the quantification and detection of a novel bone targeting parathyroid hormone conjugate (BP-PTH) in rat plasma was successfully developed. To our knowledge, we are the first group to report successful analytical detection and quantification of a peptide conjugated to a bisphosphonate in plasma. The developed method achieved a detection limit of 2.5 ng/mL from 250 μL of rat plasma. A combination of protein precipitation and solid-phase extraction was used, allowing for concentrated samples without the need of evaporation. Precision and accuracy measurements were all within accordance to EMA guidelines (195), with an average accuracy of 102.22% for all levels and CV% for all assayed samples <10%. Despite achieving satisfactory validation parameters, the chosen analytical column proved to be usable for only approximately 150 injections before becoming irreversibly damaged. The method will be re-optimized with a more appropriate analytical column in the future.

In an effort to enhance BP-PTH sensitivity in MS and further minimize unwanted analyte binding in the LC-MS/MS flow path, TMSD derivatization was used to methylate the phosphonic acid groups present in the BP moiety of BP-PTH. Lack of specificity with the derivatization agent resulted in the creation of numerous BP-PTH derivatives, with the most abundant corresponding to derivatives containing 11-15 methylations. The generation of numerous derivatives caused by the various number of possible methylation sites on the conjugate resulted in poorer MS sensitivity in comparison to non-derivatized BP-PTH.

The use of a highly specific commercial hPTH (1-34) ELISA was also explored to assess suitability for detection of BP-PTH. The ELISA was unable to establish a concentration-response relationship for unmodified BP-PTH. Modifications to BP-PTH were undertaken with the aim to generate variants that are more chemically and structurally similar to hPTH(1-34) to allow for ELISA detection. Neutralization of the phosphate groups was unsuccessful and did not lead to suitable ELISA detection.

Bibliography

1. Hadjidakis DJ, Androulakis II. Bone Remodeling. *Ann N Y Acad Sci*. 2006;1092(1):385-396.

2. Osteoporosis - Facts and Statistics. Osteoporosis Canada website https://osteoporosis.ca/about-the-disease/fast-facts/. Accessed August 3rd 2020.

3. Tarride JE, Hopkins RE, Leslie WD, et al. The burden of illness of osteoporosis in Canada. *Osteoporosis Int*. 2012;23(11): 2591–2600.

4. Seeman, E. Bone quality: the material and structural basis of bone strength. *J Bone Mineral Metabolism* 2008;26: 1-8.

5. Florencio-Silva R, Sasso GRDS, Sasso-Cerri E, Simões MJ, Cerri PS. Biology of Bone Tissue: Structure, Function, and Factors That Influence Bone Cells. *Biomed Res Int*. 2015;2015.

6. Florencio-Silva R, Sasso GRDS, Sasso-Cerri E, Simões MJ, Cerri PS. Biology of Bone Tissue: Structure, Function, and Factors That Influence Bone Cells. *Biomed Res Int*. 2015;2015.

7. Clarke B. Normal bone anatomy and physiology. *Clin J Am Soc Nephrol*. 2008;(3 Suppl 3):S131-9.

8. Sims NA, Gooi JH. Bone remodeling: Multiple cellular interactions required for coupling of bone formation and resorption. *Semin Cell Dev Biol*. 2008;19(5):444-451.

9. Feng X, McDonald JM. Disorders of Bone Remodeling. *Annu Rev Pathol Mech Dis*. 2011;6(1):121-145.

10. Lane NE. Epidemiology, etiology, and diagnosis of osteoporosis *Am J Obstet Gynecol*. 2006;194(2 Suppl):S3-11

11. Hadjidakis DJ, Androulakis II. Bone Remodeling. *Ann N Y Acad Sci*. 2006;1092(1):385-396.

12. Legrand E, Hedde C, Gallois Y, et al. Osteoporosis in men: a potential role for the sex hormone binding globulin. *Bone*. 2001;29(1):90-95.

13. Tarride JE, Hopkins RE, Leslie WD, et al. The burden of illness of osteoporosis in Canada. *Osteoporosis Int*. 2012;23(11): 2591–2600.

14. Misiorowski W. Osteoporosis in men. *Menopausal Rev*. 2017;2:70-73.

15. Buckley L, Guyatt G, Fink HA, et al. 2017 American College of Rheumatology guideline for the prevention and treatment of glucocorticoid-induced osteoporosis. *Arthritis Care Res (Hoboken)*. 2017;69(8):1095–1110.

16. Sheu A, Diamond T. Secondary osteoporosis. *Aust Prescr*. 2016;39(3):85-87.

17. Mirza F, Canalis E. Management of endocrine disease: Secondary osteoporosis: pathophysiology and management. *Eur J Endocrinol*. 2015;173(3):R131-R151.

18. Tannenbaum C, Clark J, Schwartzman K, et al. Yield of laboratory testing to identify secondary contributors to osteoporosis in otherwise healthy women. *J Clin Endo Metab*. 2002;87(10):4431–4437.

19. Sandhu SK, Hampson G. The pathogenesis, diagnosis, investigation and management of osteoporosis. *J Clin Pathol*. 2011;64(12):1042-1050.

20. . Bonjour JP, Chevalley T, Ferrari S, Rizzoli R. The importance and relevance of peak bone mass in the prevalence of osteoporosis. *Salud Publica Mex*. 2009;51(Suppl.1).

21. National Osteoporosis Foundation. Peak Bone Mass. Facts about Bone Health in Children and Adolescents. Retrieved from: https://www.nof.org/preventing-fractures/nutrition-for-bone-health/peak-bone-mass/ Accessed Jan 23 2020.

22. World Health Organization. Assessment of fracture risk and its application to screening for postmenopausal osteoporosis. Report of a WHO study group. Tech Rep Ser 843. Geneva, Switzerland: World Health Organization; 1994.

23. Appelman-Dijkstra NM, Papapoulos SE. Modulating Bone Resorption and Bone Formation in Opposite Directions in the Treatment of Postmenopausal Osteoporosis. *Drugs*. 2015;75(10):1049-1058.

24. Kearns AE, Khosla S, Kostenuik PJ. Receptor activator of nuclear factor κB ligand and osteoprotegerin regulation of bone remodeling in health and disease. *Endocr Rev*. 2008;29(2):155-192.

25. Nelson CA, Warren JT, Wang MWH, Teitelbaum SL, Fremont DH. RANKL employs distinct binding modes to engage RANK and the osteoprotegerin decoy receptor. *Structure*. 2012;20(11):1971-1982.

26. Luo G, Li F, Li X, Wang ZG, Zhang B. TNF-α and RANKL promote osteoclastogenesis by upregulating RANK via the NF-κB pathway. *Mol Med Rep*. 2018;17(5):6605-6611.

27. Simonet WS, Lacey DL, Dunstan CR, et al. Osteoprotegerin: a novel secreted protein involved in the regulation of bone density. *Cell*. 1997;89:309–319.

28. Glass DA, Bialek P, Ahn JD, et al. Canonical Wnt signaling in differentiated osteoblasts controls osteoclast differentiation. *Dev Cell*. 2005;8(5):751-764.

29. Westendorf JJ, Kahler RA, Schroeder TM. Wnt signaling in osteoblasts and bone diseases. *Gene*. 2004;341(1-2):19-39.

30. Krishnan V, Bryant HU, MacDougald OA. Regulation of bone mass by Wnt signaling. *J Clin Invest*. 2006;116(5):1202-1209.

31. Ralston SH. Genetic Determinants of Bone Mass and Osteoporotic Fracture. In: *Principles of Bone Biology, Two-Volume Set*. Vol 2. Elsevier Inc.; 2008:1611-1634.

32. Khosla S, Oursler MJ, Monroe DG. Estrogen and the skeleton. *Trends Endocrinol Metab*. 2012;23(11):576-581.

33. Saika M, Inoue D, Kido S, Matsumoto T. 17β-estradiol stimulates expression of osteoprotegerin by a mouse stromal cell line, ST-2, via estrogen receptor α. *Endocrinology*. 2001;142:2205–2212.

34. Robinson LJ, Yaroslavskiy BB, Griswold RD, et al. Estrogen inhibits RANKL-stimulated osteoclastic differentiation of human monocytes through estrogen and RANKL-regulated interaction of estrogen receptor-alpha with BCAR1 and Traf6. *Exp Cell Res*. 2009;315(7):1287-1301.

35. Marusic A, Kovacic N, Lukic I, Katavic V, Grcevic D. Understanding the role of Fas-Fas ligand system in bone. *Arthritis Res Ther*. 2012;14(Suppl 1):O20

36. Sun L, Peng Y, Sharrow AC, et al. FSH directly regulates bone mass. *Cell*. 2006;125(2):247-

37. Anderson FH, Francis RM, Selby PL, Cooper C. Sex Hormones and Osteoporosis in Men. *Calcif Tissue Int*. 1998;62(3):185-188.

38. Colvard DS, Eriksen EF, Keeting PE, et al. Identification of androgen receptors in normal human osteoblast-like cells. *Proc Natl Acad Sci U S A*. 1989;86(3):854-857.

39. Kelly PJ, Pocock NA, Sambrook PN, Eisman JA. Dietary calcium, sex hormones, and bone mineral density in men. *Br Med J*. 1990;300(6736):1361-1364.

40. Slemenda CW, Longcope C, Zhou L, Hui SL, Peacock M, Johnston CC. Sex steroids and bone mass in older men. Positive associations with serum estrogens and negative associations with androgens. *J Clin Invest*. 1997;100(7):1755-1759.

41. Carani C, Qin K, Simoni M, et al. Effect of Testosterone and Estradiol in a Man with Aromatase Deficiency. *N Engl J Med*. 1997;337(2):91-95.

42. Aguirre LE, Colleluori G, Fowler KE, et al. High aromatase activity in hypogonadal men is associated with higher spine bone mineral density, increased truncal fat and reduced lean mass. *Eur J Endocrinol*. 2015;173(2):167-174.

43. Cranney A, Papaioannou A, Zytaruk N, et al. Parathyroid hormone for the treatment of osteoporosis: A systematic review. *CMAJ*. 2006;175(1):52-59.

44. Masiukiewicz US, Insogna KL. The role of parathyroid hormone in the pathogenesis, prevention and treatment of postmenopausal osteoporosis. *Aging Clin Exp Res*. 1998;10(3):232-239.

45. Augustine M, Horwitz MJ. Parathyroid hormone and parathyroid hormone-related protein analogs as therapies for osteoporosis. *Curr Osteoporos Rep*. 2013;11(4):400-406.

46. Esbrit P, Alcaraz MJ. Current perspectives on parathyroid hormone (PTH) and PTH-related protein (PTHrP) as bone anabolic therapies. *Biochem Pharmacol*. 2013;85:1417–23.

47. Mannstadt M, Jüppner H, Gardella TJ. Receptors for PTH and PTHrP: their biological importance and functional properties. *Am J Physiol*. 1999;277:F665-675.

48. Erlebacher A, Filvaroff EH, Ye JQ, Derynck R. Osteoblastic responses to TGF-beta during bone remodeling. *Mol Biol Cell*. 1998;9(7):1903-1918.

49. Sahni S, Mangano KM, McLean RR, Hannan MT, Kiel DP. Dietary Approaches for Bone Health: Lessons from the Framingham Osteoporosis Study. *Curr Osteoporos Rep*. 2015;13(4):245-255.

50. Levis S, Lagari VS. The role of diet in osteoporosis prevention and management. *Curr Osteoporos Rep*. 2012;10(4):296-302.

51. Lips P, Van Schoor NM. The effect of vitamin D on bone and osteoporosis. *Best Pract Res Clin Endocrinol Metab*. 2011;25(4):585-591.

52. IOM (Institute of Medicine). Dietary reference intakes for calcium and vitamin D. Washington, DC: The National Academic. Press; 2011.

53. Devine A, Wilson SG, Dick IM, et al. Effects of vitamin D metabolites on intestinal calcium absorption and bone turnover in elderly women. *Am J Clin Nutri*. 2002;75(2):283–288.

54. Ebeling PR. Vitamin D and bone health: Epidemiologic studies. *Bonekey Rep*. 2014;3:511.

55. Heaney RP, Layman DK. Amount and type of protein influences bone health. In: *Am J Clin Nutr*. 2008;87(5):1567S-1570S.

56. Pouresmaeili F, Kamalidehghan B, et al. A comprehensive overview on osteoporosis and its risk factors. *Ther Clin Risk Manag*. 2018;14:2029-2049.

57. Bijelic R, Milicevic S, Balaban J. Risk Factors for Osteoporosis in Postmenopausal Women. *Med Arch (Sarajevo, Bosnia Herzegovina)*. 2017;71(1):25-28.

58. Alcohol and Other Factors Affecting Osteoporosis Risk in Women. https://pubs.niaaa.nih.gov/publications/arh26-4/292-298.htm. Accessed January 14, 2020.

59. Cheraghi Z, Doosti-Irani A, Almasi-Hashiani A, et al. The effect of alcohol on osteoporosis: A systematic review and meta-analysis. *Drug Alcohol Depend*. 2019;197:197-202.

60. Marcus R, Kiratli BJ. Physical activity and osteoporosis. In: Stevenson, J.C., and Lindsay, R., eds. *Osteoporosis*. New York: Chapman & Hall Medical, 1998:309–323.

61. Millard PS. Prevention of osteoporosis. In: Rosen, C.J., ed. *Osteoporosis: Diagnosis and Therapeutic Principles*. Totowa, NJ: Humana Press, 1996:275–285.

62. Salari Sharif P, Abdollahi M, Larijani B. Current, new and future treatments of osteoporosis. *Rheumatol Int*. 2011;31(3):289-300.

63. Patel S. Current and potential future drug treatments for osteoporosis. *Ann Rheum Dis*. 1996;55(10):700-714.

64. Lees B, Stevenson JC. The prevention of osteoporosis using sequential low-dose hormone replacement therapy with estradiol-17β and dydrogesterone. *Osteoporos Int*. 2001;12(4):251-258.

65. Gambacciani M, Levancini M. Hormone replacement therapy and the prevention of postmenopausal osteoporosis. *Prz Menopauzalny*. 2014;13(4):213-220.

66. Cauley JA, Robbins J, Chen Z, et al. Effects of estrogen plus progestin on risk of fracture and bone mineral density: the Women's Health Initiative randomized trial. *JAMA* 2003;290:1729-1738.

67. Vickers MR, MacLennan AH, Lawton B, et al. Main morbidities recorded in the women's international study of long duration oestrogen after menopause (WISDOM): a randomised controlled trial of hormone replacement therapy in postmenopausal women. *BMJ*. 2007;335:239-250.

68. Hulley S, Furberg C, Barrett-Connor E, et al. Noncardiovascular disease outcomes during 6.8 years of hormone therapy: Heart and Estrogen/progestin Replacement Study follow-up (HERS II). *JAMA*. 2002;(288):58-66.

69. Rossouw JE, Anderson GL, Prentice RL et al. Risks and benefits of estrogen plus progestin in healthy postmenopausal women: principal results from the Women's Health Initiative randomized Controlled Trial. *JAMA*. 2002;(288):321–333.

70. U.S. Preventive Services Task Force. Hormone therapy for the prevention of chronic conditions in postmenopausal women: recommendations from the U.S. Preventive Services Task Force. *Ann Intern Med*. 2005;142:855-860.

71. An KC. Selective estrogen receptor modulators. *Asian Spine J*. 2016;10(4):787-791.

72. Gennari L, Merlotti D, Valleggi F, Martini G, Nuti R. Selective estrogen receptor modulators for postmenopausal osteoporosis: Current state of development. *Drugs and Aging*. 2007;24(5):361-379.

73. Delmas PD, Ensrud KE, Adachi JD, et al. Efficacy ofraloxifene on vertebral fracture risk reduction in post-menopausalwomen with osteoporosis: four-year results from a randomized clinical trial. *J Clin Endocrinol Metab* 2002;87:3609–3617.

74. Barrett-Connor E, Mosca L, Collins P, et al. Effects ofraloxifene on cardiovascular events and breast cancer in post-menopausal women. *N Eng J Med*. 2006;(355):125–137.

75. Heaney RP. Bone mass, nutrition, and other lifestyle factors. *Am J Med*. 1993;(95):29-33S.

76. Carrié Fässler AL, Bonjour JP. Osteoporosis as a pediatric problem. *Pediatr Clin North Am* 1995;(42):811-824.

77. Jackson RD, LaCroix AZ, Gass M, et al. Calcium plus vitamin D supplementation and the risk of fractures. *N Eng J Med*. 2006;(354):669–683.

78. Chiodini I, Bolland MJ. Calcium supplementation in osteoporosis: useful or harmful? *Eur J Endocrinol*. 2018;178(4):D13-D25.

79. Tang BM, Eslick GD, Nowson C, et al. Use of calcium or calcium in combination with vitamin D supplementation to prevent fractures and bone loss in people aged 50 years and older: a meta-analysis. *Lancet*. 2007;(370):657–666.

80. Whitaker M, Guo J, Kehoe T, et al. Bisphosphonates for Osteoporosis — Where Do We Go from Here? *N Engl J Med*. 2012;366(22):2048-2051.

81. Lewiecki EM. Bisphosphonates for the treatment of osteoporosis: Insights for clinicians. *Ther Adv Chronic Dis*. 2010;1(3):115-128.

82. Poole KE, Compston JE. Bisphosphonates in the treatment of osteoporosis. *BMJ*. 2012;(344):e3211-e3211.

83. Russell RGG, Watts NB, Ebetino FH, Rogers MJ. Mechanisms of action of bisphosphonates: Similarities and differences and their potential influence on clinical efficacy. *Osteoporos Int.* 2008;19(6):733-759.

84. Sunyecz J. A. Zoledronic acid infusion for prevention and treatment of osteoporosis. *International journal of women's health.* 2010;2:353–360.

85. Harris ST, Watts NB, Genant HK, et al. Effect of risedronate treatment on vertebral and non-vertebral fractures in women with postmenopausal osteoporosis. A randomized controlled trial. *JAMA.*1999;282:1344-1352.

86. Reginster JY, Minne H, Sorensen O, et al. Randomized trial of the effects of risedronate on vertebral fractures in women with established postmenopausal osteoporosis. *Osteoporos Int.* 2000;11:83-91

87. Delmas PD, Recker RR, Chesnut CH 3rd, et al. Daily and intermittent oral ibandronate normalize bone turnover and provide significant reduction in vertebral fracture risk: results from the BONE study. *Osteoporos Int.* 2004;15:792-798.

88. Black DM, Delmas PD, Eastell R, et al. Once-yearly zoledronic acid for treatment of postmenopausal osteoporosis. *N Engl J Med.* 2007;356:1809-1822.

89. McClung MR, Geusens P, Miller PD, et al. Effect of risedronate on the risk of hip fracture in elderly women. Hip Intervention Program Study Group. *N Engl J Med.* 2001;344:333-340.

90. Brown JP, Kendler DL, McClung MR, et al. The efficacy and tolerability of risedronate once a week for the treatment of postmenopausal osteoporosis. *Calcif Tiss Int.* 2002;71(2):103-111

91. Delmas PD, McClung MR, Zanchetta JR, et al.Efficacy and safety of risedronate 150 mg once a month in the treatment of postmenopausal osteoporosis. *Bone. 2008;*42:36-42.

92. Delmas PD, Benhamou CL, Man Z, et al. Monthly dosing of 75 mg risedronate on 2 consecutive days a month: efficacy and safety results. *Osteoporos Int.* 2008;19:1039-1045.

93. Camacho PM, Petak SM, Binkley N, et al. Guidelines for the Diagnosis and Treatment of Postmenopausal Osteoporosis: AACE/ACE 2016. *Endocr Pract.* 2016;22(Supplement 4):1-42.

94. Cramer JA, Gold DT, Silverman SL, Lewiecki EM. A systematic review of persistence and compliance with bisphosphonates for osteoporosis. *Osteoporos Int.* 2007;18(8):1023-1031.

95. Gedmintas L, Solomon DH, Kim SC. Bisphosphonates and risk of subtrochanteric, femoral shaft, and atypical femur fracture: a systematic review and meta-analysis. *J Bone Miner Res.* 2013;28(8):1729-1737.

96. Migliorati CA, Siegel MA, Elting LS. Bisphosphonate-associated osteonecrosis: a long-term complication of bisphosphonate treatment. *Lancet Oncol*. 2006;7(6):508-514.

97. Yood RA, Emani S, Reed JI, et al. Compliance with pharmacologic therapy for osteoporosis. *Osteoporos Int*. 2003;14:965-968.

98. Caro JJ, Ishak KJ, Huybrechts KF, et al. The impact of compliance with osteoporosis therapy on fracture rates in actual practice. *Osteoporos Int*. 2004;15:1003-1008.

99. McCombs JS, Thiebaud P, Laughlin-Miley C, et al. Compliance with drug therapies for the treatment and prevention of osteoporosis. *Maturitas*. 2004;48: 271-287.

100. Muñoz-Torres M, Alonso G, Mezquita Raya P. Calcitonin Therapy in Osteoporosis. *Treat Endocrinol*. 2004;3(2):117-132.

101. Kallio DM, Ganat PR, Minkin C. Ultrastructural effects of calcitonin on osteoclasts in tissue culture. *J Ultrastruct Res*. 1972;39:205-216.

102. Chambers TJ, Magnus CJ. Calcitonin alters behaviour of isolated osteoclasts. *J Pathol*. 1982;136:97-106.

103. Ljunghall S, Gärdsell P, Johnell O, et al. Synthetic human calcitonin in postmenopausal osteoporosis: a placebo-controlled, double-blind study. *Calcif Tissue Int*. 1991;49:17–19.

104. Thamsborg G, Storm TL, Sykulski R, et al. Effect of different doses of nasal calcitonin on bone mass. *Calcif Tissue Int*. 1991;48:302–307.

105. Silverman SL, Chesnut C, Andriano K, et al. Salmon calcitonin nasal spray (NS-CT) reduces risk of vertebral fracture(s) (VF) in established osteoporosis and has continuous efficacy with prolonged treatment: accrued 5 year world wide data of the PROOF Study. *J Bone Miner Res*. 1998;2(Suppl 5):S174.

106. Hodson AB, Bauer DC, Dempster DW, et al. Parathyroid hormone and teriparatide for the treatment of osteoporosis: a review of the evidence and suggested guidelines for its use. *Endocr Rev*. 2005;26:688–703.

107. Neer RM, Arnaud CD, Zanchetta JR, et al. Effect of Parathyroid Hormone (1-34) on Fractures and Bone Mineral Density in Postmenopausal Women with Osteoporosis. *N Engl J Med*. 2001;344(19):1434-1441.

108. Hodsman AB, Steer BM. Early histomorphometric changes in response to parathyroid hormone therapy in osteoporosis: evidence for de novo bone formation on quiescent cancellous surfaces. *Bone*. 1993;14:523-527.

109. Zanchetta JR, Bogado CE, Ferretti JL, et al. Effects of teriparatide [recombinant human parathyroid hormone (1-34)] on cortical bone in postmenopausal women with osteoporosis. *J Bone Miner Res*. 2003;18:539-543.

110. Jiang Y, Zhao JJ, Mitlak BH, et al. Recombinant human parathyroid hormone (1–34) [teriparatide] improves both cortical and cancellous bone structure. *J Bone Miner Res*. 2003;18:1932–1941.

111. Body JJ, Gaich GA, Scheele WH, et al. A randomized double-blind trial to compare the efficacy of teriparatide [recombinant human parathyroid hormone (1–34)] with alendronate in postmenopausal women with osteoporosis. *J Clin Endocrinol Metab*. 2002;87:4528–4535.

112. Vahle JL, Sato M, Long GG, et al. Skeletal changes in rats given daily subcutaneous injections of recombinant human parathyroid hormone (1-34) for 2 years and relevance to human safety. *Toxicol Pathol*. 2002;30:312-21.

113. Palmer M, Adami HO, Krusemo YB, et al. Increased risk of malignant diseases after surgery for primary hyperparathyroidism: a nationwide cohort study. *Am J Epidemiol*.1988;127:1031-1040.

114. Lane NE, Sanchez S, Modin GW, et al. Parathyroid hormone treatment can reverse corticosteroid-induced osteoporosis: results of a randomized controlled clinical trial. *J Clin Invest*.1998;102:1627-1633.

115. Crandall C. Parathyroid hormone for treatment of osteoporosis. *Arch Intern Med*. 2002;162(20):2297-2309.

116. Schwab P, Klein RF. Nonpharmacological approaches to improve bone health and reduce osteoporosis. *Curr Opin Rheumatol*. 2008;20(2):213-217.

117. Coronado-Zarco R, Olascoaga-Gómez De León A, García-Lara A, Quinzaños-Fresnedo J, Nava-Bringas TI, Macías-Hernández SI. Nonpharmacological interventions for osteoporosis treatment: Systematic review of clinical practice guidelines. *Osteoporos Sarcopenia*.

118. Pazianas M, Abrahamsen B, Ferrari S, et al. Eliminating the need for fasting with oral administration of bisphosphonates. *Ther and clin risk mgmt*. 2013;9:395–402.

119. Major P, Lipton A, Berenson J. et al. Oral bisphosphonates. *Cancer*. 2000;88:6-14.

120. Lin JH. Bisphosphonates: A review of their pharmacokinetic properties. *Bone*. 1996;18:75-85.

121. Cremers S, Drake MT, Ebetino FH, et al. Pharmacology of bisphosphonates. *Br J Clin Pharmacol*. 2019;85(6):1052-1062.

122. Chae JW, Seo JW, Mahat B. et al. A simple pharmacokinetic model of alendronate developed using plasma concentration and urine excretion data from healthy men. *Drug Development and Industrial Pharmacy*. 2014;40:1325-1329.

123. Satterwhite J, Heathman M, Miller PD, et al. Pharmacokinetics of teriparatide (rhPTH[1-34]) and calcium pharmacodynamics in postmenopausal women with osteoporosis. *Calcified tissue international*. 2010;87(6):485–492.

124. Forteo product information. US Federal Drug Administration (FDA). 2008. Retrieved from: https://www.accessdata.fda.gov/drugsatfda_docs/label/2008/021318s015lbl.pdf

125. Reszka AA, Rodan GA. Bisphosphonate mechanism of action. *Curr Rheumatol Rep*. 2003;5(1):65-74.

126. Masarachia P, Weinreb M, Balena R, et al. Comparison of the distribution of 3H-alendronate and 3H-etidronate in rat and mouse bones. *Bone*. 1996;19:281–290.

127. Benford HL, McGowan NW, Helfrich MH, et al. Visualization of bisphosphonate-induced caspase-3 activity in apoptotic osteoclasts in vitro. *Bone*. 2001;28(5):465–473

128. Monkkonen H, Auriola S, Lehenkari P, et al A new endogenous ATP analog (ApppI) inhibits the mitochondrial adenine nucleotide translocase (ANT) and is responsible for the apoptosis

129. Russell RG, Rogers MJ, Frith JC, et al. The pharmacology of bisphosphonates and new insights into their mechanisms of action. *Journal of Bone and Mineral Research*.1996;14:53-65.

130. Sunyecz J. Optimizing dosing frequencies for bisphosphonates in the management of postmenopausal osteoporosis: patient considerations. *Clinical interventions in aging*, 2008;3(4): 611–627.

131. Schnitzer T, Bone HG, Crepaldi G, et al. Therapeutic equivalence of alendronate 70 mg once-weekly and alendronate 10 mg daily in the treatment of osteoporosis. Alendronate Once-Weekly Study Group. *Aging (Milano)*. 200;12(1):1–12.

132. Bone HG, Downs RW, Tucci JR, et al. Dose-Response Relationships for Alendronate Treatment in Osteoporotic Elderly Women. Alendronate Elderly Osteoporosis Study Centers. *J of Clin Endocrinol Metab*. 1997;82(1):265-74.

133. Yang D, Singh R, Divieti P, Guo J, Bouxsein ML, Bringhurst FR. Contributions of parathyroid hormone (PTH)/PTH-related peptide receptor signaling pathways to the anabolic effect of PTH on bone. *Bone*. 2007;40(6):1453-1461.

134. Silva BC, Bilezikian JP. Parathyroid hormone: Anabolic and catabolic actions on the skeleton. *Curr Opin Pharmacol*. 2015;22:41-50.

135. Bilezikian JP. Anabolic therapy for osteoporosis. *Int J Fertil Womens Med*. 2005;50(2):53-60.

136. Kronenberg HM. PTH: mechanism of action. In: Favus M, ed. Primer on metabolic bone diseases, 3rd Ed. American Society of Bone and Mineral Re-search. Philadelphia: Lippincott Raven. 1996;68 –70.

137. Lombardi G, Di Somma C, Rubino M, et al. The roles of parathyroid hormone in bone remodeling: prospects for novel therapeutics. *J Endocrinol Invest*. 2011;34(7 Suppl):18-22.

138. Hilliker S, Wergedal JE, Gruber HE, et al. Truncation of the amino terminus of PTH alters its anabolic activity on bone in vivo. *Bone*. 1996;19:469–477.

139. Rixon RH, Whitfield JF, Gagnon L, et al. Parathyroid hormone fragments may stimulate bone growth in ovariectomized rats by activating adenylyl cyclase. *J Bone Miner Res*. 1994;9:1179–1189.

140. Onyia JE, Helvering LM, Gelbert L, et al. Molecular profile of catabolic versus anabolic treatment regimens of parathyroid hormone (PTH) in rat bone: An analysis by DNA microarray. *J. Cell. Biochem*. 2005;95: 403-418.

141. Ishizuya T, Yokose S, Hori M, et al. Parathyroid hormone exerts disparate effects on osteoblast differentiation depending on exposure time in rat osteoblastic cells. *J Clin Invest*. 1997;99:2961-2970.

142. Krishnan V, Moore TL, Ma YL, et al. Parathyroid hormone bone anabolic action requires Cbfa1/Runx2-dependent signaling. *Mol Endocrinol*. 2003;17:423-435

143. Chenv HL, Demiralp B,Schneider A, et al. Parathyroid hormone and parathyroid hormone-related protein exert both pro-and anti-apoptotic effects in mesenchymal cells. *J Biol Chem* 2002,277:19374-19381.

144. Bellido T, Ali A, Plotkin LI, et al. Proteasomal degradation of Runx2 shortens parathyroid hormone-induced anti-apoptotic signaling in osteoblasts. A putative explanation for why intermittent administration is needed for bone anabolism. *J Biol Chem*. 2003,278:50259-50272.

145. Martin TJ. Bone Biology and Anabolic Therapies for Bone: Current Status and Future Prospects. *J Bone Metab*. 2014;21(1):8.

146. Merrick MV. Review article-Bone scanning. *Br J Radiol*. 1975 May;48(569):327-51.

147. Gil L, Han Y, Opas EE, Rodan GA, Ruel R, Seedor JG, Tyler PC, Young RN. Prostaglandin E2-bisphosphonate conjugates: potential agents for treatment of osteoporosis. *Bioorg Med Chem*. 1999 May;7(5):901-19.

148. Hirabayashi H, Fujisaki J. Bone-specific drug delivery systems: approaches via chemical modification of bone-seeking agents. *Clin Pharmacokinet*. 2003;42(15):1319-30.

149. Arns S, Gibe R, Moreau A, Monzur Morshed M, et al. Design and synthesis of novel bone-targeting dual-action pro-drugs for the treatment and reversal of osteoporosis. *Bioorg Med Chem*. 2012 Mar 15;20(6):2131-40

150. Blick, S.K.A., Dhillon, S. & Keam, S.J. Teriparatide. *Drugs*. 2008;68:2709–2737.

151. Murray TM, Rao LG, Divieti P, et al. Parathyroid hormone secretion and action: evidence for discrete receptors for the carboxyl-terminal region and related biological actions of carboxyl-terminal ligands. *Endocr Rev*. 2005;26(1):78–113.

152. Seshadri MS, Chan MR, Wilkinson RS, et al. Some problems associated with adenylate cyclase bioassays for parathyroid hormone. *Clin Sci*. 1985;68(3):311–9.

153. Doschak MR, Kucharski CM, Wright JEI, et al. Improved bone delivery of osteoprotegerin by bisphosphonate conjugation in a rat model of osteoarthritis. *Mol Pharmaceutics*, 6(2):634-40, 2009.

154. Yang Y, Panahifar A, Wu Y, et al. Bone-targeting parathyroid hormone analogues outperform unmodified PTH in the anabolic treatment of osteoporosis in rats. Podium presentation at the Annual Meeting and Exposition of the Controlled Release Society (CRS) in Chicago, USA July 11-15, 2014.

155. Henneman ZJ, Nancollas GH, Ebetino FH, et al. Bisphosphonate binding affinity as assessed by inhibition of carbonated apatite dissolution in vitro. *J Biomed Mater Res A*. 2008;85(4):993-1000.

156. Wells DA. High throughput bioanalytical sample preparation: Methods and automation strategies. 2003. 1st ed. Amsterdam: Elsevier Science B.V.

157. Thurman EM, Mills MS. Solid-phase extraction: Principles and practise. Chemical analysis: A series of monographs on analytical chemistry and its applications. 1998. Winefordner J.D. Vol. 147. New York: John Wiley & sons Inc.

158. Strata-X Polymeric SPE Information. *Phenomenex*. Retrieved from: https://www.phenomenex.com/Products/SPDetail/Strata-X/X,%20Polymeric%20Reversed%20Phase?phaseTab=true. Accessed May 28th 2020

159. McPolin, O. An introduction to HPLC for pharmaceutical analysis. Newry, UK. Mourne Training Services, 2009.

160. Hanai T. Separation of polar compounds using carbon columns. *J Chromatogr A*. 2003;989(2):183-196.

161. *LC•GC Europe-December 2001 2 LC Troubleshooting*. http://www.chromforum.com. Accessed March 30, 2020.

162. Snyder LR, Kirkland JJ, and Dolan JW. "Ionic Samples: Reversed-Phase, Ion-Pair, and Ion-Exchange Chromatography." *Introduction to Modern Liquid Chromatography*, John Wiley & Sons, Inc., Publication, 2010.

163. Wang S, Xing T, Liu AP, et al. Simple approach for improved LC-MS analysis of protein biopharmaceuticals via modification of desolvation gas. *Anal. Chem.* 2019;91(4):3156-3162

164. Xie Z, Jiang Y, Zhang D-Q. Simple analysis of four bisphosphonates simultaneously by reverse phase liquid chromatography using n-amylamine as volatile ion-pairing agent. *J Chromatogr A*. 2006;1104(1-2):173-178.

165. Ghassabian S, Wright LA, de Jager AD, et al. Development and validation of a sensitive solid-phase-extraction (SPE) method using high-performance liquid chromatography/tandem mass spectrometry (LC–MS/MS) for determination of risedronate concentrations in human plasma, *J. Chromatogr. B: Anal. Technol. Biomed. Life Sci*. 2012;(881–882):34–41.

166. Yamada M, Lee X-P, Fujishiro M, et al. Highly sensitive determination of alendronate in human plasma and dialysate using metal-free HPLC-MS/MS. *Leg Med*. 2018;(30):14-20.

167. Tsai EW, IP DP, and Brooks MA. Determination of alendronate on pharmaceutical dosage forms by ion chromatography with conductivity detection. *J. Chromatrogra*. 1992;596:217

168. Quitasol J and Krastins L. Analysis of pamidronate disodium in pharmaceutical dosage forms by ion chromatrography. *J. Chromatrogra A*. 1994;(671):273-279.

169. Usui T, Watanabe T, and Higuchi S. Determination of a new bisphosphonate, YM175, in

plasma, urine and bone by high-performance liquid chromatography with electrochemical detection. *J Chromatogr*. 1992;584(2):213-220

170. Mastanamma SK, Suresh G, Priya S, et al. A validated RP-HPLC method for the estimation of zoledronic acid. *Intl. J. Pharm sciences & research*. 2012;25:826-829.

171. Silvestro L, Tarcomnicu I, Savu RS. HPLC-MS/MS of highly polar compounds. Tandem Mass Spectrometry- Applications and Principles. 2012:494-524.

172. Matuszewski L, Matuszewska A, Mazurkiewicz T, et al. Determination of Bisphosphonates by Ion-pair HPLC. *Journal of the faculty of Agriculutre, Kyushu University*. 2011;56(2):213-216.

173 Fels JP, Guyonnet J, Berger Y, et al. Determination of (4-chlorophenyl)tiomethylene bisphosphonic acid, a new bisphosphonate, in biological fluids by high-performance liquid chromatography. *J Chromatogr*. 1988;430(1):73-79.

174. Yang Y, Liu C, Zhang Y, et al. On-cartridge derivatization coupled with solid-phase extraction for the ultra-sensitive determination of minodronic acid in human plasma by LC-MS/MS method. *J Pharm Biomed Anal*. 2015;(114):408-415.

175. W.F. Kline, B.K. Matuszewski, Improved determination of the bisphosphonate alendronate in human plasma and urine by automated precolumn derivatization and high-performance liquid chromatography with fluorescence and electrochemical detection, *J. Chromatogr. – Biomed. Appl*. 1992;583:183–193.

176. H.J. Leis, G. Fauler, W. Windischhofer, Use of 18O3-clodronate as an internal standard for the quantitative analysis of clodronate in human plasma by gas chromatography/electron ionisation mass spectrometry. *Rapid Commun. Mass Spectrom*. 2004;18:2781–2784.

177. Zhu L, Lapko V, Lee J, et al., A general approach for the quantitative analysis of bisphosphonates in human serum and urine by high-performance liquid chromatography/tandem mass spectrometry. *Rapid Commun. Mass Spectrom*. 2006;(20):3421–3426.

178. Hasan M, Schumacher G, Seekamp A, et al. LC–MS/MS method for the determination of clodronate in human plasma. *J. Pharm. Biomed. Anal*. 2014;100:341–347.

179. M.-H. Yun, K. Kwon, High-performance liquid chromatography method for determining alendronate sodium in human plasma by detecting fluorescence: application to a pharmacokinetic study in humans. *J. Pharm. Biomed. Anal*. 2006;40:168–172.

180. Muntoni E, Canaparo R, Della PC, et al. Determination of disodium clodronate in human plasma and urine using gas-chromatography-nitrogen-phosphorous detections: validation and

application in pharmacokinetic study. *J. Chromatogr. B: Anal. Technol. Biomed. Life Sci.* 2004;799:133–139.

181. Ismail Z, Aldous S, Triggs EJ, Smithurst BA, et al. Gas chromatographic analysis of didronel tablets. *J Chromatogr.* 1987;404:372-377.

182. Kataoka H, Shindoh S, Makita M. Selective determination of volatile N-nitrosamines by derivatization with diethyl chlorothiophospate and gas chromatography with flame photometric detection. *J Chromatogr A.* 1996;723(1):93-99.

183. Roelofs AJ, Coxon FP, Ebetino FH, et al. Fluorescent risedronate analogues reveal bisphosphonate uptake by bone marrow monocytes and localization around osteocytes in vivo. *J Bone Miner Res.* 2010;25(3):606-616.

184. Basics of LC/MS. Agilent. Accessed March 22 2020. Retrieved from: https://www.agilent.com/cs/library/support/documents/a05296.pdf.

185. Whittal, R.M. LC-MS 2020. Lecture in Analytical Techniques in Pharmaceutical Sciences (Lecture 4, PHARM 573). January 23 2020. University of Alberta.

186. *Why Does MS Require High Vacuum?* Shimadzu Corporation, 13 July 2017. Retrieved from www.shimadzu.com/an/ms_rquire_high_vacuum.html. Accessed March 22 2020.

187. Ho CS, Lam CWK, Chan MHM, et al. Electrospray ionisation mass spectrometry: principles and clinical applications. *Clin Biochem Rev.* 2003;24(1):3-12.

188. Dass, C., Fundamentals of Contemporary Mass Spectrometry Wiley- Interscience Series on Mass Spectrometry, ed. D.M. Desiderio, Nibbering, N.M. 2007, New Jersey, USA: John Wiley & Sons, Inc.

189. Gross, JH., *Mass Spectrometry: A Textbook.* Practical Aspects of Electron Ionization. 2004, Heidelberg, Germany: Springer-Verlag

190. Gaskell SJ. Electrospray: Principles and Practice. *J Mass Spectrom.* 1997;32(7):677-688.

191. Mallet CR, Lu Z, Mazzeo JR. A study of ion suppression effects in electrospray ionization from mobile phase additives and solid-phase extracts. *Rapid Commun Mass Spectrom.* 2004;18(1):49-58.

192. Demartini, D. R. (2013) A Short Overview of the Components in Mass Spectrometry Instrumentation for Proteomics Analyses, Tandem Mass Spectrometry - Molecular Characterization (Coelho, A. V., Ed.) InTech, Rijeka, Croatia

193. Adaway JE, Keevil BG, Owen LJ. Liquid chromatography tandem mass spectrometry in the clinical laboratory. *Ann Clin Biochem*. 2015;52(1):18-38.

194. Watson TJ and Sparkman DO. Introduction to Mass Spectrometry: Instrumentation, Applications and Strategies for Data Interpretation. John Wiley and Sons, 2011.

195. Guideline on Bioanalytical Method Validation. European Medicines Agency. 2011. Accessed May 12th 2020. Retrieved from: https://www.ema.europa.eu/en/documents/scientific-guideline/guideline-bioanalytical-method-validation_en.pdf

196 Wilson, ID. *Handbook of Methods and Instrumentation in Separation Science*. Liquid Chromatography: Detectors: Mass Spectrometry. Elsevier, 2009.

197. Black DM, Delmas PD, Eastell R, et al. Once-yearly zoledronic acid for treatment of postmenopausal osteoporosis. *N Engl J Med*. 2007;356:1809-1822.

198. Zhou W, Yang S, Wang PG. Matrix effects and application of matrix effect factor. *Bioanalysis*, 2017;9(23):1839–1844.

199. Tan A, Awaiye K. Use of Internal Standards in LC-MS Bioanalysis. In *Handbook of LC-MS Bioanalysis*. John Wiley & Sons Inc. 2013:217-227

200. Bakhtiar R, Majumdar TK. Tracking problems and possible solutions in the quantitative determination of small molecule drugs and metabolites in biological fluids using liquid chromatography-mass spectrometry. *J Pharmacol Toxicol Methods*. 2007;55:227–243

201. Chambers EE, Lame ME, Bardsley J, et al. High sensitivity LC–MS/MS method for direct quantification of human parathyroid 1–34 (teriparatide) in human plasma. *J Chromatogr B*. 2013;938:96-104

202. Kay RG, Hands JT, Hawthorne G, Constable S, Grosvenor M, Sharman JA. Validation of an ultrasensitive LC-MS/MS method for PTH 1-34 in porcine plasma to support a solid dose PK study. *Bioanalysis*. 2015;7(12):1435-1445.

203. MacNeill R, Stromeyer R, Urbanowicz B, Acharya V, Moussallie M. LC-MS/MS quantification of parathyroid hormone fragment 1-34 in human plasma. *Bioanalysis*. 2013;5(4):415-422.

204. Dolan J. A guide to HPLC and LC-MS buffer selection. *Ace HPLC Columns*. Accessed May 14th 2020. Retrieved from: https://www.hplc.eu/Downloads/ACE_Guide_BufferSelection.pdf

205. Shabir, G.A. *HPLC Method Development and Validation for Pharmaceutical Analysis*. 2004. Accessed May 14th 2020. Retrieved from: http://www.pharmtech.com/hplc-method-development-and-validation-pharmaceutical-analysis

206. Ornaf, R.M., and Dong, M.W., *Handbook of Pharmaceutical Analysis by HPLC*. Separation Science and Technology, ed. S. Ahuja, and Dong, M.W. Vol. 6. 2005: Elsevier Academic Press. 25.

207. Thompson R, LoBrutto, R. *HPLC for Pharmaceutical Scientists*, ed. Y. Kazakevich, LoBrutto, R. New Jersey: Wiley-interscience 200129, 303, 644.

208. Herodes K. LC-MS Method Validation, Selectivity: LC selectivity. *University of Tartu*. Accessed May 14th 2020. Retrieved from: https://sisu.ut.ee/lcms_method_validation/21-LC-selectivity

209. Lee HR, Kochar S, Shim, SM. Comparison of electrospray ionization and atmospheric chemical ionization coupled with the liquid chromatography-tandem mass spectrometry for the analysis of cholesteryl esters. *Intl J of Anal Chem*. 2015:1-6.

210. Chambers EE, Legido-Quigley C, Smith N, Fountain KJ. Development of a fast method for direct analysis of intact synthetic insulins in human plasma: the large peptide challenge. *Bioanalysis*. 2013;5(1):65-81.

211. Papayannopoulos IA. The interpretation of collision-induced dissociation tandem mass spectra of peptides. *Mass Spectrom. Rev*. 1995;14:49-73

212. Viswanathan, C.T., et al., *Quantitative bioanalytical methods validation and implementation: best practices for chromatographic and ligand binding assays*. Pharm Res, 2007. 24(10): p. 1962-73.

213. Wenzl T, Haedrich J, Schaechtele A, et al. Guidance Document on the Estimation of LOD and LOQ for Measurements in the Field of Contaminants in Feed and Food. *JRC Technical Reports*. 2016:14-26.

214. Layne, J. Symbiosis of Core-Shell and Fully Porous Particles: Implementing Both For Better HPLC and UHPLC Results. *Phenomenex*. 2017. Retrived from: https://phenomenex.blog/2017/06/14/core-shell-and-fully-porous-particle-webinar/?pdf=5640

215. Liebich HM, Föst C. *N*-Methylation and *N,N*-dimethylation of amino acids. An artifact production in the analysis of organic acids using diazomethane as derivatizing agent. *J. Chromatogra*. 1985;338:33-40.

216. Wasslen KV. Trimetylation Enhancement using Diazomethane (TrEnDi): A novel technique to enhance the sensitivity of MS-based analyses of biological molecules. Masters Thesis. 2014. Carleton University, Ottawa, Canada.

217. Gunawardena G. Methyl Ester Synthesis Using Diazomethane. *Chemistry Libretexts*. 2019. Accessed April 2nd 2020. Retrieved from:

https://chem.libretexts.org/Bookshelves/Organic_Chemistry/Map%3A_Organic_Chemistry_(Wa de)/21%3A_Carboxylic_Acids/21.07%3A_Methyl_Ester_Synthesis_Using_Diazomethane

218. Shioiri T, Aoyama T, Mori S. Trimethylslyldiazomethane. *Organic Syntheses*. 1990;68:1

219. Wong ASY, Ho ENM, Wan TSM, et al. Liquid chromatography–mass spectrometry analysis of five bisphosphonates in equine urine and plasma. *J Chromatogr B Analyt Technol Biomed Life Sci*. 2015;998-999:1-7.

220. Ogawa H, Hagiwara H, Chihara T, et al. Methylation of alcohols and phenopls adsorbed on silica gel with diazomethane. *Bulletin Chem Soc Jpn*. 1987;60:627.

221. Nishiyama H, Nagase H, Kiyotaka O. Reaction of some amides and thioamides with diazomethane catalyzed by silica gel. *Tetrahedron Lett*. 1979;20(48):4671-4674.

222. Ardrey RE. *Liquid chromatography-mass spectrometry: an introduction*. Chichester, UK: John Wiley and Sons Ltd. 2003.

223. Fei N., Sauter B., Gillingham D. The pKa of Brønsted acids controls their reactivity with diazo compounds. *Chem. Commun*. 2016;52:7501.

224. The Biology Project, Introduction to ELISA Activity. *University of Arizona, Department of Biochemistry and Molecular Biophysics*. 2000. Accessed May 18th 2020. Retrieved from: http://www.biology.arizona.edu/immunology/activities/elisa/main.html

225. Overview of ELISA. ThermoFisher Scientific. Accessed May 18th 2020: Retrieved from: https://www.thermofisher.com/ca/en/home/life-science/protein-biology/protein-biology-learning-center/protein-biology-resource-library/pierce-protein-methods/overview-elisa.html

226. ELISA Fundamental Principle, How ELISA Works- Immunoassays. *Bosterbio*. Accessed May 18th 2020. Retrieved from:

https://www.bosterbio.com/protocol-and-troubleshooting/elisa-principle

227. van Oss CJ. Hydrophobic, hydrophilic and other interactions in epitope-paratope binding. *Mol Immunol*. 1995;32:199–211.

228. Reverberi R, Reverberi L. Factors affecting the antigen-antibody reaction. *Blood Transfus*. 2007;5(4):227-240. 95